«An investigation of bio potentials for the pre-diagnosis of heart dysfunction using a novel portable high resolution electronic analyzer and software»

Thesis submitted to the Faculty of Computing, Engineering & Technology of Staffordshire University in partial fulfillment of the requirements for the degree Doctor of Philosophy

Author: ANDONOPOULOS JOHN

Supervised by:
Prof. Noel Shammas
Prof. Steve Grainger
Dr. Ian Taylor
Prof. Theodore Ganetsos

January 2011

I. Acknowledgments

Completing a PhD is truly a marathon event, and I would not have been able to complete this journey without the aid and support of many people over the past four years. I must first express my gratitude towards my principal supervisor, Professor Noel YA Shammas whose expertise, understanding, and patience, added considerably to my research experience.

I would like to thank the other members of my committee, Dr Ian Taylor, and Prof. Steve Grainger for the assistance they provided at all levels of the research project.

I want to express my gratitude to Dr. Theodore Ganetsos, for his supervision, advice, and guidance from the very early stage of this research. He provided me with direction, technical support and became more of a mentor and friend, than a professor. I am indebted to him more than he knows.

In addition, I want to thank my friend and associate Nikolaos Laskaris for his advice, and crucial contribution, which made him a backbone of this research and so to this research. Also I would like to thank my friend Anastasios Arvanitis for his assistance to the research editing.

I gratefully thank Mrs Tracy Davies for her continuous support through all these years.

Finally, I would also like to thank my family for the support they provided me through my entire life and in particular, I must acknowledge my wife and best friend, Sofia, without whose love, encouragement and editing assistance, I would not have finished this research.

I dedicate this research to my grandmother, Maria.

II. Abstract

An electrocardiogram (ECG) is a bioelectrical signal which records the heart's electrical activity versus time. It is an important diagnostic tool for assessing heart functions. The interpretation of ECG signal is an application of pattern recognition. The techniques used in this pattern recognition comprise: signal pre-processing, QRS detection, creation of variables and signal classification. In this research, signal processing and programs implementation are based in Matlab environment. The processed simulated signal source came from the SIMULAIDS® interactive ECG simulator™ device and the actual heart signals came from actual patients that suffer from various heart disorders, as well as healthy persons that hadn't recorded any form of heart condition in the past.

For the creation of the database in this research, 5 types of ECG waveform were selected from the ECG simulator device. These are normal sinus rhythm (NSR), ventricular tachycardia (VT poly), ventricular fibrillation (VF), Atrial fibrillation (A FIB) and supra ventricular tachycardia (SVT). An essential part of this research was the development of a portable high resolution ECG device, capable of connecting with, either an ECG simulator device, or recording real human data. This device is able to produce higher resolution than normal ECG devices and high values of Signal to Noise Ratio (SNR).

Matlab was used to develop a program that could further examine, analyze and study the ECG samples. Since the heart waveform can be simulated by cubic spline interpolation, this feature was used by the implemented Matlab program. The ECG samples were normalized and processed to produce 4 specific coefficients. These 4 coefficients of cubic spline were used in the applied methodology in order to evaluate and separate the various heart disorders with mathematical terms and equations. The database created was compared with the real human samples that were taken and passed through the same data process. Through this step, the entire data process and implementation was not only confirmed, but also proved that the capability to diagnose heart disorders was possible.

Based on the results of the applied methodology, the categorization of heart disorders without actual clinical examination is possible. Further analysis of each group of results, can lead to heart disorder prediction. Also given are further suggestions to plan experiments for future work.

Table of Contents

List of figures:

List of Tables:

List of abbreviations and acronyms:

- AIC - Akaike information criterion
- AGC - Automatic gain control
- AMI - Acute myocardial infarction
- ANS - Autonomic nervous system
- AP - Action potential
- APD - Action potential duration
- AR – Autoregressive
- AV – Atrioventricular
- BSP – Body Surface Potentials
- CHF - Congestive heart failure
- CO - Cardiac output
- CSA - Compressed spectral arrays
- CTM - Measure of central tendency
- CWT - Continuous wavelet transform
- CV - Coefficient of variation
- DWD - Discrete Wigner distribution
- DWT - Discrete wavelet transform
- ECG - Electrocardiogram
- FIR - Finite impulse response
- FFT - Fast Fourier Transform
- FHRV - Fetal heart rate variability
- FPE - Final prediction error
- HF - High frequency
- HR - Heart rate
- HRV - Heart rate variability
- LF - Low frequency
- LF/HF - The ratio of the power estimates for the LF and HF components
- LMS - Least mean square
- MAP - Monophasic action potential MI - Myocardial infraction
- MP - Matching pursuit
- NN sequence - Normal Sinus to Normal Sinus sequence
- PCA – Principal Component Analysis
- pNN50 - The percentage of difference between adjacent normal RR intervals greater than 50 ms computed over the entire 24 hour ECG recording
- QMF - Quadrature mirror filter
- QRS - Q-, R-, and S-waves in electrocardiogram
- QT - QT time interval
- RLS - Recursive least square

- RMSSD - Root mean square of successive differences
- RR - RR time interval
- RT - RT time interval
- RWED - Running windowed exponential distribution
- SA - Sinoatrial
- SD - Standard deviation
- SDA - Selective discrete Fourier transform algorithm
- SDANN - Standard Deviation of the Averages of NN Intervals in All 5-Minute Segments of a 24-Hour Recording SDNNIDX - The mean of the standard deviations of all normal RR intervals for all five minutes segments of a 24 hour ECG recording
- SVM – support vector machines
- SPWD - Smoothed pseudo Wigner distribution
- STFT - Short-time Fourier transform
- SV - Stroke volume
- SURE - Stein's unbiased risk estimate
- TFR - Time frequency representation
- TI NN - Triangular interpolation of the normal-to-normal histogram
- ULF - Ultra low frequency
- VLF - Very low frequency
- VRD - Ventricular repolarization duration
- WD - Wigner distribution
- WP - Wavelet packet
- WT - Wavelet transform

1. Introduction

1.1 Aims of investigation

In 1992, 42% of adult deaths in USA was caused by heart diseases as scientific researches point that as the mean average of population getting older heart diseases are growing. A timely diagnosis and prevention is very needful and also there is a tension to avoid costly and same times dangerous methods of examination and surgical operation.

Electrocardiogram is common practice for diagnosis of heart diseases and is based on measurement of electrical activity on the body surface caused by the function of heart.

Eithoven in 1903 developed further the theory of cardiac signals which was acquaintance from 1889, while he is also the person in charge for the import of significances that is used until today while it determined and the points from which the signals should be received. Finally it developed the basic theory round the ECG, central regard of which is the modelling of heart as a time-rating dipole.

The fundamental practice for recording the cardiac signals is the measurement of a voltage difference between two points in the body. Eithoven had assign three leads (I, II, III) derived from the arms and the left leg. Since then, 9 other leads developed in order the examiner to have a complete picture of the heart function.

The Einthoven three lead recordings are reported with Latin numbers I, II, III. These are defined as:

$$I = B_{LA} - B_{RA}$$
$$II = B_{LL} - B_{RA}$$
$$III = B_{LL} - B_{LA}$$

where RA = Right Arm, LA = Left Arm, LL = Left Leg. The three signal recordings are not independent of each other but are related with II = I + III.

In today it is scientifically accepted that the same diseases in two different patients have the same influence in the cardiosignal and differentiate its morphology

in the same way giving us the opportunity to recognize the disease. The unchangeable morphology of the two derivatives of the cardiosignal gives also the possibility to proceed in the study and creation of patterns that recognize the disease. So, patients that are examined have the same heart disorders in order to see which parameters of the cardiosignal remain stable, which change and if there is any relation between this change and the gravity of the disease. Another way to exam the heart functionality is by measuring the chaotic morphology of the cardiac signal.

The principal aim of the project is to develop new algorithms for analysis of the electro cardio signal waveform and also to create a portable and accurate ECG analyser in order to succeed a) timely diagnosis, b) avoid costly diagnosis, c) improvement of today methods, d) improve the pro- surgical planning –decrease the surgical risk and e) supply the research of the heart and heart diseases.

In order to success the original goal, initially a development of an ECG analyser containing new and powerful signal processors and also analog filters had to be made. A computer software developed in Matlab for analysing the cardiac signals, placing the input signals into digital filters and lead to scientific results about the methodology and the diagnosis of a disease followed and initiated the research.

1.2 Project Objectives

The principal objectives of the work are:
➢ Literature survey of previous and current developments in the field.
➢ Develop (design and construction) of an electro cardiographer with high resolution in very low bio-electrical signals. Portable and connectable with computers.
➢ Development of software in Matlab based on the theoretical analysis about these bio-signals. This program will provides the possibility of a very circumstantial analysis of cardiac signals either to time domain or to frequency domain.
➢ Creation of a database consisted of simulated cardio signals categorized in groups. A deep mathematical, physical and statistical analysis will be carried out in order to find any common points between signals of the same disease or

even a pattern than a disease follows and change the cardiac signal in the time domain, frequency domain, first and second derivative or chaos.

➢ Further development of the software in order to be able to compare new signals with signals of the database and through an analysis of derivatives, chaos and a comparison is capable for diagnosis.

➢ Compare real human samples with the theoretical model.

➢ Finalization of the portable device and statistical analysis of the capability.

1.3 Summary

In the following chapter of the research, a detailed analysis of the way a human heart works and sends biosignals throughout the body is explained. A more comprehensive analysis of the cardiovascular signals is quoted.

In chapter three, a physiological background of the heart is analyzed thoroughly with the analysis of signal variability to be expanded in every detail. Notable interest shows the induction of chaos theory in ECG in this chapter. Another very interesting part of this chapter is where common heart rhythms and arrhythmias are explained.

In chapter four the methods of investigation are discussed. This includes not only the ECG hardware created for this research, but also the software that was implemented with the application "MATLAB". The ways of acquiring an ECG from adults and kids are also mentioned.

The main function used in this research, that is Cubic Splines, and the necessary routine creation are thoroughly explained in chapter five. Here the main simulating device used for exporting various heart conditions in order to create a well established signal database is introduced. A way to correlate the factors of the various heart conditions collected and analyzed is explained and presented with real human samples compared with the theoretical model.

In the last chapter, conclusion and further development of the research are presented.

2. Literature survey

2.1 The heart and electrical signals

The human heart, one of the most studied organs in biology, is a hollow mass of mainly striated muscle fibers. It is situated slightly to the left of the middle of the thorax, underneath the breastbone (the sternum), at a position surrounded by the lungs (Figure 1). It is most essential to life, since its function is to pump blood through the blood vessels to the entire body by repeated, rhythmic contractions. It is the active center of the human cardiovascular system, circulating blood in the entire organism as a medium for transporting substances such as oxygen, nutrients, blood cells, enzymes, antibodies, as well as collecting the corresponding counterparts as wastes, toxins or external agents for disposal.
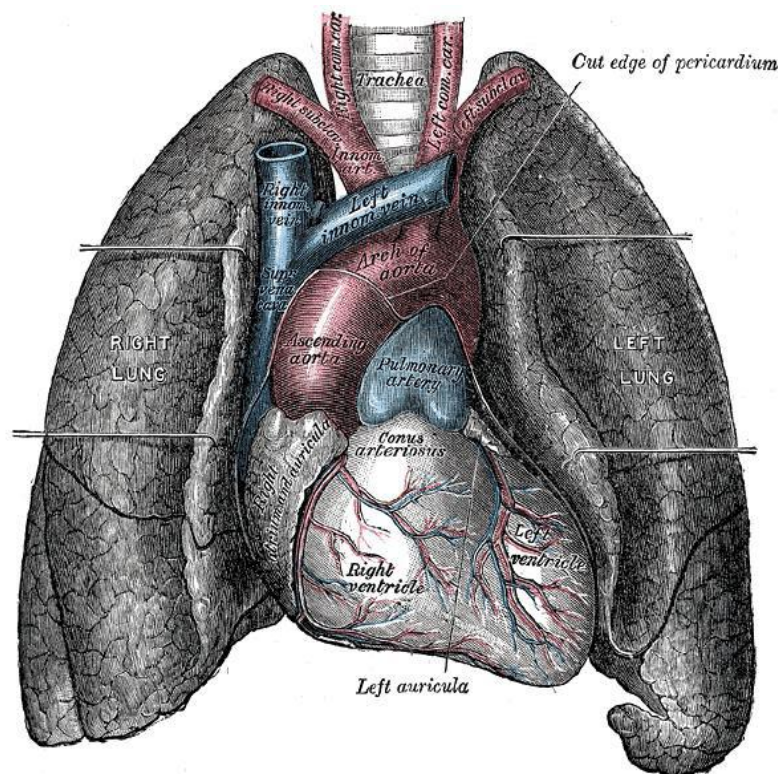
Figure 1. *Heart and lungs.[1]*

The heart consists of four chambers, namely the two upper atria and the two lower ventricles. The number of chambers followed the evolutionary pattern of the

vertebrates, which prevents a blend of arterial and venous blood in the closed circulatory system.

The high energy consumption of homeotherms, *i.e.* the avian and mammals, requested a higher efficiency of oxygen transport by clearly separating oxygenated and deoxygenated hemoglobin within the circuit. Indeed, the number of the chambers in the heart in terms of their specific functions as well as their structures and geometries are important in the expression of the pathology of this organ studied in this work. The atria serve as buffers for blood entering the heart from which it is transferred to the ventricles. The ventricles are the actual pumps that propel the blood into the circulatory system. The valves between the atria and ventricles maintain coordinated unidirectional blood flow from the atria to the ventricles. Thevenous blood returning from the peripheral vessels enters the right atrium, through which it passes to the right ventricle and is sent to the lungs through the pulmonary artery. The blood, rich with oxygen and free of carbon dioxide by diffusion at the pulmonary alveoli, is passed to the left atrium from which it enters the left ventricle. The latter forces the blood into the aorta from which it enters the entire circulatory system (figure 2).
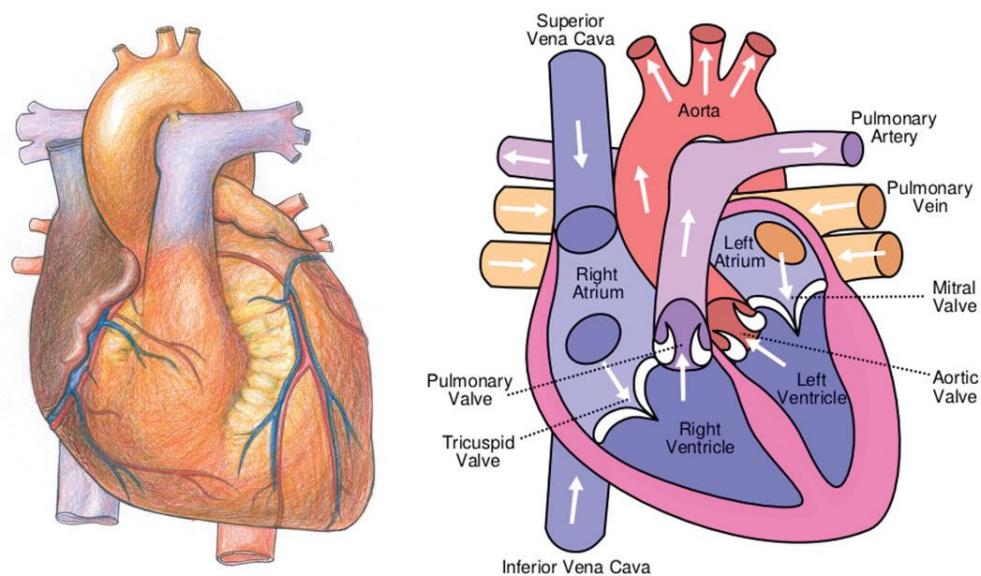
Figure 2. *Heart as the main pump of the cardiovascular system. Schematic diagram of blood flow in the human heart and nomenclature of principal anatomical features.[2]*

Every normal single beat of the heart involves a sequence of these well-organized events, which constitutes the cardiac cycle. In a cardiac cycle, the aforementioned sequence consists of three major stages, namely the atrial systole, the ventricular systole and the complete cardiac diastole. The atrial systole is the phase which comprises the contraction of the atria and the corresponding influx of blood into the ventricles. Once the blood has fully left the atria, the atrioventricular valves close, preventing backflow into the atria. This closing of the valves (semilunar and atrioventricular) is the origin of the familiar beating sounds of the heart. The ventricular systole consists of the ventricular contraction and the efflux of blood into the circulatory system. Once the blood is expelled from the ventricles, the pulmonary and aortic semilunar valves close. The final complete cardiac diastole involves the relaxation of the atria and ventricles in preparation for the refilling phase of circulating blood. The whole cycle of blood circulation within the system is governed almost completely by the fluid mechanics regulated by the muscular contraction of the heart.

2.1.1 Bioelectricity of the heart

The cardiac muscle, a spontaneously contracting, self-exciting tissue, develops the driving force governing the fluid mechanics of the circulatory system by converting biochemical energy to kinetic energy. The contraction of the muscle is triggered by an electric stimulation, that is, the onset of a bioelectric signal called the action potential (AP).
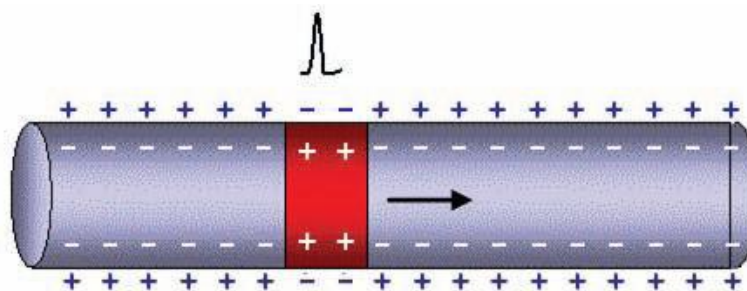
Figure 3. *Schematic of action potential propagation over a cell membrane.*

The action potential is the general term for an all-or-none active electric impulse traveling along the cell membrane (Figure 3).

In the neural system, it functions as a messenger between cells, while in muscles, it regulates the contraction of fibers. It is generated by exchanges of electrically charged ions across the cell membrane via ion channels, [3] creating a local potential bias above a triggering threshold between the two sides of the membrane. In its relaxed state, the inside of a cardiac myocyte is at a negative potential with respect to the outside, the resting potential. If the absolute value of this resting potential is reduced below a threshold level, a cascade of ion kinetics is induced, entailing chain reactions of potential dynamics propagation to the surrounding cell membrane (figure 4).

The resting potential of a cell membrane is generated by an electrochemical equilibrium of charges (ions) on each side of the membrane. The action potential reflects the local acute non-linear depolarization from this resting potential, followed by a repolarization phase of return to the resting potential.
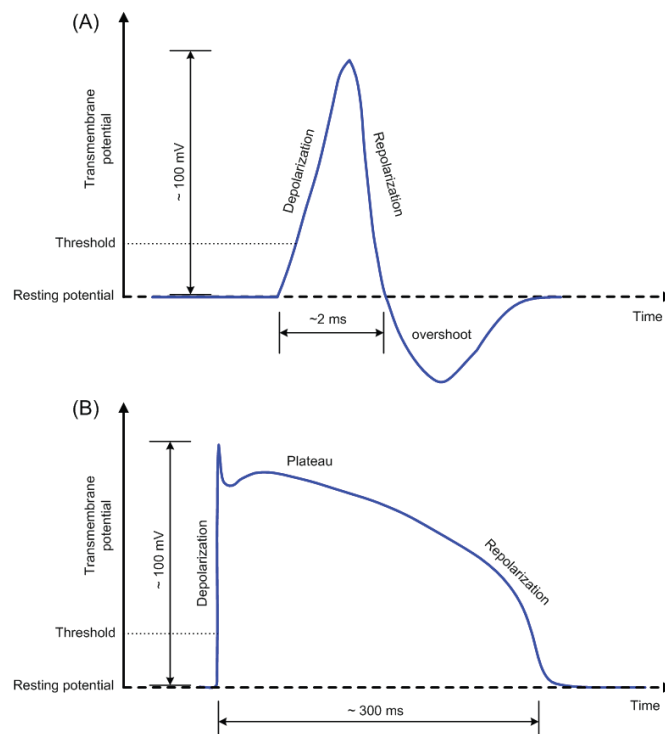
Figure 4. *Action potentials.* **(A)** *AP of neurocytes.* **(B)** *AP of cardiomyocytes [4]*

The dynamics of the inward and outward electric current is regulated by the opening and closing of the gates (ion channels) and is ruled by the electrochemical diffusion of the ions [5]. The transport of ions that regenerate the initial equilibrium is an active procedure carried out by the ion pumps. There is a brief time interval, called the refractory period, during which the membrane is not excitable between two successive action potentials.

In the case of cardiac muscle, the action potential is the signal that activates the contraction of the cardiomyocytes by propagating from cell to cell over the whole tissue. There are, nonetheless, preferential pathways along fast conducting bundles that effect the organization of the contraction of the chambers.
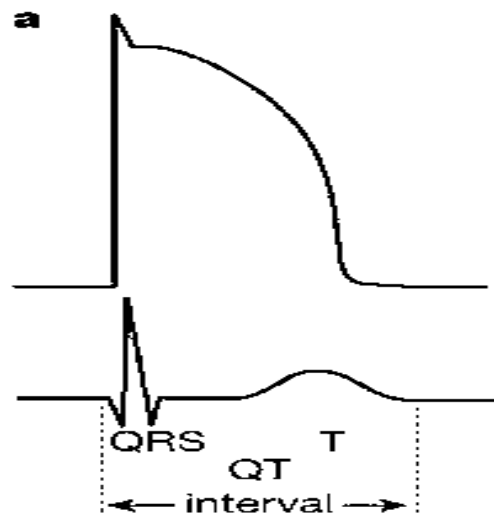
Figure 5. *Temporal relationships between the ventricular action potential (top) and the ECG (bottom). The QRS complex, T wave and QT interval are indicated. Both signals are functions of the same timescale on the x axis; the y axis plots voltage, with a gain that is roughly 100-fold higher for the ECG than for the action potential (that is, the absolute signal amplitude is about 100-fold smaller for the ECG).[6]*

The rhythmic sequence of the cardiac cycle is initiated by the sinoatrial (SA) node and regulated by the atrioventricular (AV) node. The sinoatrial node, known as the cardiac pacemaker, is located in the upper front wall of the right atrium and is responsible for the initiation of action potential propagation that contracts the atria. Once the propagation reaches the atrioventricular node, situated in the lower right atrium, it is conducted through the bundle of His, the left and right bundle branches, and to an extensive network of Purkinje fibers which trigger the contraction of the

ventricles. The AV node regulates the timing of transmission of the excitation to the ventricles, creating a delay between the contractions of the two groups of chambers which enhances the filling of the ventricles prior to their contraction.

The physiological activity of the myocardium involves associated electromagnetic phenomena that are expressed as electric potential dynamics inside the entire body. As early as in the 19th century it became clear that the heart generated electricity. The first to systematically approach the heart from an electrical point of view was Augustus Waller, working in St Mary's Hospital in Paddington, London. [7] He used a mercury capillary electrometer to measure the electromotive changes on the body surface arising from the beat of the mammalian heart, and of the human heart in particular (figure 6).
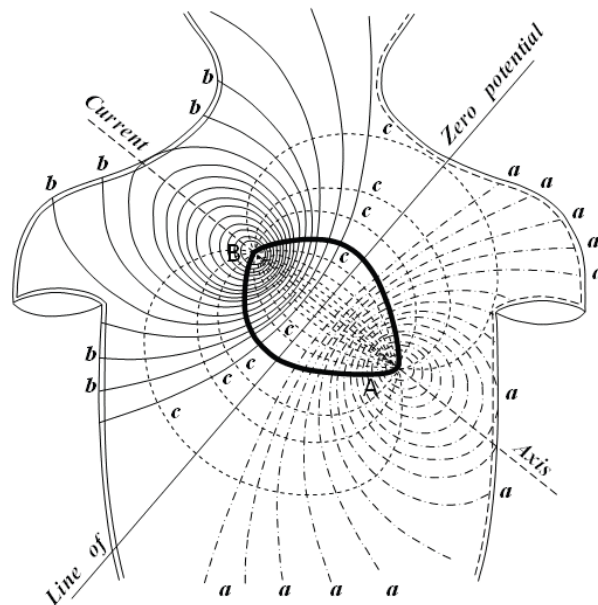
Figure 6 *Potential inequalities over the body surface,[7]*

2.1.2 Body surface potentials and Electrocardiogram

The electromagnetism linked to the electrophysiology of the heart is a direct expression of the cardiac mechanical function. Hence, the observation of the electric activity as body surface potentials (BSP) is an efficient and non-invasive manner of estimating the functional state of the heart. The time course of the resulting potential differences between any two points on the body surface is called Electrocardiogram (ECG).
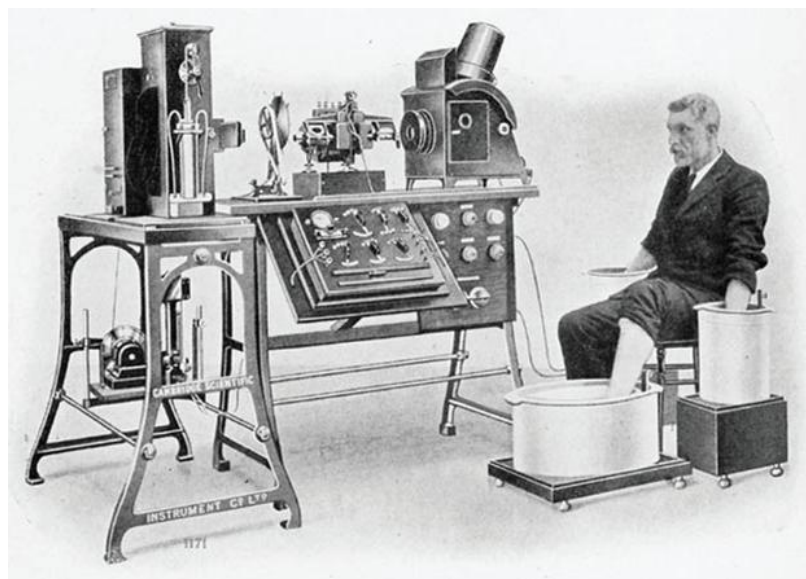
Figure 7. *Picture of an early ECG recording performed by Willem Einthoven in 1903.[8]*

Following Waller, a major breakthrough in cardiac electrophysiology was reached when Willem Einthoven, working in Leiden, the Netherlands, used a string galvanometer in 1901 to record ECGs. By measuring the potential differences between the two hands and the left foot (figure 7), Einthoven assigned the letters P, Q, R, S and T to the various deflections, and described the electrocardiographic features of a number of cardiovascular disorders.[9] He received the *Nobel Prize in Physiology or Medicine* for his discovery in 1924.

Nowadays, the electrodes used in clinical practice to record the *standard 12-lead ECG* are placed on the two hands (VR and VL), the left foot (VF), and at six

precordial positions (V1 to V6) as presented in figure 7. These *nine* electrodes located over the surface of the human body capture the electric activity of the heart from different angles reconstructing the spatial dynamics of the heart's electric activity. A display of the three limb leads in the form of a triangle on the frontal plane is referred to as Einthoven's triangle. The mean value of the instantaneous potentials is used as the reference of the ECG signals, known as the Wilson Central Terminal (WCT) reference (figure 8). The ECG is the prime tool in cardiology, and has its main function in screening and diagnosis of cardiovascular diseases in clinical practice. Because of the strong link (direct and indirect) between cardiac function and electric potential dynamics observable on the body surface, many cardiac diseases can be monitored through the expressed potential differences.
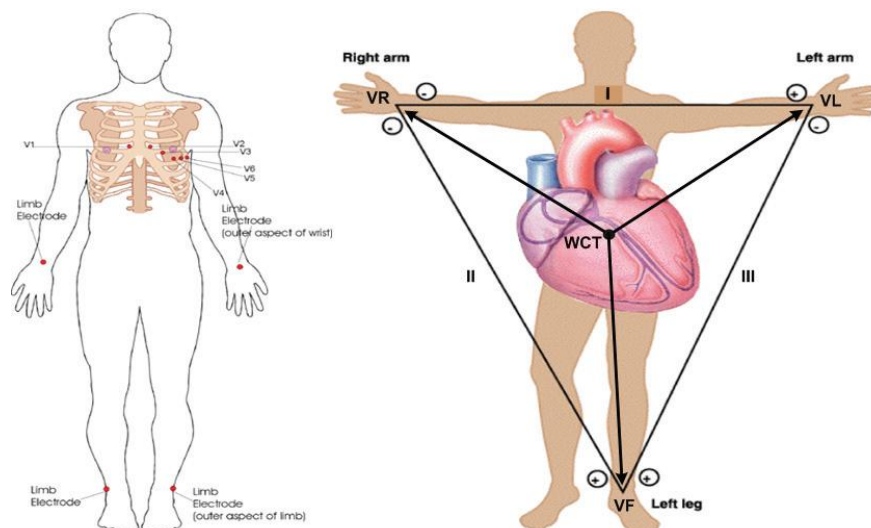
Figure 8. *Electrode positions of a standard 12-lead ECG and the derived leads. The three limb electrodes form an equilateral triangle in the frontal plane called the Einthoven triangle (right panel). The potential reference for all other leads is Wilson's Central Terminal (WCT) defined as the mean value of the potentials at electrodes VR, VL and VF, corresponding to the position of the center of gravity of Einthoven's triangle.[4]*

According to the well-established definition of waveforms observable on each lead, the ECG has a wide use for indicating pathologies such as cardiac arrhythmias, ischemia, or conduction abnormalities.
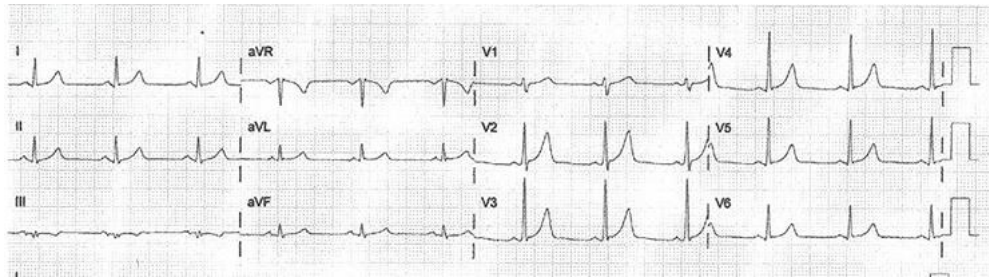
Figure 9. *An example of standard ECG recording during normal sinus rhythm. The twelve derivations are potential differences specifically defined between electrodes. I, II and III are potential differences between the limb electrodes as shown in figure 8. aVR, aVL and aVF are the "augmented" VR, VL and VF, respectively, signifying the 1.5-fold voltage between the corresponding electrode and the WCT reference. This is a historical custom in which, for instance, aVR was measured as VR $-\frac{1}{2}(VL + VF)$, which simply resulted as $aVR = \frac{3}{2}VR$. V1 to V6 are the potential differences between the corresponding precordial electrodes and the WCT reference.[4]*

2.1.3. Electrophysiology

Electrophysiology is the study of the electrical properties of biological cells and tissues. It involves measurements of voltage change or electric current on a wide variety of scales from single ion channel proteins to whole organs like the heart. In neuroscience, it includes measurements of the electrical activity of neurons, and particularly action potential activity. Classical electrophysiology techniques involve placing electrodes into various preparations of biological tissue. The principal types of electrodes are simple solid conductors, such as discs and needles (singles or arrays), tracings on printed circuit boards, and hollow tubes filled with an electrolyte, such as glass pipettes. The principal preparations include first of all living organisms, excised tissue (acute or cultured), dissociated cells from excised tissue (acute or cultured), artificially grown cells or tissues, or hybrids of the above. [10]

Many particular electrophysiological readings have specific names:

- For the heart it is called Electrocardiography

- For the brain Electroencephalography
- From the cerebral cortex Electrocorticography
- For the muscles Electromyography
- For the eyes Electrooculography
- For the retina Electroretinography
- For the olfactory receptors in arthropods Electroantennography
- For the auditory system Audiology

2.1.3.1. Electrophysiology of the Heart

Like all living cells at rest, the cardiac muscle cell or myocyte is polarized, so that the potential inside the cell, which called intracellular space, is negative with respect to the outside, which called interstitial space.

The transmembrane potential is defined as the potential difference across the surface membrane of the cell. It is controlled primarily by three factors. The first is the concentration of ions on the inside and outside of the cell, particularlyNa^+, K^+, Cl^-, and Ca^{2+}. The second factor is the permeability of the cell membrane to those ions through specific ion channels. The last factor is the activity of electrogenic pumps (e.g., Na^+/K^+-ATPase and Ca2+ transport pumps) that maintain the ion concentrations across the cell membrane. Because K+ concentration is high inside the cell and low outside, a chemical gradient for K+ to diffuse out of the cell is found. In opposite, Na^+ and Ca^{2+} chemical gradients for an inward diffusion are found. The natural tendency of sodium and potassium ions is to diffuse across their chemical gradients to attempt to reach their respective equilibrium potentials, with sodium diffusing into the cell and potassium diffusing out.

However, the resting cell membrane is approximately 100 times more permeable to potassium than to sodium, so that more potassium diffuses out of the cell than sodium diffuses in. This permeability to potassium is due to potassium channels that are open at the resting voltage. As a result, the dominant outward leak of potassium ions produces a polarizing current that establishes the cell's resting potential of roughly -70 mV [11].

2.1.3.2. The Action Potential of a Single Cell of Working Myocardium

By applying an external stimulus, cells of excitable tissues can be polarized. An action potential can be produced by a sequence of influx and out flux of multiple captions and anions through the cell membrane. Once a cardiac cell is getting excited, an electrical stimulation to the cells that lie adjacent to it and furthermore to all the cells of the heart will be propagated [12]. The action potential has five phases, numbered from zero to four. A typical action potential for a cardiac myocyte in the left ventricle is shown in figure 10.
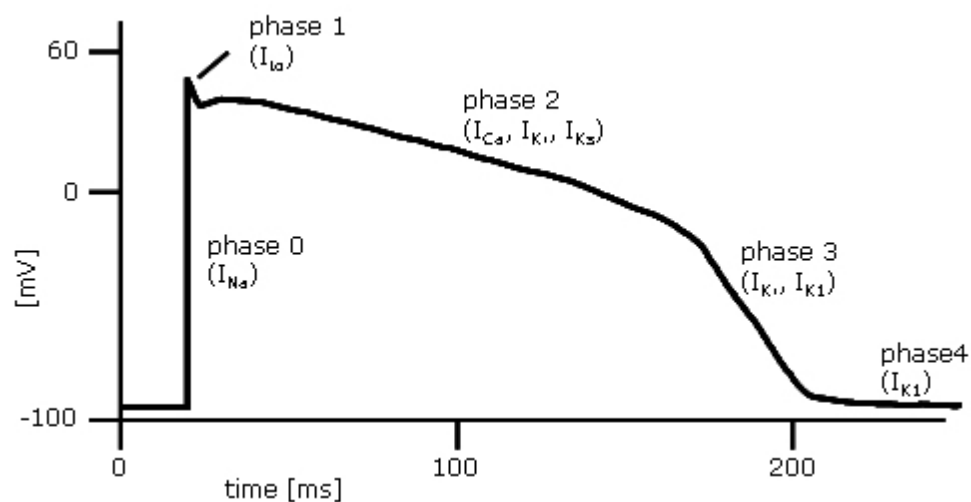
Figure 10. *The Action Potential of a single cell of working Myocardium.[13]*

Phase 4 represents the resting transmembrane potential, in other words, this voltage can be measured if the cell is not stimulated. This phase of the action potential is associated with the diastole of heart chambers. Phase 0 is known as the rapid depolarization phase. The maximum rate of depolarization of the cell, dV_{max}/dt, is determined by the slop of curve corresponding to this phase. This phase is associated with opening of the fast Na^+ channels, rapidly increasing the membrane conductance to Na^+ (gNa) and a rapid influx of Na^+ ionic current (INa) into the cell. In fact, the

fast sodium channel has two gates, the h gate and m gate, whose interaction allows Na^+ to enter the cell through this channel. At rest, the m gate is closed and h gate is open, but when the transmembrane potential approaches a threshold (about -60 mV), the m gate opens quickly while the h gate closes slowly. After a very short time, both gates will be open changing the sign of the transmembrane voltage to positive value (round +20 mV), to the so-called overshoot. The closure of the fast Na^+ channel after a short time and the slower outflow of potassium through the potassium channels are tending to restore the initial state of the membrane generating the phase 1. The balance between inward movement of Ca^{2+} (ICa) through Ltype calcium channels and outward movement of K+ through potassium channels sustains the phase 2 (or so-called plateau) of the action potential. Cardiac myocytes have different characteristics of the plateau phase. During this phase the fast sodium channels are not active keeping the cell immune to any external stimulus. Therefore, it is called refractory period. In the phase 3 of the action potential, K^+ will be accumulated in the xtracellular space leaving the intracellular space. This action is responsible for the repolarization of the cell. The cell can be depolarized again in this period by very large stimuli, therefore it is called refractory relative period. Finally, K^+ channels close when the transmembrane potential is set back to the resting phase and the initial concentration of ions is rapidly restored by means of Na-K pumps and Na-Ca exchangers. The myocytes throughout the heart have different time course of action potentials (figure 11).
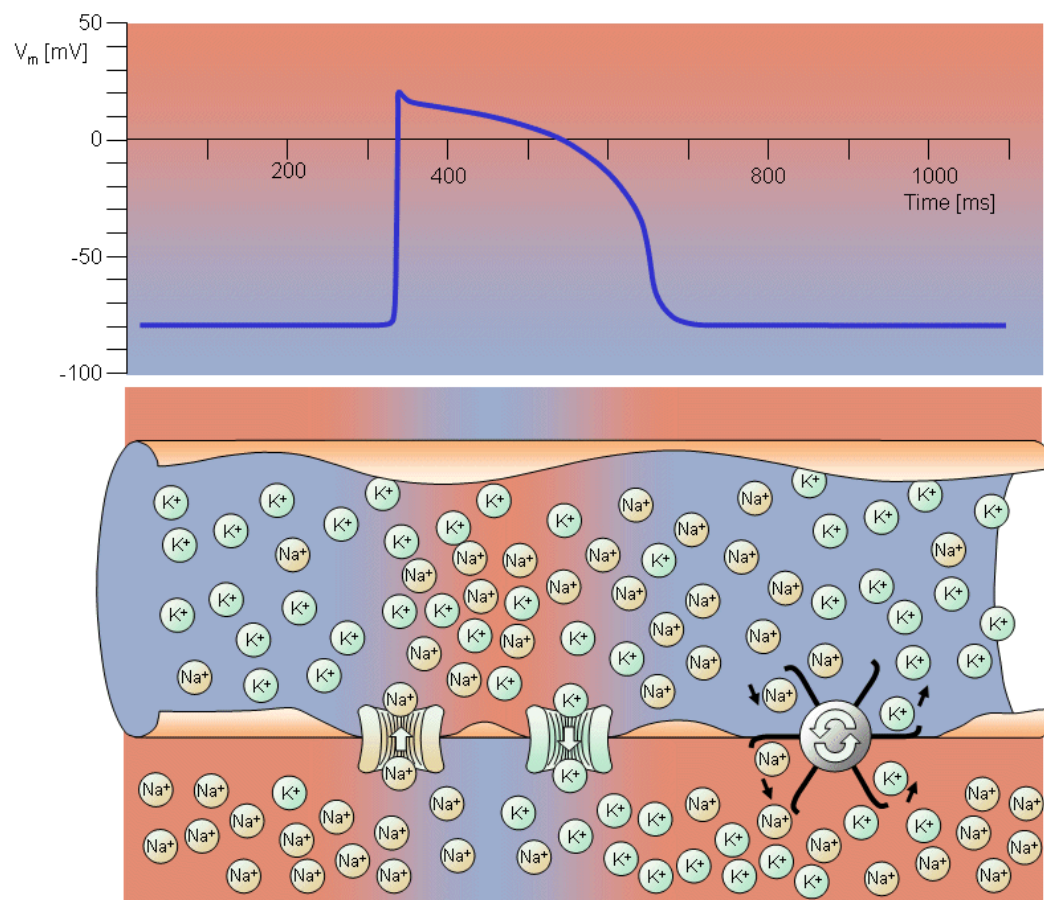
Figure 11. *The resting voltage and action potential electrophysiology of a single cell of working Myocardium[14].*

2.1.3.3. Excitation Propagation and Cardiac Contractions

Cardiomyocytes consist of three systems: a sarcolemmal excitation system that participates in spread of action potential (AP) and functions as a switch initiating intracellular events giving rise to contraction, an intracellular excitation-contraction coupling (ECC) that converts the electric excitation signal to a chemical signal and activates the contractile system, a molecular motor based on formation of chemical bridges between actin and myosin.

1. **The Excitation System**: This system is responsible to maintain the resting potential, create an action potential and facilitate spreading the AP. The cardiac cycle

is initiated from the excitation system of SA node. The rapid change in the voltage during an AP causes the activation in the excitation system. Consequently, the neighboring cells will be depolarized. As a result, an electrical impulse, also called the cardiac electrical wavefront, propagates through the conduction system of the heart and spreads from cell to cell throughout the myocardium in the way that the atrial and ventricular contraction (depolarization) and relaxation (repolarization) will happen with the correct timing in the healthy heart [15].
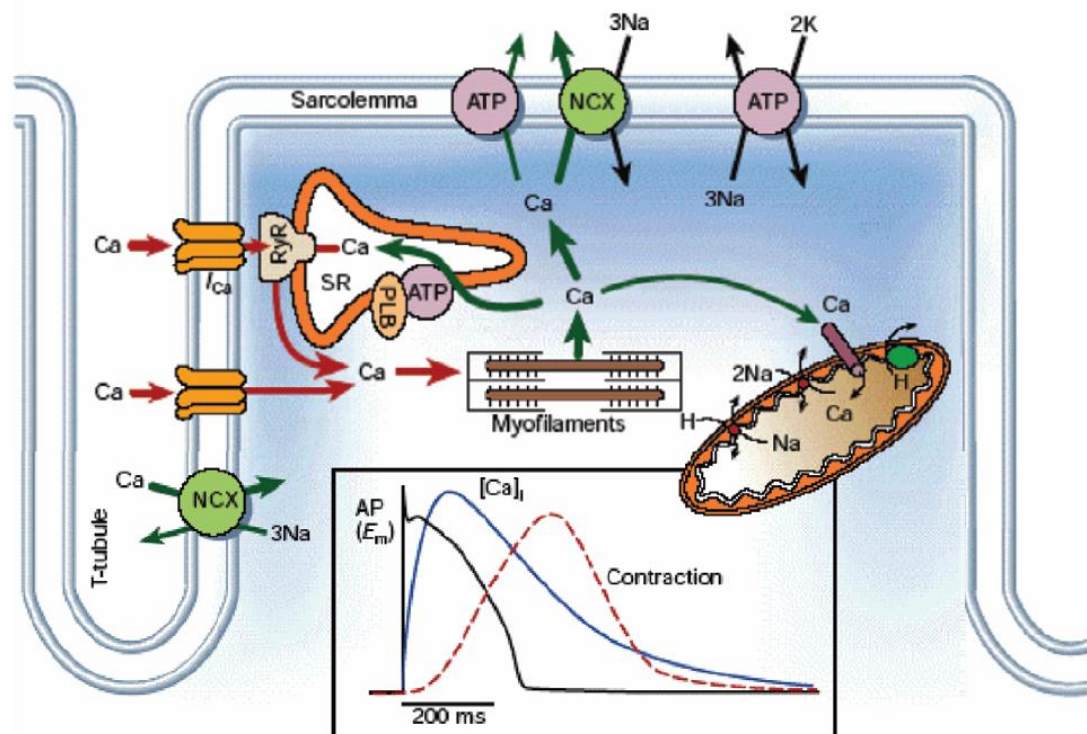
Figure 12. *Schematic diagram of the major cellular components involved in contraction of the myocyte.[16]*

2. **The Excitation-Contraction Coupling System:** Excitation-contraction coupling (ECC) is established by the sarcotubular system, an arrangement of specialized sarcoleman and intracellular membranes that controls and amplifies the ability of AP to switch the contractile system on and off by creating electrochemical signals between the sarcolernma and intracellular organelles. When a myocyte is depolarized by an AP. calcium ions enter the cell during phase 2 of the action

potential through L-type calcium channels triggering a subsequent release of calcium that is stored in the sarcoplasmic reticulum (SR) increasing the intracellular calcium concentration from about 10^{-7} to 10^{-5} M. The released calcium binds to troponin-C (TN-C) that is part of the regulatory complex attached to the thin filaments. When calcium binds to the TN-C, this induces a conformational change in the regulatory complex such that troponin-I (TN-I) exposes a site on the actin molecule that is able to bind to the myosin ATPase located on the myosin head. This binding results in ATP hydrolysis that supplies energy fora conformational change to occur in the actin-myosin complex [17].

3. The Contractile System: The building block of the contractile system is the sarcomere. The result of the changes made by the released calcium in ECC is a movement between the myosin heads and the actin. The actin and myosin filaments slide past each other thereby shortening the sarcomere length. This ratcheting cycle occurs as long as the cytosolic calcium remains elevated. At the end of phase 2 of APcycle ends when new ATP binds to the myosin head, displacing the ADP and the initial sarcomere length is restored.

2.1.3.4. The Generation of an Electrocardiogram and the Dominant Cardiac Vector

The Electrocardiogram (ECG) represents a temporal and spatial summation of the extracellular fields of the action potentials generated by millions of cardiac cell. It describes the different electrical phases of the cardiac cycle. ECG provides a measure of the electrical currents generated in the extracellular fluid by the changes in the APs. At any given instant, only a group of cells out of millions of individual cells in the myocardium depolarizes simultaneously. They can be represented as an equivalent current dipole source to which a vector is associated, describing the dipole's time-varying position, orientation, and magnitude [15]. The dominant vector describing the main direction of the electrical wavefront can be defined as a summation of the vectors of all current dipoles in the heart at a certain time instant.

2.2. Cardiovascular variability signals

The sinus rhythm fluctuates around the mean heart rate, which is due to continuous alteration in the autonomic neural regulation, i.e. sympathetic-parasympathetic balance. Periodic fluctuations found in heart rate originate from regulation related to respiration, blood pressure (baroreflex) and thermoregulation.

Parasympathetic (vagal) regulation to the heart is inhibited simultaneously with inspiration, and the breathing frequency coincides with fluctuations observed in heart rate [18]. Furthermore, thoracic stretch receptors and peripheral hemodynamic reflexes also result in respiratory arrhythmia [19]. Respiratory arrhythmias are consequently due to parasympathetic regulation and can be excluded by atropine or vagotomy [19]. The maximal amplitude of respiratory related heart rate fluctuation is found at breathing rate of 6 cycles per minute, because the fluctuation increases as respiration rate achieves the frequency of the intrinsic baroreflex-related heart rate fluctuations [20].

The fluctuations due to blood pressure regulating mechanisms originate from self-oscillation in the vasomotor part of the baroreflex loop [20]. These fluctuations coincide with synchronous oscillations in blood pressure called Meyer waves [21]. Increase of sympathetic nerve impulses strengthen and sympathetic or parasymphatetic blockade weaken these fluctuations in heart rate [22, 23].

Changes in peripheral resistance produce low frequency oscillations in heart rate and, for example, in systolic blood pressure. Thermal stimulation given on the skin can be used to stimulate the oscillations, which are originally due to thermoregulatory adjustment of peripheral blood flow [20]. These fluctuations are controlled by the sympathetic part of the autonomic nervous system.

The overall autonomic function is controlled by a central command from the brain. However, the autonomic nervous system operates as a feedback system, and heart rate is thus regulated by many reflexes which may increase or decrease the sympathetic or parasympathetic activity or both of them [24]. Reflexes can act simultaneously and their interactions may be complex. The arterial baroreceptor reflex originates from receptors located in the arteries such as carotid sinuses and aortic arch. The increase in blood pressure excites baroreceptors producing an

augmented efferent vagal and reduced sympathetic activity. Peripheral arterial chemoreceptors located in the carotid and aortic bodies produce, most often, an increase in the rate and depth of respiration. Because this reflex influence on heart rate through respiration, the effects may be covered by other respiratory responses. The coronary chemoreflex (Bezold-Jarisch reflex) can cause bradycardia and is significant in pathological states such as myocardial ischemia and infarction. Atrial receptors stretched by the increase in atrial volume and some of them by atrial contraction, the response being linked directly to atrial pressure. These volume receptors cause an increase in heart rate and operate through the sympathetic nerves producing their response very slowly. There exist also other cardiovascular reflexes coming from receptors located e.g. in pulmonary arteries, lungs and muscles.

The physiological importance of heart rate can be demonstrated by an axiomatic relation in which cardiac output (CO) can be defined by a product between heart rate and stroke volume (SV) as $CO = HR \cdot SV$. Because heart rate and stroke volume are not independent of each other, the definition of cardiac output is not always so straightforward in terms of physiological adjustment.

The rate of depolarization of the cardiac pacemaker defines heart rate. The sinoatrial (SA) node, the atrioventricular (AV) node and the Purkinje tissue can be regarded as potential pacemaker tissues in a heart. As the fastest depolarization rate is found in the sinoatrial node and the depolarization impulse spreads through the conduction system to other pacemakers before they spontaneously depolarize, the sinoatrial node usually defines the heart rate. However, failing to produce a normal pacemaker impulse, other pacemaker tissues can act as a cardiac pacemaker.

Table 1. *Model of a normal ECG*

Parameter	Reference Value
Heart Rate	60-100 beats per minute (BPM)
P wave	Duration <0.12 s / Amplitude <0.25 mV
P-R interval	Duration <0.12-0.20 s
P-R segment	Duration 0.1 s
QRS complex	Duration 0.04-0.12 s / Amplitude 0.5-1 mV
Q-T interval	Duration 0.39-0.42 s
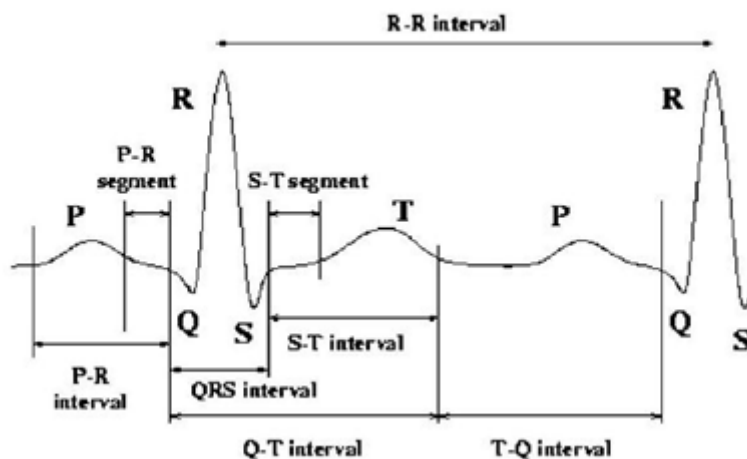
Figure 13. *ECG Analysis*

Autonomic neural regulation of the heart is determined by its sympathetic and parasympathetic parts. The parasympathetic nerves are connected to the sinoatrial node, the AV conducting pathways and the atrial and ventricular muscles as well as coronary vessels. Sympathetic nerve fibers innervate the SA node, the AV conducting pathways, coronary vessels and the atrial and ventricular myocardium [25]. Both divisions of the autonomic nervous system always have some activity which continuously regulates the function of the heart. Heart rate response therefore presents a balance between sympathetic and parasympathetic (vagal) regulation which can be considered also as an antagonist function.

Heart rate has a major effect on ventricular repolarization duration (VRD), but the autonomic nervous system also regulates directly the repolarization of the ventricles. In addition, electrolytic factors, age and gender have an effect on it. It has been shown that when the autonomic nervous system regulates VRD there are similar periodic fluctuations as seen in heart rate [26].

2.2.1. Changes of signal variability connected to specific diseases

A decrease in vagal neural activity into the heart may result in diminished HRV after myocardial infarct (MI) leading to the prevalence of symphatetic neural

regulation and to electrical instability [27]. Reduced heart rate variability is also associated with an increased risk for ventricular fibrillation and sudden cardiac death [28, 29]. Changes in long term RR interval dynamics with beat-to-beat RR interval alternans is concluded to precede the spontaneuous onset of sustained ventricular tachyarrhythmias [30]. Results obtained using spectral analysis of HRV suggests a change of sympatho-vagal balance toward symphatetic dominance and a diminished vagal tone in patients surviving an acute myocardial infarction [27, 31]. Cardiac diseases such as congestive heart failure, coronary artery disease and essential hypertension are also associated with a reduced vagal and an enhanced sympathetic tone, which change heart rate variability dynamics [20, 32]. Because HRV analysis can be regarded as a noninvasive, reproducible and an easy to use method reflecting the degree of autonomic control of the heart [33], it has been widely used to diagnose the autonomic dysfunction due to diabetic neuropathy (34, 35, 36]. It has been generally observed, that overall HRV is reduced and sympatho-vagal balance may be altered during tilt maneuver or standing in diabetic patients [32, 25].

Although HRV is used in a wide range of clinical applications, diminished HRV has only been generally accepted as a predictor of risk after acute myocardial infarction and as an early warning of diabetic neuropathy. Diminished HRV can predict mortality and arrhythmic events independently of other risk factors after acute myocardial infarction, and long-term HRV analysis have proven to be a more definite predictor compared to a short-term analysis [27]. Heart rate variability analysis should also be joined with other risk factors so as to improve the predictive use. Any heart disease (left ventricular hyperthrophy, heart failure, etc.) can modify repolarization duration [37]. Anomalies in repolarization duration are signs of electrical instability in the heart and can lead to malignant arrhythmias such as ventricular fibrillation and Torsades de Pointes. Analysis of ventricular repolarization duration dynamics provides essential information on a propensity for ventricular arrhythmias, because some life-threatening arrhythmias arise in myocardial tissue. Altered dynamics of the VRD, and the events of the alternating T wave amplitude particularly in patients with the long QT syndrome as well as with structural heart disease at fast heart rates, suggest that the analysis of the ventricular repolarization dynamics may provide an important clinical tool [38].

2.2.2. Other events modifying signal variability

Several pharmaceutical interventions can be used to modify heart rate dynamics as shown by human [39] and animal [3] studies. Atropine administration has been used to prove the connection between vagal neural activity and high frequency (respiratory related) fluctuation in RR interval time series [23]. Scopolamine significantly augments heart rate variability [40] which suggests an increasing coincident vagal activity into the heart. The effect of β-adrenergic receptor blockades has been studied after myocardial infarction [41, 42]. There are also studies on the effect of antiarrhythmic drugs such as flecainide and propafenone, as well as encainide and moricizine on the heart rate dynamics [31, 43, 5]. A study of the effect of β-adrenergic blocker (nadolol) on ventricular repolarization duration and its dynamics was made. The finding was that the length of repolarization duration was shorter, the signal variance was greater and the spectral pattern was shifted to higher frequencies due to this medication. A change of the dynamic relationship between ventricular repolarization duration and heart rate has been observed as a consequence of nadolol administration with normal patients [26, 44].

Heart rate variability has been employed to investigate the short and long term autonomic responses to physical and mental exercise. It has been observed that the increase in respiratory related fluctuation, the total HRV reduction and the recorded signal become more nonstationary as the intensity of the dynamic physical exercise increases [45]. Heavy physical exercise has been shown to augment low-frequency (LF) fluctuations in heart rate, and the recovery of the spectral pattern may last even 48 hours after finishing exercise [46]. The sympatho-vagal balance seems to change towards sympathetic dominance e.g. in hypertensive patients. Long term physical exercise has positive effects on hemodynamics and neural control mechanisms, for example, by lowering the arterial pressure in hypertensive patients [47] and increasing baroreflex gain in patients with ischemic heart disease [48] An overall observation, also related to dynamic mental stress, is an increase of the sympathetically- and a decrease of vagally-mediated fluctuations in heart rate [7].

2.2.3. Various time series

RR interval time series

The basic procedure used for determining the heart rate and its fluctuations is described below. An electrocardiogram (ECG) is measured, using appropriate data acquisition equipment. The time elapsing between consecutive heart beats is defined as that between two P waves, when a P wave describes the phase of atrial depolarization. In practice, it is the QRS complex that is used to obtain the time period between heart beats. This complex is detected in the R wave, because it has a very clear amplitude and better frequency resolution than the P wave, and a much better signal-to-noise ratio. The time interval between the P and R waves can be assumed and has been shown to be constant [21]. Defining the times of occurrence of two consecutive R waves as *s(t)* and *s(t+1)*, *t = 1,..., N*, the expression $x(t) = s(t + 1) - s(t)$ is obtained for a time period in milliseconds. This *x(t)* is called the RR interval time series or else the times to which it refers are simply called RR intervals. A heart rate time series [min−1] can be obtained by *y(t) = 1000 · (60/x(t))* and the mean heart rate is simply $HR = N^{-1} \sum_{t=1}^{N} y(t)$. These formulae indicate a nonlinear relationship between the values in a given time series, which should be taken into account when comparing the results obtained by time and frequency domain approaches [49]. At the moment, RR intervals seem to be the more frequently used time series in heart rate variability (HRV) analysis. For a discussion of the choice between different time series (tachograms), [50]

VRD time series

QT time interval in electrocardiographic signals has been used to perform both static and dynamic analyses of the duration of the ventricular repolarization. There exist difficulties in the detection of the onset of Q wave and the offset of T wave due to poor signal-to-noise ratio and varying ECG morphology. For these reasons other

estimates, such as RTmax interval, has been widely used. Moreover, this provided a motivation to investigate and compare the noise sensitivity of different

QT interval estimates. Because Q-S time interval is a result of the depolarization period of the ventricles, it is actually more correct to measure the time interval between the R and T waves as one is interested in the changes occurring within the ventricular repolarization period. R wave has been used to estimate the start of the repolarization period because searching for the offset of S wave can be difficult. The maximum (apex) of T wave has been often regarded as a more reliable estimate for the end of the repolarization period than the T wave offset. The total repolarization duration, i.e. time interval between the offsets of S and T waves, can further be analyzed with respect to early and late repolarization duration as well as repolarization area [51]. In this work the objective will be on the measurement of the repolarization duration in the ambulatory ECG.

The 24-hour ambulatory ECG has certain problems and drawbacks because the signal is corrupted by noise from various sources and also several conditions may alter the ECG morphology. The ambulatory ECG is usually acquired with a sampling frequency of 128 Hz giving a time resolution of 7.81 ms for each sample, which is too low for QT interval variability measurement. It has been suggested that the QT interval should be determined at least with resolution of 1 ms, which would require 1 kHz sampling frequency for ECG signal. In an ambulatory measurement setting, with data acquisition times lasting up to 24 hours, the sampling frequency cannot be that high, because then the amount of the stored data rises rapidly. In present ambulatory ECG analysis systems the possibility of exporting a beat-to-beat QT time series extracted with high time resolution is also lacking. These problems have been solved by exporting raw ECG data and, by oversampling ECG signal [52] or by interpolating waveforms [53] a better time resolution for the time interval measurement results.

APD time series

The local ventricular repolarization duration can be measured by placing a contact electrode in a ventricular muscle. Rate-dependent dynamics of VRD obtained from the right ventricular apex provides an example. This approach can solve the above mentioned problems related to the ambulatory QT measurement. However, measuring monophasic action potentials (MAP) is an invasive procedure. The

duration of repolarization phase, which is termed as action potential duration (APD), is estimated as a time interval between the onset and offset of the action potential. The offset is defined as the maximal positive derivative of the upstroke phase of the action potential waveform. The offset can be defined at time points where the waveform has come down 15, 30, 50 and 90 % from the maximal amplitude of the MAP. Most often used definitions are 50 and 90 % points. The APD time series are extracted from the consecutive waveforms and the beat-to-beat analysis is performed.

2.2.4. ECG waveform detection

The RR and QT interval measurement [54] was based on an implementation of an algorithm described previously [55] and the detection scheme will be briefly reviewed here. The basic concept of the algorithm is to look for the zero crossing points, the crossings of certain experimentally-determined threshold values, as well as the local maximum or minimum values of the differentiated ECG signal $d(t)$ and its low-pass filtered version $f(t)$.

The differentiator and the low-pass filter were modified according to the sampling rate in order to obtain an optimal frequency response. The sampling rate of the analyzed ECG was one parameter of the waveform detection procedure and in this way, the preprocessing filters and the algorithm itself can adapt to the different sampling rates.

The flowchart of the implemented waveform detection procedure is shown in Tikkanen's work [54] The first step is to calculate the signals $d(t)$ and $f(t)$, which is done for the whole period of the ECG selected for analysis. The waveform detection procedure continues by determining the initial value of the threshold value H_n used to search the maximum absolute value of the QRS in the signal $f(t)$. The threshold value $Hn+1$ is continuously updated during the waveform detection using the equation [55].

$$H_{N+1} = 0.8 * H_n + (0.16 + |f(PK_n)|) , \qquad (2.1)$$

Where $|f(PK_n)|$ is the absolute value of the signal $f(t)$ at the detected fiducial R wave position of the beat n.

The initialization of the average of RR intervals RR_{av} and the first RR interval value are then obtained. The RR_{av} value is later used to check the calculated value of a new RR interval and thus provides a basis for identifying the QRS complex.

The initial position of a QRS complex is detected using an adaptive threshold method determined by the RR interval average value [54]. After that, the algorithm continues to search the position of the R wave. In the present approach, the fiducial point of the R wave was detected using three methods: at the maximum amplitude upwards or downwards from the baseline, or at the zero crossing point of the signal *f(t)* during the QRS complex. The last technique was implemented in the original algorithm by Laguna *et al.* (1990). It was found that, in some cases, a more accurate definition can be obtained, if the fiducial point of the R wave is defined at the maximal upward amplitude of QRS. With this algorithm, an accurate determination of the R wave is an absolutely necessary condition for a reliable Q wave detection. After detecting the R wave position and updating the threshold H_n and RR_{av} , the onset of Q wave is searched keeping the R wave position as a reference point. Here it should be mentioned, that examining the pattern of the Q wave is made by analyzing the differentiated signal *d(t)* and not the signal *f(t)*, because the signal *d(t)* includes the high frequency components of the Q wave. Next the T wave maximum and T wave end are detected from the signal *f(t)*. The following definition for the limits of a search window calculated from the R wave position was used:

$$(bwind; \ ewind) \ = \ (a * RR_{av}; \ b * RR_{av}) \qquad (2.2)$$

where *a* and *b* are parameter values in the procedure. This definition is a slightly different one from the given by Laguna et al. As the threshold for T wave end was used the value *Hs = f(Ti)=2, Ti* denoting the position of the maximal downward or upward slope after the T wave maximum.

Finally, a value of QT interval is calculated using the relation $QT(n) = T_{end}(n) - QT_{onset(n)}(n)$, where $T_{end}(n)$ and $QT_{onset(n)}(n)$ are the positions of T wave end and the onset of the QT time interval during the beat *n*. The analysis of the next cardiac beat is started 150 ms after the last T wave end is defined.

The effects of the four alternative definitions of the QT interval onset on the analysis of QT interval dynamics were compared: true QRS onset, R wave maximum,

ascending or descending maximal slopes of the R wave. One reason for this was quite practical: in some circumstances dealing with ambulatory ECG, the determination of the QRS onset seems to be uncertain e.g. because of a missing Q wave and the relatively low sampling rate. In the original implementation of this algorithm, the Q wave onset found is rejected if the difference between Q wave and R wave fiducially points are larger than 80 ms [55]. In that case, QRS onset is defined in the onset of R wave.

2.2.5. Ambulatory HRV data

The aim of recording RR intervals has been to gain information about the neural regulation of the heart and the circulatory system. Observing the changes occurring over long periods of time (i.e. several hours) requires ambulatory recording, which is usually performed using standard commercial equipment (Holter devices). This provides procedures for ECG signal acquisition and analysis, extracting the RR interval time series from the ECG signal and analyzing them. The sampling frequency typically used for an ECG signal with Holter devices is 128 Hz (as explained in 2.2.3.), which means a timing accuracy of 7.81 ms for R wave detection. Thus a low sampling frequency produces inaccuracies in RR interval measurement and bias in the analysis. A timing accuracy of the order of 1 ms would be desirable for the assessment of chaos, for example.

One factor affecting ambulatory HRV measurement is circumstances that vary with time, i.e. the fact that external conditions can be far from stable. This may produce nonstationary changes in a time series and make the assessment of the physiological events more difficult, or even impossible, than under stable laboratory conditions. A method for separating non-periodic (nonstationary) changes from periodic ones has been proposed by Sapoznikov D, Luria M & Gotsman M [59]. Variable conditions may also produce periodic fluctuations which become summed in the time series, making it difficult to distinguish the regulatory processes from each other. This can obviously lead to misinterpretations in some circumstances.

2.2.5.1. Accuracy of HRV measurement

The accuracy of spectral estimates performed on RR intervals obtained from ambulatory Holter systems has been studied by Pinna G, Maestri R, Cesare AD, Colombo R & Minuco G [56]. It has been observed that the centre and dispersion of the estimation error changes from one Holter system to another. There are large inter-recorder differences and variable spectral distortion among selected spectral bands. Use of the Fourier spectral estimate gave more stable results than did the AR spectral estimate in ten minute ECG sequences. The main factor limiting the accuracy of the RR interval measurement was the low frequency with which the ECG signal was sampled, a topic discussed theoretically by various scientists [56, 57] concluded that spectral analysis of RR interval time series with very low variability may be seriously altered when performed on an ECG signal acquired using a Holter system.

The accuracy of spectral estimates of HRV was investigated by generating a simulated RR interval time series of variable length (180-540 seconds) using an autoregressive model from a set of recordings and adding Gaussian noise [58]. The accuracy of Fourier (Blackman-Tukey) and AR spectral estimates could then be evaluated in terms of the normalized bias and variance. The results showed that the bias (systematic error) of the estimate was a less important factor than the variance (random error). Both decreased as the length of the time series increased, but the variance decreased more rapidly. The power estimate was most stable in the HF band, while that in the VLF band had the highest variance. No minimum length was proposed for a time series, but it was concluded that even with the shortest record the bias made a less significant contribution to the estimates. It was pointed out that a relative high variability in spectral parameters is typical of RR interval time series, and that this should be noted in the analysis of the short time series.

2.2.5.2. Reproducibility of HRV measurements

There are a number of factors that affect HRV measurements, and obtaining precisely controlled conditions is problematic. Furthermore, variability is always seen between repeated measurements. From this point of view, it is essential to study both short-term (over several days or couple of weeks) and long-term (over 6-7 months)

reproducibility of the analyses, even though this can be a tedious task.A few published investigations on the reproducibility of HRV exist, e.g. [9, 59, 60, 23, 61].

An investigation the short-term reproducibility of HRV measurements in patients with chronic stable angina and found no significant changes in the time or frequency domain parameters between two 24 hour ambulatory ECG recordings was made [67]. The short-term and mid-term (over one month) stability of spectral parameters studied in healthy young subjects in the past [9]. It was observed that the intra-observer and inter-observer reproducibility of spectral analyses are high under controlled conditions. No employment of any standardization for breathing frequency or volume was made.

A study of the short and long-term reproducibility of HRV measurements in normal subjects was made [60]. The conclusion was that time domain parameters, as evaluated over the whole 24 hour recording, can be expected to be reproducible during relatively stable conditions but frequency domain parameters calculated for ten minute ECG sequences were reproducible only under known stable conditions, as factors of other than neural origin can greatly alter the spectrum. The measurement of total power needed resting conditions to produce reproducible results. Respiratory oscillations in the spectrum (high frequency component) can be measured reproducibly during controlled breathing. The low frequency component was reproducible, particularly at rest and during tilt, which indicates that these fluctuations are quite stable. The reproducibility of the power estimates when normalized by reference to the total power seemed to be no better than that of the real values. It should be noted that the time domain parameters were not reproducible if they were evaluated from ten minutes sequences instead of the whole 24 hour period.

The results of analyses performed on signals of short (e.g. five to ten minutes) and long (possibly 24 hours) duration seem to differ. A suggestion is that analyses of long signals may homogenize the results and give better reproducibility of the frequency domain parameters [60]. In analyses performed on 24 hour recordings, the results have often been calculated for short sequences and then averaged over the whole recording. The authors also conclude that frequency domain parameters should be evaluated from short signals and under controlled conditions to minimize the effects of disturbing factors [60]. Recording the respiratory activity would probably help to explain the RR interval fluctuations. It should be mentioned that the amount of heart rate variability depends on the subjects. Thus, the reproducibility observed in the

case of normal subjects, for example, cannot be assumed to occur in patients with cardiac diseases [60].

2.2.5.3. Artifacts in RR interval time series

When the activity of the autonomic nervous system (ANS) is evaluated in terms of HRV, variations in the sinus rhythm of the heart and the RR interval time series analyzed should contain only normal RR intervals. The RR intervals obtained from ambulatory recordings, however, often include abnormal intervals, which do not represent the sinus rhythm and differ in length from normal RR intervals. These can arise from rhythm disturbances (ectopic beats) or errors in the detection of QRS complexes of technical or physiological origin. These artifacts lead to spurious transient spikes in the resulting RR interval time series. The computation of HRV indices can be unfavorably affected by the presence of even a small number of such transients. In addition to high-frequency transient spikes, non-periodic low frequency changes in the sinus rhythm, i.e. normal physiological or emotional responses of the heart, which are easily encountered in long-term recordings, can have adverse effects on some HRV indices.

As the interest in HRV increases, more efforts are being made to understand the effects of artifacts and artifact processing techniques on HRV measurements [62, 63, 64]. If the number of transient spikes in a RR interval time series is small, it is possible to reject them or correct for them, and thus to obtain a smooth signal consistent with normal RR intervals. Data segments containing frequent artifacts, however, should be rejected from further analysis. Detrending can be used to remove the effects of non-periodic low-frequency changes in RR intervals. The amount of rejected data and the artifact detection criteria and correction techniques used should be taken into consideration when discussing the reliability and reproducibility of different HRV approaches.

2.2.5.4. Errors in the detection and classification of QRS complexes

The detection of QRS complexes (R waves) always precedes the further processing of a RR interval time series. Achieving an accurate, artifact-free RR interval time series requires optimal electrode positioning. Ambulatory ECG recording is exposed to many technical and physiological disturbances which are not easily prevented or controlled, and consequently errors in the automatic detection of QRS complexes cannot always be avoided. That is, the accuracy of QRS detection can be affected; the detector can miss normal QRS complexes or spuriously detect additional events within normal RR intervals. A missed R wave will lead to an interval, which is approximately twice as long as the average interval, while a detection of an additional event within a normal interval will lead to two shorter intervals, the sum of which equals the real interval. Unfortunately combinations of missed and false detections exist, resulting in difficulties in artifact identification.

It can be impossible to tell on the basis of RR interval data alone whether the cause of an artifact is physiological or technical. In addition, information is needed on the underlying shape of the ECG signal. Considering the activity of the ANS system, however, the origin of the artifact is not important, since all abnormal RR intervals are not useful for further analysis. A review of software QRS detection in ambulatory monitoring has been published by Pahlm & Sornmo (1984) [65]

Along with detecting QRS complexes, most algorithms used with commercial long-term ECG devices attempt to classify them according to type, as "normal" (i.e. originating from sinus rhythm) or "abnormal" (ectopic). Randomly occurring ectopic (extra) beats are frequently encountered in normal "subjects" but if an ectopic beat is mistakenly analyzed as normal, an artifact is induced into the time series, since the RR intervals connected with an abnormal beat differ in length from normal intervals. Thus the role of this classification can be very important, however errors in QRS classification are not rare [66, 64]. Therefore systems including QRS classification may require effective artifact correction in the same way as systems without this classification. While single ectopic beats can be corrected to allow further analysis, segments containing pathological rhythm disturbances are usually rejected. The classification of ectopic beats can, according to their occurrence in time relative to

surrounding beats, form the basis for the selection of the correction method [67]. Ectopic beats can be interposed extra-systoles, compensated extrasystoles, or phase-shifted extra-systoles.

Disturbances of physiological origin

Errors in QRS detection arise from disturbances and extraordinary waveforms in the measured ECG signal [65, 68]. Abnormal initiations of the heart beat (ectopic beats) can lead to a variety of morphologies of QRS complexes and cause difficulties in both their classification and their detection. Potential physiological sources of errors also include: abnormally large P or T waves, and myopotentials similar enough to QRS complexes in amplitude and frequency content to cause spurious detection. Variations in the position of the heart with respect to the measuring electrodes and changes in the propagation medium between the heart and the electrodes, both being dependent on the position and breathing of the patient, can cause: sudden changes in the amplitude of the ECG signal and morphology of the QRS complex, leading to missed QRS complexes, as well as low frequency baseline shift. The ability of the QRS detector to tolerate variations in ECG waveforms depends on the recognition criteria themselves and the pre-processing of the raw ECG data, of which the most essential part is filtering [69, 14].

Disturbances of technical origin

Like physiological changes in the ECG signal, the tolerance of different QRS detection procedures can vary with respect to technical disturbances [69,14]. These include movement of electrodes (relative to the skin and heart) or other changes in conductivity between the electrodes and the skin, which can result in rapid baseline shift. Capacitively or inductively coupled disturbances, e.g. power line interference and extra peaks originating from the movement of wires or discharges of static electricity when clothes, skin, electrodes and wires chafe against each other in the presence of dry air and skin can also cause disturbances.

Problems at the electrode-skin interface

Most of the disturbances in automatic QRS detection are connected with electrodeskin impedance, since poor conductivity between the electrodes and the skin both reduces the amplitude of the ECG signal and increases the probability of

disturbances[70]. Along with pathological arrhythmias, problems at the electrode-skin interface are the most common reasons for having to reject large segments of RR interval data in HRV analyses. The need to take account of the interaction of the skin with the electrodes is commonly described in the literature dealing with the non-invasive recording of surface potentials, but the mechanism of the disturbances caused by rapid impedance changes has been not described. The reason may lie in the fact that problems with electrode contacts can be avoided if the electrodes are correctly attached, electrode paste is used and the tests are performed at rest. Even at normal activity levels, electrode paste usually improves conductivity between the skin and the electrodes enough to prevent problems. Movement of the electrodes relative to the skin and the heart, caused by rapid motion on the part of the subject, can give rise to sudden changes in electrode-skin impedance and consequently a baseline shift in the measured ECG signal. These problems due to unavoidable movement of the electrodes are especially frequent in exercise tests, and are accentuated further if the electrodes are loose or the subject has unusually high skin impedance.

The larger the electrode-skin impedance, the smaller the relative impedance change needed to cause a major shift in the baseline of the ECG signal, and if the skin impedance is extraordinarily high, it may be impossible to detect the QRS complexes reliably in the presence of body movement. In such cases the sudden baseline shifts may be of such amplitude that they lead to the saturation of the voltage amplifier or confuse the automatic gain control (AGC). The exact electrode-skin impedance depends largely on the electrode and the type of electrolyte used, the properties of the subject's skin and the measurement frequency. If the skin is dry, the electrode-skin impedance can be as high as several hundred kilo-ohms at frequencies below 100 Hz. Three-electrode leads are usually better than two-electrode ones, since a separate ground electrode is available.

If the electrode-skin impedance is high, a distribution of charges and subsequent potential difference can be generated on both sides of the interface or between the electrodes. The origin of such a potential difference can be electrode offset potential or an unequal local distribution of charges on the skin surface generated, for example, by static electricity. When an impedance change takes place at the electrode-skin interface, the potential differences drive a current over the electrodeskin – tissue – skin - electrode circuit, or parts of it, and a shift in voltage is measured by the differential amplifier. Due to the transient form of the current and the high-pass

property of the ECG amplifier, the baseline returns to normal after some time. Once the skin impedance becomes lower due to sweat gland activity, baseline shifts are no longer generated. Besides eliminating these impedance changes, the improved conductance puts an end to the unfavorable effects of static electricity, because the charges are rapidly equalized over the body surface and on the electrodes. When the sweat glands are filled with conducting sweat (sweat can be considered the equivalent of 0.3 % saline), many low-resistance parallel pathways result, thus significantly reducing the electrode-skin impedance and alleviating the problems [71]. A further lowering of the impedance takes place due to hydration of the skin.

2.2.5.5. Non-periodic changes in RR intervals

Conventional mathematical analysis methods such as standard deviation, correlation and power spectrum analysis presuppose that the data are stationary in the wide sense. This means that in the case of HRV analysis the sinus rhythm of the heart can be approximated as stable. This approximation holds best over a short period and under steady-state conditions. In addition to the transient spikes mentioned earlier, non-periodic changes in the heart rhythm can impair the stationarity of the signal and have adverse effects on HRV indices. Non-periodic changes can be induced in a RR interval time series by normal responses of the heart to physical activity, emotional stimuli or reflexes of various kinds.

The question might arise as to whether it is permissible to correct an RR interval time series for abnormalities if their background is physiological. As discussed earlier, a correction procedure should be employed for ectopic beats, since they do not carry information on the sinus rhythm, but the need to correct for nonperiodic changes in the sinus rhythm, e.g. by removing the changes in the HR trend, depends largely on the application and on the mathematical HRV indices used. When day-to-day variation is to be studied in a single subject, for example, it is important to detrend the data series so that the statistics regarding frequently-occurring parameters can be compared. If conventional methods are used, the correction of non-periodic changes in heart rhythm should be preferred, since rough nonstationary sequences in the RR interval data can bias the results of the analysis. Detrending is usually applied to cut down on the effects of nonperiodic low-frequency changes in RR intervals.

2.2.5.6. Limitations and effects of artifacts

In view of the non-periodic nature of the artifacts in RR interval time series, it is clear that spectral domain methods in general and time domain methods based on the calculation of standard deviations and mean values are sensitive to artifacts in the automatic measurement of RR intervals. Experiments have shown that pNN50 and indices based on the calculation of standard deviation are more sensitive to artifacts than the HRV index (the number of normal-to-normal intervals of modal duration) or TI NN (triangular interpolation of the normal-to-normal histogram) [72]. A comparison of methods for the removal of ectopy is also presented [62].

Mulder (1992) describes the effect of artifacts in considerable breadth, placing emphasis on spectral methods [67]. The impulse-like deviation in RR interval time series caused by errors in QRS detection, both missed R waves and additional triggers, and also interposed ectopic beats have a similar effect on the power spectrum in that power is increased at all frequencies. The effect of a phase-shifted ectopic beat is similar in form but smaller in amplitude. As the number of corrupted beats (not consecutive) increases, the total spectral variability grows linearly, while in the case of more consecutive artifacts, e.g. intervals of twice the normal length the Fourier transform of an artifact complex is no longer flat but follows the form of a sinc-function, adding more power to the lower frequencies. As can be observed in Figure 14, the effect of compensated ectopic beats is markedly different, i.e. their contribution is large at higher frequencies and small at lower frequencies.

Responses of the heart to physical activity or emotional stimuli clearly affect the mean values, standard deviation and low frequencies of the RR spectrum (see Figure 14). Detrending is usually used to remove low frequency baseline shifts by subtracting a fitted polynomial. There is also another method, based on the ratio between the peak power and bandwidth of the LF range in the power spectrum [66]. A wavelet filtering approach is used to remove very slowly oscillating components from RR interval data [74].In long term measurements, stationarity can be achieved better if the data are first divided into shorter segments which are analyzed one by one and then averaged. When using Fourier transform-based approaches, however, compromises must be made between the requirements of stationarity and good

frequency resolution, since the frequency resolution of the FFT algorithm is better if longer segments are analyzed at a time.
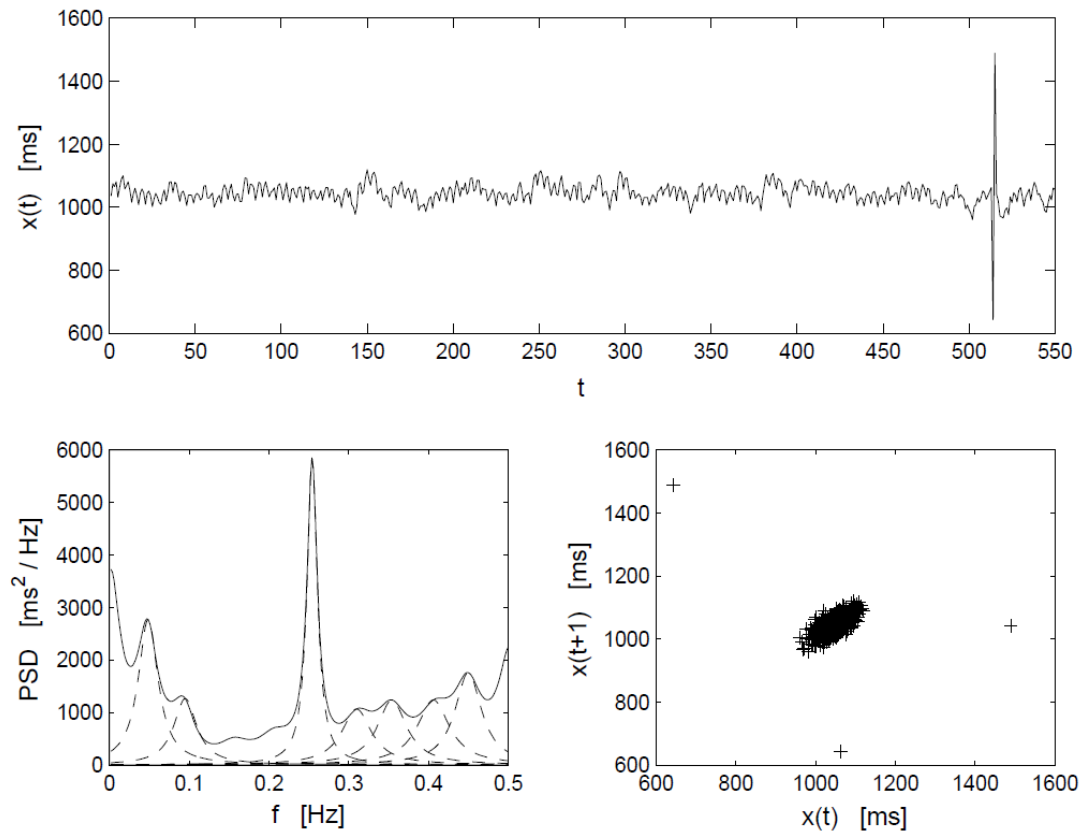
Figure 14. *RR time series obtained from a healthy young subject when asleep (top). The ECG signal includes a compensated ectopic beat, producing the sequence normal-short-long-normal in the RR intervals. Power spectrum estimated by the modified covariance method with a model of order 20 (bottom left). The estimate include the sum spectrum (solid line) and the spectra of the separate components (dashed lines). First-order difference plot of the RR intervals (bottom right).[75]*

2.2.5.7. Correction of abnormal RR intervals

The decision as to whether a deviating interval should be corrected or not, usually forms the most difficult step in the removal of abnormal intervals. A segment of an RR interval time series is accepted for further analysis if the number of qualified

intervals exceeds a preset acceptance percentage which varies widely according to the application and the patient group, a typical figure being around 95 % as in Mulder *et al*. [67] and Pitzalis *et al*. [60]. There are no specific recommendations in the literature as to the maximum number of artifacts one can interpolate or accept.
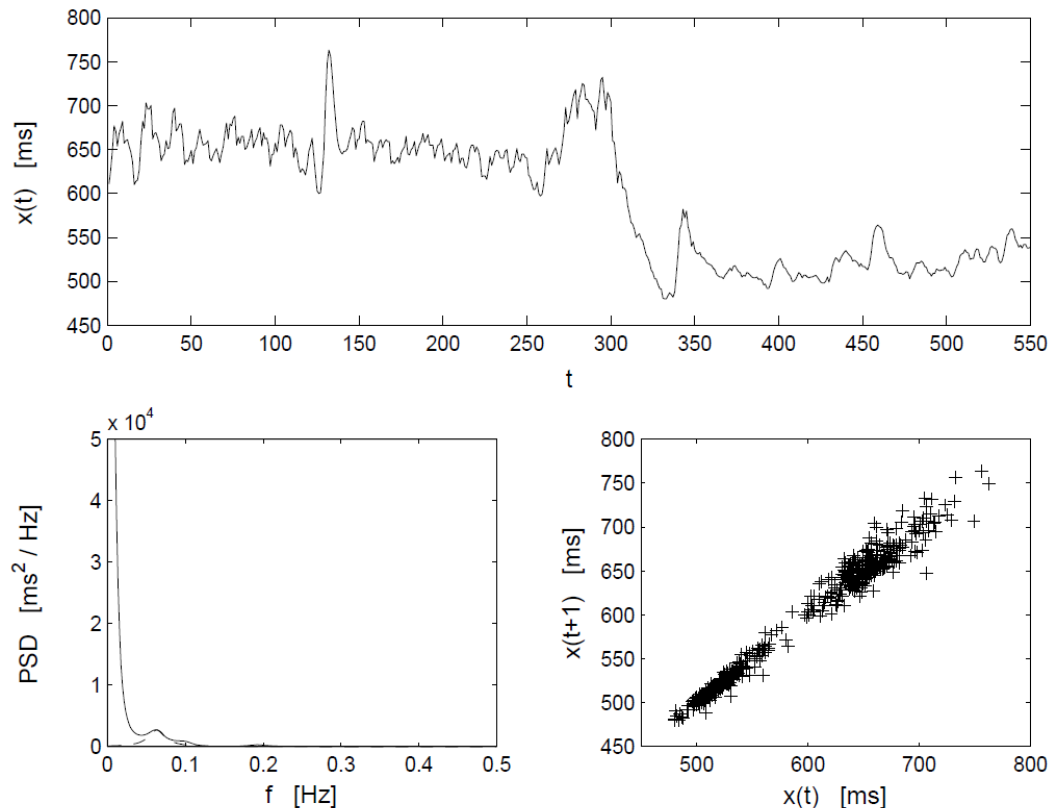
Figure 15. *RR time series obtained from a healthy young subject, including an abrupt change in RR intervals due to physical activity (top). Power spectrum estimated by the modified covariance method with a model of order 20 (bottom left). First-order difference plot of the RR intervals (bottom right). [75]*

2.2.5.8. Detection and correction of artifacts

Error detection algorithms attempt to distinguish normal intervals from abnormal ones. The optimum would be for the algorithm to adapt to the data and derive the error detection criteria from the distribution indices of the normal-to-normal intervals. An algorithm which automatically identifies artifacts and corrects them in a RR interval time series is presented by Berntson *et al*. [76]. It can be noticed from the literature, however, that relatively simple detection criteria supported by additional visual verification are still being used in computerized artifact detection in

connection with HRV measurement. This is explained by the fact that results obtained with simple procedures are not distinctively poorer than those arising from more complex solutions [67]. As the normal intra-subject and inter-subject variability in heart rhythm is large, automatic adjustment of the criteria can be difficult. Short and sudden surges are usually treated successfully by most methods, but the decision on whether deviating intervals resulting from non-periodic physiological fluctuations should be corrected is more problematic. So far, researchers have wanted to solve the most critical questions during the visual verification after computerized detection.

The simple artifact detection criteria described in the literature include absolute upper and lower limits for acceptable intervals (e.g. 300 - 1500 ms), absolute or relative differences from the previous RR interval (e.g. 20 - 40 %), from the following RR interval, from the previous accepted interval, from the mean, from the mean updated by previously accepted intervals or from a fitted polynomial representing the baseline. Malik *et al.* [71] used four simple detection criteria and found none of them to be significantly better than the others. As a single detection criterion always has its particular weaknesses, a combination of criteria should be preferred [64]).

There are two basic methods for removing individual artifacts from an analysis: total exclusion of abnormal intervals or substitution of a better matching value. The exclusion approach is widely used, suits well for time domain analysis, and can also be used with frequency domain analysis if only a few beats are to be excluded, where as the substitution approach is used relative widely with both time domain and frequency domain analysis.

The substitution can take the form of simply replacing the abnormal value with a local mean or median value, but more sophisticated procedures include linear, non-linear or cubic spline interpolation methods or more complicated predictive modeling. The substitution approach can be used with good justification in a physiological sense if the artifact is known to be of technical origin, while if it is due to a physiological or mental factor, both approaches can be used with success. The comparison, by Lippman *et al.* [62], of methods for removing ectopy from 5- minute RR sequences showed that the simple deletion method and the more complex non-linear predictive interpolation method gave the best results. In general, the removal of abnormal intervals tends to increase the low frequency component of the spectrum and reduce the standard deviation, but it should be noted that the sum of the intervals after correction does not always equal the sum of the original intervals. A correction

procedure, presented by Mulder [67], attempts to retain the total time, and this approach can be successful if the sinus rhythm is not disturbed during a period of disturbances; however, short intervals connected with phase-shifted extra systoles can make it impossible to preserve the sum of the intervals.

3. Analysis of signal variability

3.1. Interpolation of the ECG signal

As seen earlier, the ECG was interpolated in order to increase the sampling rate of the measured signal. That is important because of the relatively low sampling rate (often 128 Hz) of the ambulatory ECG. The objective is to increase sampling rate to obtain, for example, a more accurate measurement of the end of the T wave. Speranza *et al.* [52] utilized this technique in order to gain an improved resolution of the RT interval variability measurement. They checked the performance of the technique and showed that the interpolation caused a distortion in the QRS complex, but did not affect the T wave. The difference was less than 3 % of the peak-to-peak amplitude of the original signal, when the ECG was sampled at 250 Hz and interpolated to 1 kHz, and was comparable to the signal digitized at 1 kHz [52].

Interpolation is the process of increasing sampling rate by an integer factor *M*, that is, upsampling by *M*. First, the time base of the signal is changed so that *M − 1* zero valued samples are placed between each sample pair of the original signal *x(t)* (*t = 1, 2, …., N*). This new sequence is defined by

$$v(t) = \begin{cases} x\left(\frac{t}{M}\right), & \text{t} = 0, \pm M, \pm 2M \\ 0, & \text{otnerwise} \end{cases}, \tag{3.1}$$

For instance, when having a signal sampled at 128 Hz and interpolating it to 1024 Hz sampling rate (interpolation by factor 8), 7 zeros are placed between each sample pair. Thus, the time interval between each sample pair changes from 7.81ms to 0.98 ms.

A symmetric, linear phase, FIR digital filter was used. This filter resamples data at a higher rate using low-pass interpolation. This allows the original data *x(t)* to pass through the filter unchanged and interpolates *M − 1* values between data samples such that the mean square error between them and their ideal values is minimized [78]. The length of the designed filter is 2*ML*+ 1, where *M* is an integer factor used to increase sampling rate and *L* is an integer factor determining the degree of the filter. The cutoff

frequency α was given in radians ($0 < \alpha \leq 1,0$), so that the input data is assumed to be band-limited with the frequency $\alpha\pi/M$.

The increase in sampling-rate obtained by the addition of $M - 1$ zeros between successive values of $x(t)$ results in a signal $y(t)$ whose spectrum $Y(\omega_y)$ is an M-fold periodic repetition of the input signal spectrum $X(\omega_x)$ [79]. Since only the frequency components of $x(t)$ in the range $0 \leq \omega_y \leq \pi M$ are unique, the images of $X(\omega)$ above $\omega y = \pi/M$ should be rejected by passing the sequence $V(t)$ through a lowpass filter. The frequency response of the filter can be ideally given as

$$H_M(\omega_y) = \begin{cases} C, & 0 \leq |\omega y| \leq \pi/M \\ 0, & otherwise \end{cases}, \tag{3.2}$$

where C is a factor required to normalize the sequence $y(t)$.

3.2. Time domain analysis and indices

Time domain analysis of RR interval time series covers histogram and scattergram analysis, and the calculation of several common statistical indices. In many studies, these indices are compared with frequency domain parameters, and the correlations between these parameters are also calculated.

When dealing with the interpretation of parameters such as histograms, it should be pointed out that they do not in general contain any information on periodic fluctuations in RR intervals. Respiration frequency, for example, cannot be observed on the basis of these parameters, nor can the variance related to a specific frequency band (i.e. spectral component) be measured by these indices if RR intervals without any band-pass filtering are considered. Time domain indices tend instead to rather measure the average variability in time series or maximum amplitude of the variability, depending on the nature of the index considered. See Kleiger *et al.* [80] and references therein, for a more detailed discussion on the use of time domain parameters.

There are several statistical indices which have been used to describe heart rate variability, e.g. average, median, deviation between maximum and minimum values (range), standard deviation (sd) and root mean square of successive differences

(RMSSD). The formulation of these is well known and they do not require complex calculations. The statistical properties of a time series $x(t)$ are often described using basic indices such as the mean x and standard deviation sx, which can be obtained from the given data as follows:

$$\bar{x} = \sum_{t=1}^{N} x(t)/N, \qquad\qquad s_x = \sqrt{\sum_{t=1}^{N}(x(t) - \bar{x})^2 /N} \qquad\qquad (3.3)$$

The variance is the square of the standard deviation, $var(x(t)) = s_x{}^2$. The coefficient of variation and the range, i.e. the deviation between the maximum and minimum values in a time series, are formulated as

$$CV_x = 100 * s_x/\bar{x} \qquad\qquad (3.4)$$

$$d_x = \max_t[(x(t)) - \min_t(x(t))] \qquad\qquad (3.5)$$

The mean square of successive differences (RMSSD) is calculated for the purposes of HRV analysis by

$$RMSSD_x = \sqrt{\sum_{T=1}^{N-1} \frac{[x(t)-x(t+1)]^2}{N}} \qquad\qquad (3.6)$$

Certain "modified" indices also exist, such as "the percentage of difference between adjacent normal RR intervals greater than 50 ms computed over the entire 24 hour ECG recording" (pNN50) or "the mean of the standard deviations of all normal RR intervals for all 5 minutes segments of a 24 hour ECG recording" (SDNNIDX) [81, 82].

3.3. Analysis of distribution

The distribution of RR intervals can be analyzed in terms of a histogram of the time series [83, 84] in which the "frequencies" in the histogram bins may be expressed in absolute numbers or as relative "frequencies" of the time series values. The histogram has also been presented either by drawing a line between the bins or by giving the portions of the time series values numerically [85].

A few parameters generated for the analysis of RR interval histograms are introduced in Baevskij *et al.* [85]. The bin having the largest "frequency" is termed

the mode of histogram and the "amplitude" of this mode has also been observed. The width of the histogram base, i.e. the maximal deviation in time series values, has been proposed as another basic measure of RR interval variability. Several parameters may be constructed from these three elementary measures.

Casolo *et al.* [86] used the width of the histogram base as a measure of total variability, and defined the width at levels of 10% and 50% of the maximum height of the histogram. Odemuyiwa *et al.* [87] approximated the shape of the histogram as a triangle in order to reduce the effect of less marked variabilities.

The results produced by the histogram naturally depend on the bin width used. If a large bin width is chosen, the histogram will be vague in shape, while a small bin width will accentuate unimportant details. It is worth noting that the bin width of a histogram should remain constant in order to allow rational comparison of the absolute results. A simple estimate for bin width is given by Scott D [88]

$$H_N = 3.49(s_x/N^3), \tag{3.7}$$

where s_x is the standard deviation of N time series values. The estimate takes the variability in time series into account by using the standard deviation. This expression can be used successfully with approximately Gaussian data [88]. In practice, the bin width can be selected to be near the estimate H_N. The estimation of frequency distributions has been studied in Willard K & Connelly D [89], where different non-parametric methods using both simulated and real data are compared and improvements to the histogram are proposed.

3.4. Frequency domain analysis

Spectral estimates can be studied by integrating over a given frequency band or by decomposing the spectrum into components. The first approach can be performed with Fourier and autoregressive (AR) techniques, but the latter is possible only with AR techniques.

One problem affecting integration of the spectrum is definition of the frequency bands. Doing this signal by signal would be quite a laborious task, because it would mean checking all the estimates manually. Frequency ranges can be defined by an

experimental procedure or obtained from the literature and kept constant, but problems will arise when the locations of components vary between signals. The definition of frequency ranges has been studied experimentally by Jaffe *et al.*[90], where the aim is to optimize the ranges to some extent. Use of the spectrum decomposition procedure gives estimates for the component spectrum and powers. In addition, the central frequencies as well as the power estimates can be utilized to search for the appropriate components. Use of the maximum of component spectrum and the band width of the component to detect periodic fluctuations is discussed in Sapoznikov *et al.* [73]. The mean, median and central frequency has been used to obtain the characteristic frequency of a specific band in Korhonen [91]. Several definitions exist for the frequencies of the components in a RR interval time series spectrum, as summarized in the following short description:

- The *very low frequency* (VLF) component is found at frequencies $f < 0.04$ Hz [25]. These fluctuations in RR intervals are due to thermoregulation mechanisms [20]. Some low frequency trends or nonstationarities may also exist, which can be observed in the form of increased power at low frequencies in the spectrum.

- The *low frequency* (LF) component is usually observed around $f = 0.1$ Hz. This is mainly due to the systems regulating blood pressure [25, 92] and reflects the autonomic sympathetic tone in heart rate regulation [93,94] although it has also been suggested that parasympathetic regulation plays some role in it [19, 23].

- The *high frequency* (HF) component will be often found in the frequency band $0.15 < f < 0.40$ Hz, which is related to the frequency of respiration (e.g. cycle length T = 4 *s*, $f = 0.25$ Hz) [95, 21] and is often called *respiratory sinus arrhythmia (RSA)*. The amplitude and frequency of this component are closely related to the respiration volume and frequency [96, 97]. The HF component has been considered a measure of parasympathetic neural regulation of heart rate [98, 94, 23].

Sometimes an *ultra low frequency* (ULF) component is defined with a frequency band of $f < 0.0033$ Hz [8]. The balance between sympathetic and

parasympathetic neural regulation is often measured by the ratio of the power estimates for the LF and HF components (LF/HF ratio) [22, 94] An RR time series for a healthy young subject is shown in Figure 16, together with a spectrum estimated using an AR model, showing the components of spontaneous RR fluctuation described above and a pole diagram representing the locations of the poles of the parametric model on the complex z-plane. In this example, the model order was selected by visually examining the spectrum when the order 16 gave a reasonable result. The power spectrum estimate represent the sum spectrum (solid line) and the spectra of the separate components related to respective pole pairs (dashed lines).

3.4.1. On the use of spectral analysis

The use of frequency domain analysis in different clinical circumstances has been extensively reviewed in Rienzo *et al.* [99], Malliani *et al.* [22], Kamath & Fallen [25] and Öri *et al.* [81]. Spectral analysis has been often performed for RR interval time series including 256 or 512 values [102], the recording lasting several minutes depending on the heart rate. Analyses of this kind can provide information on *short term* fluctuations in RR intervals.

Short term fluctuations and their changes over several hours can be studied with ambulatory recordings (24 hour Holter recordings), a long recording being segmented into shorter RR interval time series of 512 values, as for instance described in Cerutti *et al.* [100] and Furlan *et al.* [102]. Such a short time series can be assumed to conform better with the stationarity requirement for the relevant spectrum estimation. Circadian variation in spectral parameters has been studied in Furlan *et al.* [102] and Huikuri *et al.* [93], and long term RR interval recordings in Bianchi *et al.* [103], Rienzo *et al.* [104], Malik *et al.* [105].
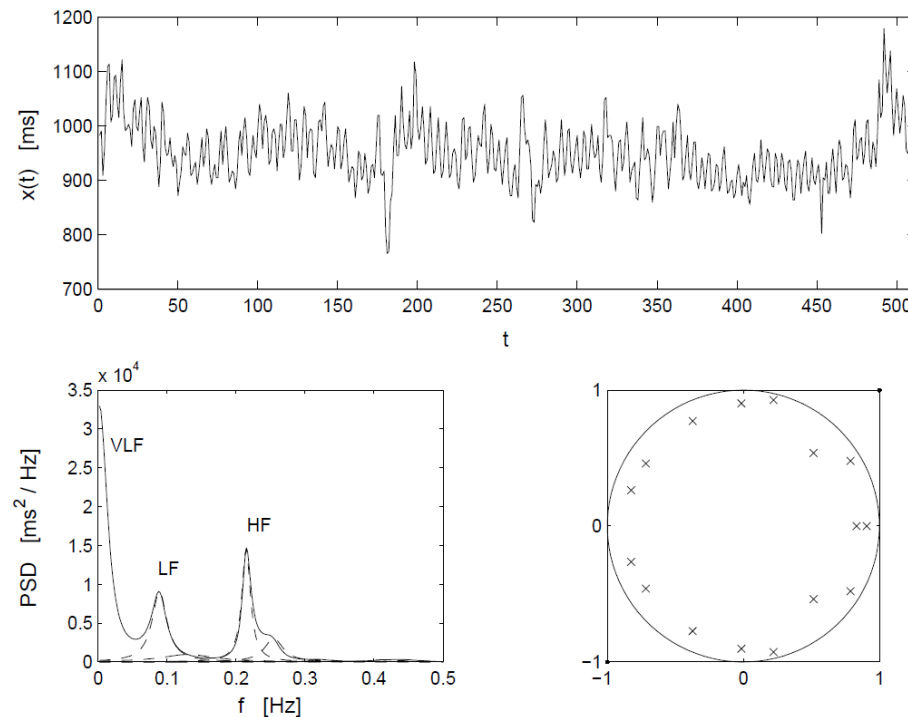
Figure 16. *RR time series obtained from a healthy young subject under resting conditions (top). Power spectrum estimated by the modified covariance method with a model of order 16 (bottom left). The corresponding pole diagram (bottom right).[202]*

and Saul *et al.* [95]. Long term variation in autonomic neural regulation has been studied using the VLF and ULF components mentioned above, and the spectrum has been calculated from the whole 24 hour recording. The spectrum has been reported to have the shape $1/f$ [107, 106].

2.3.4.2. Mathematical background to spectral analysis

The RR interval time series includes information of wide origin and its nature will hardly allow an assumption of wide sense stationarity in the strict statistical sense under any conditions. The RR intervals should rather be understood as being approximately stationary at most, whereupon the analysis would give relevant results in a medical sense. There may exist sections which can very well be assumed to be (almost) stationary, and also sections that are far from allowing such an assumption. It

is often necessary to divide a recording into shorter stationary sequences. Nonstationarities include transient phenomena and slowly varying changes (trends), the identification of which is more difficult. The theory of many approaches is nevertheless based on the assumption of signal stationarity. In this context, a calculated spectrum for a RR interval time series, for example, is understood as a "model" for periodic fluctuations rather than as a "true" spectrum.

Let $x(t)$ be a stationary process defined at discrete values $t = 0, \pm1, \pm2, ...$ The autocovariance function will be written as [108]

$$r(k) = E\{(x(t) - \mu)(x(t + k) - \mu)\} \quad, \qquad k = 0, \pm1, \pm2, \ldots$$

(3.8)

and the autocorrelation function will then be r(k) = r(k)/r(0). Here the mean value of the process $x(t)$ is defined, using the expectation operator $\mu = E\{x(t)\}$. For a wide-sense stationary process, the mean value is constant and the autocorrelation satisfies the property r(n_1, n_2) = r($n_1 - n_2$) = r(k).

Assuming that $x(t)$ is a zero mean stationary process, there must exist an orthogonal process $Z(\omega)$ such that [108]

$$x(t) = \int_{-\pi}^{\pi} \exp(i\omega t)\, dZ(\omega)$$

(3.9)

and $E\{|dZ(\omega)|2\} = dH(\omega)$, where $dH(\omega) = h(\omega)d\omega$, $-\pi \le \omega \le \pi$ and $\omega = 2\pi f$. This is called the *spectral presentation of a discrete stationary process*. The autocovariance sequence is

$$r(k) = \int_{-\pi}^{\pi} \exp(i\omega k)\, h(\omega)\, d\omega$$

(3.10)

and the power spectral density is

$$h(\omega) = \frac{1}{2\pi} \sum_{k=-\infty}^{\infty} r(k) \exp(-i\omega k) \quad, \qquad -\pi \le \omega \le \pi \quad.$$

(3.11)

3.4.3. Spectrum estimation using a periodogram

Let us divide the N-point process $x(t)$ into K non-overlapping segments, each having M points. The Fourier transform of the p:th segment can be written as

$$X^p(\omega) = \sum_{t=1}^{M} x(t) \exp(-i\omega t) \quad, \qquad -\pi \leq \omega \leq \pi \quad .$$
(3.12)

The periodogram estimate of the spectral density function of a single data segment is given by

$$\hat{P}_x^p(\omega) = M^{-1}|X^p(\omega)|^2 \quad, \qquad p = 1, \ldots, K \quad .$$
(3.13)

If the periodograms of K segments are averaged, the estimate is called a Bartlett averaged periodogram. It should be noted here that the periodogram is only one way of estimating the spectrum of the process, and is by no means a "definition" of the spectrum.

Modifications of the averaged periodogram also exist, among which the Welch periodogram is introduced. In this method, data segments are allowed to overlap by 50% or 70%, for example, and each data segment will be weighted with a window function before calculating the periodogram. As a result, one has for the periodogram of each segment

$$\tilde{P}_x^p(\omega) = \frac{1}{MU}|\sum_{t=1}^{M} x(t)w(t) \exp(-i\omega t)|^2 \quad .$$
(3.14)

The factor $U = M{-}1t{=}1(t)2$ is a normalization factor for the power in the window function $w(t)$. The Welch periodogram estimate will be then an average of these periodograms:

$$\hat{P}_x^w(\omega) = \frac{1}{L} \sum_{p=1}^{L} \tilde{P}_x^p(f) \quad .$$

(3.15)

The statistical properties of periodograms are discussed by Priestley (1981) and Kay (1988).

Sometimes one may need to approximate a periodogram more closely, which can be done by using the *zero padding* procedure [109]. This is performed by extending the data set with zeros, and taking the Fourier transform of the whole data set. This operation does not achieve any better resolution in the spectrum, however, although the frequency spacing will be denser. Zero padding actually interpolates the values of the measured spectrum at more frequencies, producing a smoother spectrum.

3.5. Parametric modeling of time series

Parametric modeling of time series has some advantages over non-parametric (Fourier) methods. Here only autoregressive (AR) models are examined and the focus is on spectral estimation, which has been the main object of interest in HRV analysis. There are many algorithms for obtaining estimates for AR parameters, e.g. methods based on estimation of the autocorrelation sequence (Yule-Walker), the Burg algorithm, and least squares linear prediction algorithms (including the modified covariance method) [109, 110]. There are also adaptive algorithms such as least mean square (LMS) and recursive least square (RLS), which update the parameter estimates as a new data sample becomes available [110].

Estimation of the signal spectrum with AR models enables the frequencies of spectral components to be determined more exactly than by non-parametric estimation. The frequency estimates can be calculated after determining the poles of the parametric model. Tracking of the pole locations in the complex z-plane can be utilized when monitoring spectral changes in time series, for example. Furthermore,

the powers of the spectral components and their balance can be estimated more accurately. Estimation of the AR spectrum does not need windowing of the time series as can be the case with the Fourier spectrum.

Let us define an autoregressive model for a stationary time series $x(t)$ as follows:

$$\sum_{k=0}^{p} a_k x(t-k) = e(t) \quad , \qquad a_0 \equiv 1 \quad ,$$

(3.16)

where ak are the model parameters to be estimated, $e(t)$ is the residual time series or error process, and p is the model order. The estimates for the model parameters, $\hat{a}_k$ can now be regarded as the "components" observed in the power spectrum estimate, which are to be fitted into the time series $x(t)$ in order to minimize the process $e(t)$ in some sense.

The power spectrum of the process $x(t)$ is given as $Px(z) = H(z)H(1=z)Pe(z)$, which can be written

$$P_x(z) = \frac{\sigma_e^2}{A(z)A(1/z)} \quad ,$$

(3.17)

where the Z transform of the above recursion is

$$H(z) = \frac{1}{1 + \sum_{k=1}^{p} a_k z^{-k}} = \frac{1}{A(z)}$$

(3.18)

and $Pe(z) = \sigma^2_e$ denotes the spectrum of the residual time series. Let us estimate the power spectrum of $x(t)$. Assuming an AR process of order p, it can be written:

$$\hat{P}_{AR}(z) = \frac{\hat{\sigma}_e^2}{\prod_{k=1}^{P}(z - p_k)(z^{-1} - p_k^*)} \quad ,$$

(3.19)

where $\hat{\sigma}_e^2$ is the estimated variance of $e(t)$, and pk are the poles of the model. This can also be given by using the estimates $\hat{a}_k$ and denoting $z = \exp(i\omega)$:

$$\hat{P}_{AR}(\omega) = \frac{\hat{\sigma}_e^2}{|1 + \sum_{k=1}^{p} \hat{a}_k \exp(-i\omega k)|^2} \quad .$$

(3.20)

The spectrum of the single component can be estimated by the following expression:

$$\hat{P}_k(z) \approx \frac{c_k}{(z - p_k)(z^{-1} - p_k^*)} \quad ,$$

(3.21)

assuming that $\omega \approx \omega_k$ and $z = \exp(i\omega)$. For the constant c_k can be written

$$c_k \approx \frac{\hat{\sigma}_e^2}{\prod_{j \neq k}(z - p_k)(z^{-1} - p_k^*)} \quad , \qquad z_k = \exp(i\omega_k) \quad .$$

(3.22)

Now the frequency ω_k is related to the pole pk. It is assumed that a part of the estimate $\hat{P}_{AR}(z)$, c_k, will be constant when $\omega \approx \omega_k$. The AR spectrum estimate should follow the relation $\hat{P}_{AR}(z) \approx \sum_k \widehat{P_k}(z)$, i.e. the spectrum is the sum of the spectrum estimates of the components.

3.6. Estimation of the powers related to components

It was defined, above, the spectrum estimate of a single component related to the pole pk. It may sometimes also be useful to estimate the power associated with a component. In HRV analysis, powers are estimated in order to evaluate the strength and balance of autonomic regulation.

The power of a component observed at frequency ωk can be estimated by utilizing the residue of the function analyzed [111, 110]

$$\hat{P}(\omega_k) = q \, \Re\{\operatorname*{Res}_{p_k}\{\frac{\hat{P}_{AR}(z)}{z}\}\} \quad, \tag{3.23}$$

where the residue of $\widehat{P_{AR}}(z)/z$ is determined for the pole pk. The operation $\Re\{\cdot\}$ denotes the real part of the function. The total power associated with the spectrum and the residues of the function are related as follows:

$$\frac{1}{2\pi j} \oint f(z)dz = \sum_{k=1}^{n} \operatorname*{Res}_{p_k} f(z) \quad. \tag{3.24}$$

Furthermore, the total power of the signal should be equal to the sum of the power estimates of the components, $P_{tot} \approx \sum_{k} \hat{P}(\omega_k)$. Finally, the estimated power of a single component is calculated by

$$\hat{P}(\omega_k) = q \, \Re\{\frac{(z-p_k)\hat{\sigma}_e^2}{z\hat{A}(z)\hat{A}(\frac{1}{z})}\} \quad, \tag{3.25}$$

where $z = pk$ and $\hat{A}(z) = \Pi_{k=1}^{P}(1 - P_k^{-1})$. Now $q=1$ for a real pole and $q=2$ for a complex pole. $\hat{\sigma}_e^2$ is the estimate for the prediction error variance at the given model order.

In HRV analysis, the power estimates are sometimes presented in *normalized units* [n.u.] instead of *absolute units* [ms^2]. The power estimate in normalized units will be [94]

$$\hat{P}(\omega_k)_{\text{n.u.}} = 100 \cdot \frac{\hat{P}(\omega_k)}{P_{tot} - \hat{P}_0} \quad, \tag{3.26}$$

where $\hat{P}_0$ represents the power estimate of very low fluctuations in a signal (*f<0.03Hz*) and P_{tot} the total power of the signal. It is obvious that *0 < $\hat{P}(\omega k)n.u. \leq 100$*.

Model order selection

It is essential to choose an appropriate model order, but the task can be a problematic one. The order of the AR model has a major effect on the spectral estimate for a time series. Too low an order will result in a smoothed spectrum, and

too high an order will increase the resolution of the spectrum and may introduce spurious peaks. The estimate for the power associated with a single component is also dependent on the order that is selected. The orders $p = 15 - 20$ are often satisfactory with RR interval time series, giving a meaningful spectrum. Minimization of the prediction error variance is alone not a sufficient method for model order selection in the case of AR models, since $\hat{\sigma}_e^2$ decreases as the order increases [112], but this decrease should smooth out after a certain order, indicating that the optimum has been reached. The autocorrelation function of a residual time series can also be studied, and if the model order is correct the residuals should be uncorrelated. The locations of the poles in the complex z-plane should then be quite stable.

Several *penalty function methods* for model order selection exist that utilize the prediction error variance, e.g. FPE (final prediction error) and AIC (the Akaike information criterion)[112]. It is expected that these criteria may fail in real world time series. They provide a basis for model order selection, but the final decision has to be made by a subjective inspection. If one can assume that the properties of time series do not change significantly from one such series to another, one probably will not make a serious mistake by choosing a relatively high model order and keeping it constant.

Bispectrum estimation

A potential tool for future RR interval variability analysis may be the estimation ofthe bispectrum. The power spectrum is based on the second order statistics of the time series, but the bispectrum make use of third order statistics. By definition, a gaussian random process has a zero higher-order spectrum of order two (bispectrum) [113], which allows the study of the deviation from the gaussianity or to suppress gaussian noise. The method also contains information about the phase character of the signal, which is failed with the methods based on the second order statistics. Moreover, the bispectrum estimation can be used in detection and characterization of the nonlinearities by analysis of quadratic phase coupling in the frequency domain. A preliminary study on quadratic phase locking in HRV can be found in Calcagnini *et al.* [114]

3.7. Time frequency analysis

There may be a need for monitoring the spectral properties of the signal as time elapses, especially, when "long" time periods are under consideration. The temporal location of the spectral components may give more information than one single spectrum. The short-time Fourier transform (STFT) is a linear Time Frequency Representation (TFR) used to present changes in the signal that vary with time. The Fourier transform does not explicitly show the time location of the frequency components, but some form of time location can be obtained by using a suitable pre-windowing window [115]. The STFT can be defined for $x(t)$ as

$$S_x^g(t, \omega) = \int x(s)\, g^*(s-t) \exp(-i\omega s)\, ds \quad .$$

(3.27)

$S_\omega^g(t,\omega)$ is a local spectrum of the signal $x(s)$ around the analysis time s, because multiplying by the short window $g^*(s - t)$ suppresses the signal outside the neighborhood around the time $s = t$. The properties of the window $g^*(s)$ also have an effect on the calculated STFT [115, 116].

The time-frequency resolution of the STFT is limited by the time-frequency product, i.e. having a small time resolution means poor frequency resolution, or vice versa. The resolution is also constant as a function of the frequency, which is due to the window chosen for the STFT [116].

As an example of quadratic TFRs, the Wigner distribution (WD) is given:

$$W_x(t, \omega) = \int x(t+v)\, x^*(t-v) \exp(-i\omega\tau)\, d\tau \quad , \qquad v = \tau/2 \quad .$$

(3.28)

Detailed reviews of several types of time frequency representation and their application can be found in Cohen [117], Hlawatsch & Boudreaux-Bartels [115] and Loughlin [118], for instance.

3.8. Time-variant spectral analysis

Techniques have recently been developed and demonstrated that allow the tracking of spectral parameters as time elapses. Approaches of this type have also been called time-variant spectral analysis or time-frequency analysis. For a detailed description of the algorithms and methodologies proposed and for some experimental studies, see references Basano *et al.*[119], Bianchi *et al.* [103], Cerutti *et al.* [100], Keselbrener & Akselrod [120], Lee & Nehorai [121], Mainardi *et al.* [122, 123], Novak *et al.* [96, 97]. The advantages of these methodologies are associated mainly with reducing the influence of nonstationarities and monitoring transient cardiac events occurring in long-term recordings.

In Cerutti *et al.* [100], a procedure of compressed spectral arrays (CSA) was implemented which can reduce the spectral data obtained from 24 hour ambulatory ECG recordings. The method was based on the calculation of AR spectral estimates for successive RR interval segments, and checking whether a new spectrum differs significantly from the preceding one.

Time-variant spectral analysis was introduced into HRV analysis by Lee & Nehorai [121], and particularly for the analysis of 24 hour ambulatory recordings by Bianchi *et al.* [103]. Here the AR parameters are estimated by the recursive least square (RLS) approach, and the time-variant power spectrum is given as

$$\hat{P}_{AR}(\omega, t) = \frac{\hat{\sigma}_e^2(t)}{\hat{A}(z, t)\hat{A}(z^{-1}, t)} \quad , \qquad z = \exp(i\omega) \quad ,$$

(3.29)

with $\hat{A}(z, t) = 1 + \sum_{k=1}^{p} \hat{a}_k(t) z^{-k}$ and t denoting the time index. Mainardi *et al.* [122] introduced two algorithms for recursive tracking of the pole displacements of an estimated AR model. The procedure was formulated and tested in more detail in Mainardi *et al.* [123]. The algorithms were based on the classical linearization approach and recursive calculation of the roots of a polynomial (Bairstow method).

The discrete Wigner distribution (DWD) was applied to heart rate variability analysis in Novak & Novak [96], and a modified algorithm was proposed for auto- and cross-DWD. The cross-terms were suppressed by means of a smoothing data window and a Gauss frequency window [97]. This approach has been employed

further in a study of the influence of respiration on heart rate [96], showing its ability to estimate spectral changes in nonstationary RR interval time series.

Keselbrener & Akselrod [120] proposed a selective discrete Fourier transform algorithm (SDA) for time-frequency presentation of cardiovascular time series. This approach is very close to the STFT, and involves calculating the spectra with short time windows, but SDA utilizes a shorter window for high frequencies in the spectrum and a wider window for low frequencies.

Fourier transform-, autoregressive and time-frequency representation (TFR)-based power spectral estimators applied to nonstationary time series are compared in Pola *et al.* [124], the results of which show that TFRs such as SPWD (smoothed pseudo Wigner distribution) and RWED (running windowed exponential distribution) should be utilized when good time resolution or the preservation of instantaneous power is essential. RWED has proved to be efficient in reducing the cross-term amplitudes, but SPWD is more capable of evaluating the mean power in the time-frequency plane. It can also be concluded that one problem entailed in the classical estimators is the dependence of the time resolution on the observation window, which often means a poor time resolution for the oscillations observed in cardiovascular time series.

On the whole, increased interest is being shown in time-variant spectral analysis or the monitoring of spectral parameters as a function of time. These techniques seem to offer approaches for overcoming the requirement for signal stationarity.

3.9. Wavelet analysis

The wavelet transform (WT) is a fairly new approach in the field of biomedical time series analysis, and only a few published articles exist on its use in HRV analysis, although it seems to possess some obvious advantages over classical time-frequency analysis methods, see Akay *et al.* [115] and Tsuji & Mori (1994). The motivation for applying the wavelet transform to the analysis of ECG signal and RR interval time series lies mainly in the monitoring of nonstationary signals and the long-term evolution of the power spectrum.

General and also more detailed theoretical discussions on the wavelet transform and its applications to biomedical signal processing can be found in references Akay (1995), Clouet *et al.* [15], Cohen & Kovacevic [126], Hess-Nielsen & Wickerhauser [127], Karrakchou *et al.* [128] Rioul & Vetterli [116], Thakor & Sherman [129] and Unser & Aldroubi [130]. WT as a tool in the time-dependent spectral analysis approach to stochastic processes has been discussed by Priestley [131], especially the term "frequency" in connection with nonstationary time series.

3.9.1. Continuous wavelet transform

As a starting point, the continuous wavelet transform (CWT) is introduced and then extended to the theory of discrete (multiresolution) wavelet and wavelet packet transform, which are used to decompose the signal. CWT is defined for a signal $x(t)$ by [132]

$$\mathcal{W}x(a,b) = \int_{-\infty}^{+\infty} x(t)\psi_{a,b}(t)\,dt \quad,$$

(3.30)

where a and b is the scaling and translation factor. Different versions of wavelet functions $\psi_{a,b}(t)$ are obtained from the basic wavelet by

$$\psi_{a,b}(t) = |a|^{-\frac{1}{2}}\psi(\frac{t-b}{a}) \quad,$$

(3.31)

where a and b are real numbers ($a \neq 0$). The wavelet function $\psi_{ab}(t)$ has a constant norm in the space $L^2(\mathbb{R})$ of square integrable functions due to the normalizing factor $|\alpha|^{-\frac{1}{2}}$. The continuous wavelet transform is invertible with [126]

$$x(t) = \frac{1}{C_\psi} \int_{-\infty}^{+\infty} \int_{-\infty}^{+\infty} \mathcal{W}x(a,b)\psi_{a,b}(t)\,\frac{da\,db}{a^2}$$

(3.32)

if the wavelet function satisfies the admissibility condition

$$C_\psi = \int_{-\infty}^{+\infty} \frac{|\hat{\psi}(\omega)|^2}{|\omega|} \, d\omega < +\infty \quad ,$$

where $\hat{\psi}(\omega)$ is the Fourier transform of the wavelet function $\psi_{a,,b}(t)$. The constant C_ψ is finite only if $\hat{\psi}(0) = 0$ or equivalently

$$\int_{-\infty}^{+\infty} \psi(t) \, dt = 0 \quad .$$

To ensure that the wavelet function decays quickly to zero and is thus well localized in the time domain, the following relation should be fulfilled [132]

$$\int_{-\infty}^{+\infty} (1 + |t|^\alpha)|\psi(t)| \, dt < +\infty \quad , \quad \alpha > 0 \quad ,$$

(3.33)

which is a subtly stronger condition than integrability of the function $\psi_{a,b}(t)$. This also satisfies the admissibility condition as $|\hat{\psi}(\omega)| \leq B|\omega|^\beta$ *with* $\beta = $ min $(\alpha, 1)$ B being a constant.

By analogy with the Fourier transform, which uses a complex exponential *exp(iωt)* as its basis function, the wavelet transform utilizes the function $\psi_{ab}(t)$ to represent a signal as a linear superposition of basic functions. The physical term frequency ω is related to complex exponential functions and does not have a direct interpretation when other functions such as wavelets are being considered (Priestley 1996). One can observe from the above formulation that wavelets are indexed with the parameters *a* and *b* instead of the variable ω. Actually, wavelet functions are located in time by the parameter *b*, while *a* denotes to the width of the wavelet. This leads to the interpretation that the wavelet transform can describe local properties of a time series *x(t)* in the neighborhood of each time point rather than global ones as the standard Fourier transform do.

It was shown earlier that the short time Fourier transforms $S_x^g(t, \omega)$ is a function of the variables *t* and ω that has a certain location in time. The width of the window *g(t)* was constant for all ω, so that all frequencies were evaluated with the same

resolution. In the case of wavelet transform, a large value of the scaling factor a stretches the basic wavelet function and allows the analysis of low frequency components of the signal. The small value of a gives a contracted version of the basic wavelet, and then allows the analysis of high-frequency components, respectively. In other words, the wavelet transform uses a short time interval for evaluating higher frequencies and a long time interval for low frequencies, high frequency components of short duration can be observed successfully. The properties naturally depend strongly on each wavelet function.

The frequency resolution of the wavelet transform is poor at high frequencies and good at low frequencies, which means that the time resolution at high frequencies will be good and that at low frequencies, will be poor [117]. The time-frequency resolution even in this case cannot be arbitrarily good, but is thus limited by the rules analogous to the well known Heisenberg's uncertainty principle.

Priestley [117] derived an expression for the time-dependent spectrum of a stochastic process:

$$E\{|a_{m,n}|^2\} \sim 2\pi h_t(\omega_m) \quad , \qquad t = n/2^m, \quad \omega_m = 2\pi 2^m \quad , \tag{3.34}$$

which allows the squared modulus of wavelet coefficients to be interpreted as a time-dependent spectrum. It is assumed here that the mother wavelet has a complex form $(t) = exp(2\pi it)$, and its squared Fourier transform $|\hat{\psi}m(\omega)|^2$ is suitably concentrated around $\omega = \omega m$. Although the term frequency should be understood with care and in a somewhat heuristic sense, time-frequency analysis is probably one of the most powerful features of the wavelet approach in this context.

3.9.2. Discrete wavelet transform

By choosing fixed values $a = \alpha_0^m$ and $b = nb_0 \alpha_0^m$, $m, n = 0, \pm1, \pm2, \ldots$, got for the discrete wavelet transform (DWT) [132]:

$$\begin{aligned} \mathcal{W}x(m,n) &= \langle x(t), \psi_{m,n}(t) \rangle \\ &= \int_{-\infty}^{+\infty} x(t)\psi_{m,n}(t) \, dt = a_0^{-m/2} \int_{-\infty}^{+\infty} x(t)\psi(a_0^{-m}t - nb_0) \, dt \quad . \end{aligned}$$

Values $\alpha_0 = 2$ and $b_0 = 1$ construct discrete wavelets $\psi_{m,n}(t) = 2^{-m/2} \psi (2^{-m} t-n)$ used in multiresolution analysis constituting an orthonormal basis for $L^2(\mathbb{R})$. To obtain a complete characterization of $x(t)$ using discretized wavelets $\psi m,n(t)$, and further, to recover $x(t)$ from the discrete transform in a numerically stable manner, wavelet function should constitute a frame. The transform between the signal and the wavelet function should be bounded above and below:

$$A \, ||x(t)||^2 \leq \sum_{m,n} |\langle x(t), \psi_{m,n}(t) \rangle|^2 \leq B \, ||x(t)||^2$$

(3.35)

with $A > 0$, $B < 1$. If frame bounds A and B are equal, then the frame is called tight.

3.9.3. Multiresolution wavelet analysis

In multiresolution analysis successive approximation subspaces Vj fulfill the property $Vj \subset Vj+1$ with

$$\overline{\cup_{j=-\infty}^{+\infty} V_j} = L^2(\mathbb{R}) \quad \text{and} \quad \cap_{j=-\infty}^{+\infty} V_j = 0 \ .$$

The multiresolution feature follows from the condition that all the spaces are scaled versions of the central space $V0$:

$$x(t) \in V_j \iff x(2^j \cdot) \in V_0 \ .$$

The space $V0$ has to be also invariant under integer translation:

$$x(t) \in V_0 \Rightarrow x(\cdot - n) \in V_0$$

for all $n \in \mathbb{Z}$. A scaling function $\varphi_{m,n}(t) \in V_0$ is also required which is an orthonormal basis in V_0, where $\varphi m,n(t) = 2^{-m/2} \varphi(2^{-m} t - n)$. Under these assumptions, the

multiresolution scheme involves an orthonormal wavelet basis of $L2(\mathbb{R})$, $\psi m, n\ (t)\ =\ 2 - m/2\ \psi(2 - m\ t\ -\ n)$ so that

$$P_{m-1}x(t) = P_m x(t) + \sum_{n=-\infty}^{+\infty} \langle x(t), \psi_{m,n}(t) \rangle \psi_{m,n}(t)\ ,$$

where *Pm* is the orthogonal projection onto space *Vm*. The signal *x(t)* is consequently obtained by

$$x(t) = \sum_{m,n=-\infty}^{+\infty} \langle x(t), \psi_{m,n}(t) \rangle \psi_{m,n}(t)\ .$$

The decomposition of the signal *x(t)* using discrete analysis wavelet functions $\psi j,k(t)$ and discrete scaling functions $\varphi K;k(t)$ can be given on different scales as follows:

$$x(t) = \sum_{j=1}^{K} \sum_{k=-\infty}^{\infty} d_j(k)\psi_{j,k}(t) + \sum_{k=-\infty}^{\infty} a_K(k)\phi_{K,k}(t)\ ,$$

where *dj(k)* are the wavelet coefficients (detailed signals) at scale 2^j and $\alpha_K\ (k)$ is the scaling coefficients (approximated signal) at scale 2^K. In Figure 17, the idea of discrete wavelet analysis is presented by means of a wavelet decomposition tree. A decomposition onto dyadic scales associates the frequency content of the signal and scales as

$$2^{-j} \leq \Delta\omega_j \leq 2^{l-j}\pi$$

for *j* = 1, 2,.... The signal spectrum includes the range $0\ -\ \pi$ rad and $\Delta\omega_j$ is the frequency band corresponding the level *j*.

3.9.4. Sub band filtering

Multiresolution analysis comprises a hierarchical and fast scheme to compute the wavelet coefficients of an analyzed signal. The scheme involves the computation

of sequentially coarser approximations of $x(t)$ and the difference in signals between two consecutive levels. In the sub band filtering approach the computation consists of the analysis and the synthesis steps which correspond to the decomposition and the reconstruction stages in wavelet analyses [133]. The discrete wavelet transform can be implemented by the scaling (low pass) and wavelet (high pass) filters

$$h(n) = \frac{1}{\sqrt{2}} \langle \phi(t), \phi(2t - n) \rangle$$

(3.36)

and

$$g(n) = \frac{1}{\sqrt{2}} \langle \psi(t), \phi(2t - n) \rangle = (-1)^n h(1 - n)$$

(3.37)
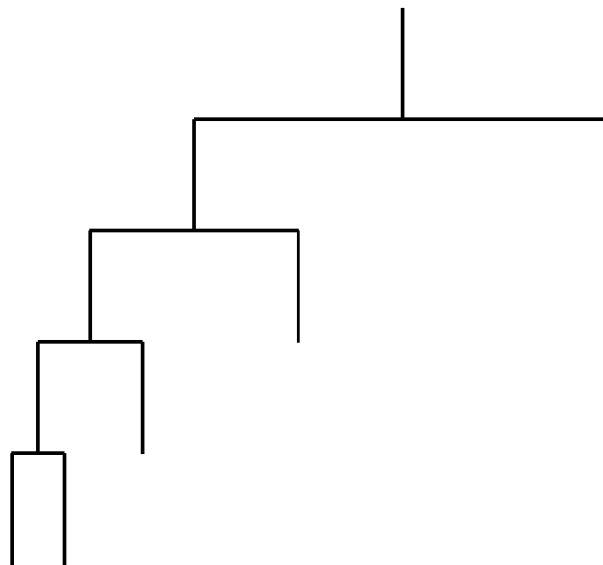
Figure 17. *A wavelet signal decomposition presented by a tree structure.[6]*

being quadrature mirror filters (QMF) [132]. The estimation of the detail signal at level j will be done by convolving the approximate signal at level $j-1$ with the coefficients $g(n)$. Convolving the approximate signal at level $j-1$ with the coefficients $h(n)$ gives an estimate for the approximate signal at level j. The analysis step (decomposition stage) involves filtering the approximate signal and retaining every other sample of the filter output (down sampling). The synthesis step then involves up sampling and filtering to obtain a reconstructed signal. In Figure 18, the

decomposition and reconstruction stages in a sub band filtering scheme establishing a filter bank are presented.

3.9.5. Wavelet packet analysis

If one defines the scaling function W0(t) = φ(t) and the wavelet function W1(t) = ψ(t), then it can be written for functions Wm(t), m = 0, 1, 2, …, as

$$W_{2m}(t) = 2 \sum_{n=0}^{2N-1} h(n)W_m(2t - n)$$

(3.38)

and

$$W_{2m+1}(t) = 2 \sum_{n=0}^{2N-1} g(n)W_m(2t - n) \quad .$$

(3.39)

53
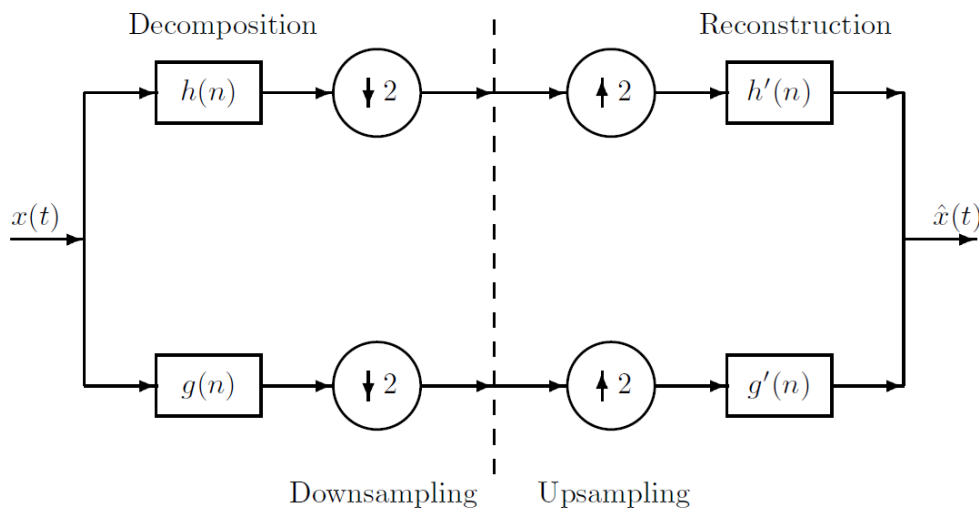
Figure 18. *A schematic presentation of a sub band filtering procedure using filter banks. The operations ↓2 and ↑2 stand for down sampling and up sampling by two.[6]*

The analyzing functions called wavelet packet atoms are given in an orthogonal case as

$$W_{j,m,n}(t) = 2^{-j/2}W_m(2^{-j}t - n) \quad ,$$

(3.40)

where j is a scale parameter, n is a time-localization parameter and parameter m gives roughly the number of "cycles" included in the oscillating waveform. Wavelet packet can be considered as a waveform whose oscillations persists for many cycles but are still finite. With fixed value of j the function $Wj,m,n(t)$ analyzes the signal around the position $2j \cdot n$ at the scale $2j$. The analyzed frequencies are roughly given by $n{=}2N$ with $n = 0, 1,..., (2j − 1)$.

Wavelet packet analysis is a generalization of wavelet analysis offering a richer decomposition procedure. Both detailed and approximated signals are split at each level into finer components. A set of details and approximations is called the wavelet packet decomposition tree.

3.9.6. Optimization of the wavelet packet decomposition

Wavelet (multiresolution) decomposition allows searching an optimal decomposition among L trees if a signal of length $N = 2^L$ has been decomposed at L levels. Wavelet packet analysis involves the selection of an optimal decomposition tree among at most 2^L different subtrees of depth L. The optimization can be based on e.g. the minimization of the entropy of analyzed signal, where the optimized decomposition is called the best tree. The idea is to look at each node of the decomposition tree and quantify the information to be gained by performing each split.
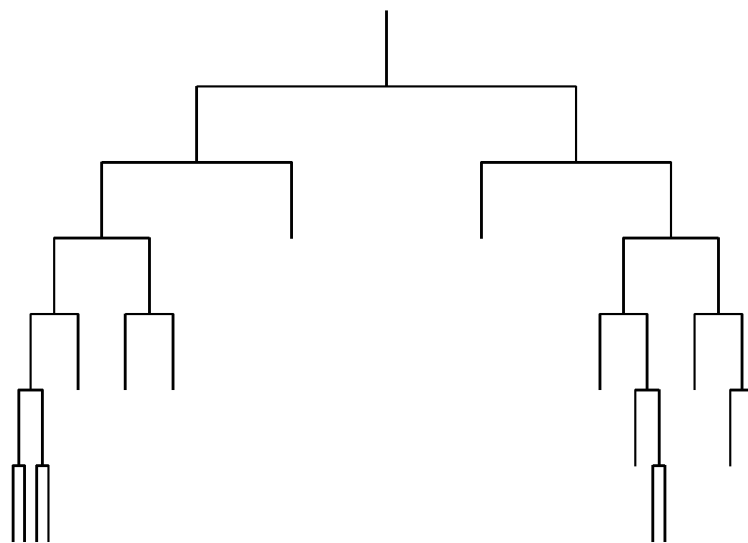
Figure 19. *A wavelet packet signal decomposition presented by an optimized tree structure.[6]*

The entropy can be obtained by many approaches, for example, the Shannon entropy [15] is defined as $\mathcal{E}(x) = \sum_t x^2(t) \cdot \log\left(x^2(t)\right)$. In Figure 19, the optimized wavelet packet decomposition tree is shown, which schematically presents the idea of this procedure.

3.10. ECG signal preconditioning

There are many sources of noise in a clinical environment that can degrade the ECG signal. A noisy ECG signal extracted from the MIT/BIH database is shown in Figure 20.
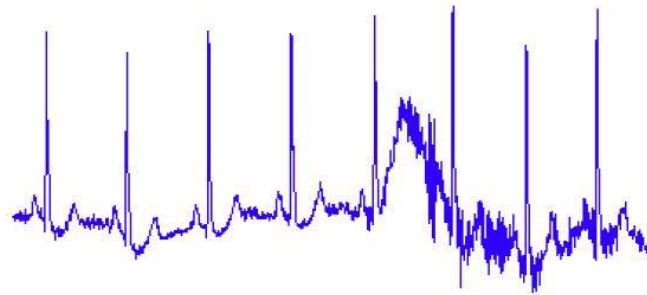
Figure 20. *Typical ECG signal with noise*

The common sources of ECG noise are:

- Power line interference,
- Muscle contraction noise,
- Electrode contact noise,
- Patient movement,
- Baseline wandering and ECG amplitude due to respiration,
- Instrumentation noise generated by electronic devices used in signal processing,
- Electrosurgical noise, and other, less significant noise resource.

A brief description of these noise signals will be discussed as follows (Friesen G. M. and Jannett C. T. et al., 1990) [134]:

Chapter 3: Analysis of signal variability

- Power line interference

Power line interference consists of 50 Hz pickup and harmonics, which can be modeled as sinusoids and combination of sinusoids (Furno G. S. and Tompkins W. J., 1983). Typical parameters: Frequency content-50 Hz (fundamental) with harmonics; Amplitude-up to 50 percent of peak-to-peak ECG amplitude.

- Muscle contraction noise,

Muscle contraction noise causes artificial milivolt-level potentials to be generated. The baseline electromyogram is usually in the microvolt range and therefore is usually insignificant. Typical parameters: Standard deviation-10 percent of peak-to-peak ECG amplitude; Duration-50 ms; Frequency content-dc to 10000 Hz.

- Electrode contact noise,

Electrode contact noise is transient interference caused by loss of contact between the electrode and skin, which effectively disconnects the measurement system from the subject. Typical parameters: Duration-1s; Amplitude-maximum recorder output; frequency-50 HZ time constant-about 1s.

- Patient movement,

Patient movements are transient (but not step) baseline changes caused by variations in the electrode skin impedance with electrode motion. Typical parameters: Duration-100-500 ms; amplitude-500 percent of peak-to-peak ECG amplitude.

- Baseline wandering and ECG amplitude due to respiration,

The drift of the baseline with respiration can be represented as a sinusoidal component at the frequency of respiration added to the ECG signal. Typical parameters: Amplitude variation-15 percent of peak-to-peak ECG amplitude; Baseline variation-15 percent of p-p ECG amplitude variation at 0.15 to 0.3 Hz

- Instrumentation noise generated by electronic devices used in signal processing, and artifacts generated by electronic devices in the instrumentation system.

- Electrosurgical noise,

Electrosurgical noise completely destroys the ECG and can be represented by a large amplitude sinusoid with frequencies approximately between 100 kHz and 1 MHz. Typical

parameters: Amplitude-200 percent of peak-to-peak ECG amplitude; Frequency content-Aliased 100 kHz to 1 MHz; Duration-1-10s.

Motivation

The frequency of the baseline wander, as stated before, is usually in a range below 0.1 Hz in rest ECG and 0.65 Hz during stress test. Therefore, its presence will be reflected in the higher level DWT approximation coefficients. This is actually the basic phenomenon behind this approach aiming to eliminate the distortion of baseline wander in measured ECG signals. This elimination is accomplished by decomposing the noisy ECG signal, contaminated with baseline wander into a certain number of levels n using Discrete Wavelet Transform (DWT). The highest level , i.e. the nth level, approximation coefficients (AC) are supposed to represent the low frequency baseline variation signal. In the filtering algorithm proposed here, the nth level AC are set to zeros. When a mother wavelet, e.g. coifflet 4, is arbitrarily chosen and DWT decomposition is carried out on one ECG signal with a sample frequency equal to 1 kHz, it was noticed that each of the $8th$, $9th$ and $10th$ level approximation coefficients, when time-aligned to the original ECG, resemble the baseline wander. Figure 20 shows this resemblance. It is not very clear, as seen from figure 20, which level approximation coefficients represent the baseline wander signal the best in general. However, the following two issues need to be further investigated:

1. Which mother wavelet should be applied for DWT analysis on the noisy ECG to achieve the best results?
2. What value of n should be chosen? In other words, up to which level the ECG signal needs to be decomposed?

In order to answer these two questions, the following simulation is carried out.

Simulation

Before dealing with real ECGs, artificial signals were chosen for experimentation. These artificial signals are in fact mixtures of artificial free-of-noise

---

ECG signals and artificial baseline variation signals. Thus, with a clear knowledge of the component signals, the performance of filtering could be judged.
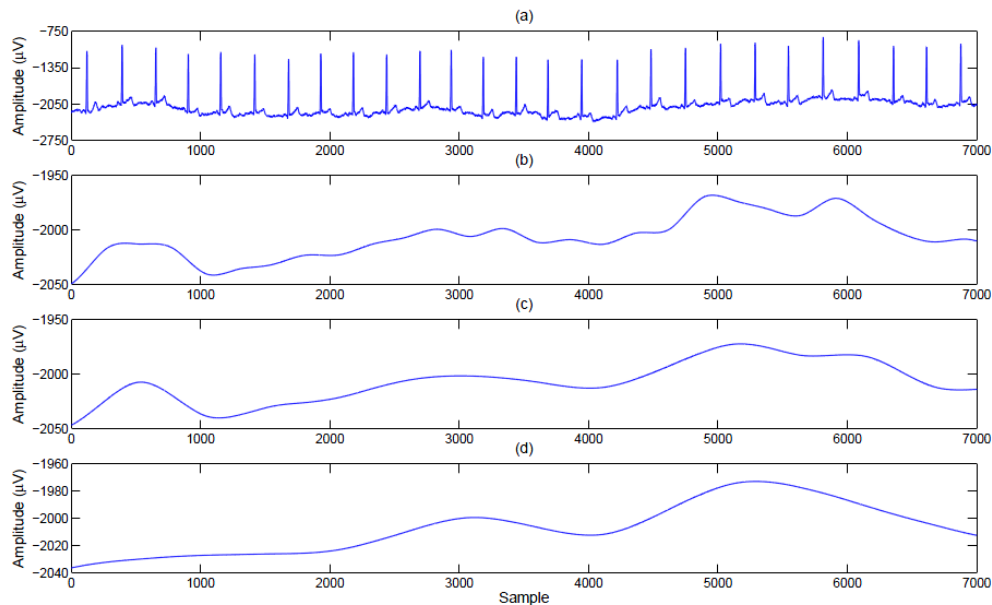
Figure 21. *The 8th, 9th and 10th level approximation coefficients for an ECG signal with a sample frequency equal to 1 kHz and using Symlet4 as mother wavelet: (a) the ECG signal (b) the 8th level approximation coefficients (c) the 9th level approximation coefficients (d) the 10th level approximation coefficients.[135]*

Artificial noise-free ECG beats were generated by means of the algorithm used to generate noise-free ECG for Savitzky-Golay filter simulator and filter in *Matlab* Environment (Signal Processing Toolbox). Figure 22 shows an example of the generated noise-free ECG . The sampling frequency was assumed to be 1 kHz, or in other words the span of 1000 samples is 1 second. The data length was taken to be 25000 samples, i.e. 25 seconds. In this case each beat should have a span of 1000 samples for 60 bpm (beats per minute) ECG and hence there would be 25 beats in total. For different bpm, the span of ECG beat was varied accordingly and hence the total number of ECG beats. To find out the suitable mother wavelet and the decomposition level n, tests were carried out on 650 artificially generated noisy ECG signals. Thirteen noise-free ECG signals in the range of 60 to 180 bpm (increment step value of 10 bpm) were created as discussed above. At the same time, a set of fifty sinusoidal signals with frequencies ranging from 0.01-0.5 Hz (with increment step

value of 0.01 Hz) were created in order to simulate the baseline wander. Thereafter, as result, 650 test signals in total were synthesized by mixing the artificial ECG signals with artificial baseline wander signals in one to one correspondence. Now, on each of the 650 test signals, the mixture signals, DWT analysis was carried out taking a total of 29 mother wavelets under consideration, i.e. symlet1, symlet2, ... symlet12, coiflet1, coiflet2, ... coiflet5, Daubechies1 (Haar), Daubechies2, ..., Daubechies12. By applying DWT decomposition a symmetric boundary value replication of the signal under decomposition in each level is employed during the convolution with analysis filters or synthesis filters in order to deal with border distortions. The extension is done on both sides with the length of the half of the low-pass filter or high-pass filter. On every test signal, for each of the mother wavelets, the following procedure was adopted.
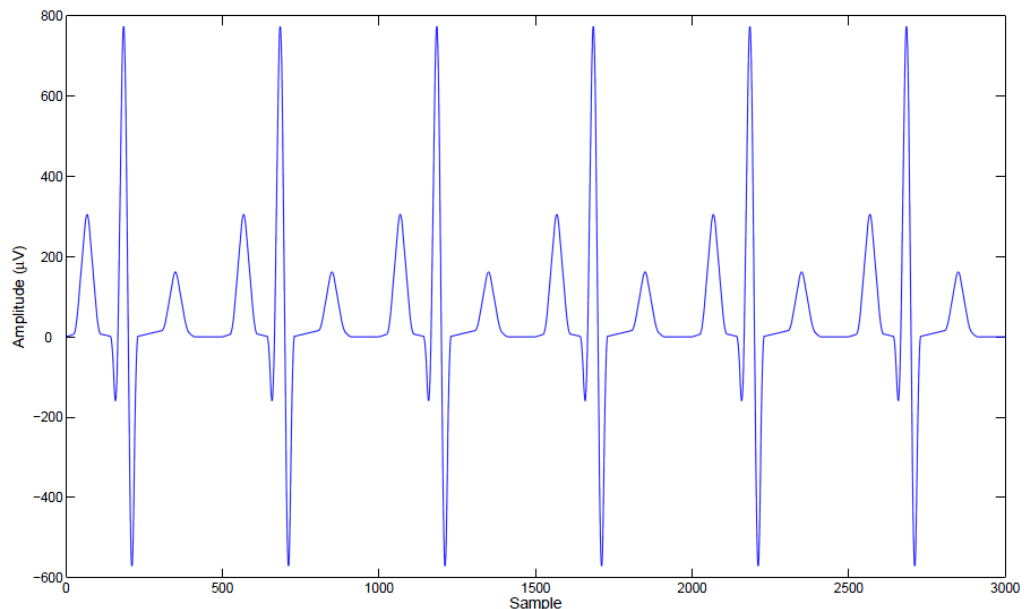
Figure 22. *An example of the noise-free ECG generated by Savitzky-Golay filter simulator in Matlab environment. The sample frequency is 1kHz and the heart rate is 120 beats per minute.[135]*

1. Initialize n=1; i.e. no. of decomposition levels for DWT.
2. Decompose the test signal till *n* levels (maximal n here is chosen equal to 12) and get the DWT coefficients An, Dn, $Dn-1$, $Dn-2$,...,$D1$, where Ai = ith level approximation coefficients and Di = ith level details coefficients.

3. Perform the following two reconstructions:

- *First Reconstruction*: With *An* to be all zeros, a reconstruction of the signal is possible. The signal, reconstructed in this way is called the *ECG reconstruction*. It should resemble the original noise-free ECG (with which the test signal is synthesized) for higher values of n.

- *Second Reconstruction*: Set all the coefficients other than *An* (i.e. the details coefficients, *Dn*, ..., *D*1) to zeros and reconstruct the signal. The signal, reconstructed in this way is called the *Baseline Reconstruction*. It should resemble the original baseline variation signal (with which the test signal is synthesized) for higher values of *n*.

4. Judge the resemblance between the original and reconstructed signals by means of correlation. Two correlation coefficients (*CE* & *CB*) were calculated, where *CE* is the percentage result correlation between the original noise-free ECG and the *ECG reconstruction*, or *First Reconstruction* and *CB=* correlation between original baseline variation signal (low frequency sinusoid) and the 'baseline Reconstruction'.

5. Repeat steps 2 to 4 for *n* = 1,...,12.

6. Furthermore, the whole above-mentioned process from step 1 to 5 was repeated for 29 different mother wavelets applied on the same test signal. Finally, for each test signal, two matrices were constructed, the first one includes all *CE* values and the other one includes all *CB* values. Each matrix is of size 12×29 and has the structure illustrated in figure 23.
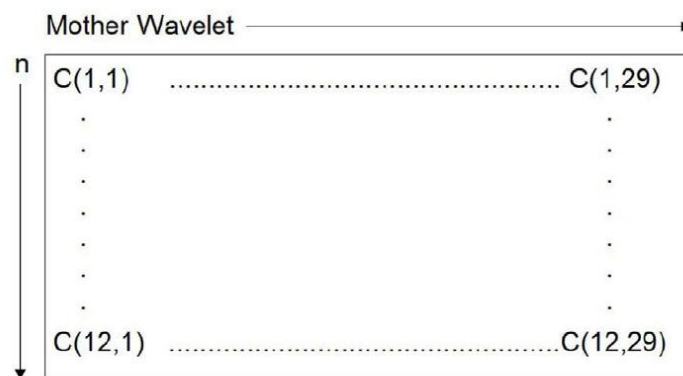
Figure 23. *The structure of each matrix derived from the baseline simulation process: C*

devotee either CE or CB. The 1st to 12th column represents Symlet Wavelets of 1st to 12th order (sym1, sym2, ...sym12), the 13th to 17th column represents ₁, Coiflet Wavelets of 1ˢᵗ to 5th order (coif1, coif2, ... coif5) and the remaining 18ᵗʰ to 12ˡʰ column represents Daubechies Wavelets of 1ˢᵗ to 12ˡʰ order (db1, db2, ..., db12,). For 650 test signals, there were 1300 correlation matrices in total, half for CEs and half for CBs. In addition two more matrices were computed, the first one is denoted as CE_{mean} and represents the mean matrix of the 650 CE matrices, whereas the second one is denoted as CB_{mean} and represents the mean matrix of the 650 CB matrices[135]

<u>Simulation Result</u>

At this stage, the positions of the first L greatest elements in both matrices. CE_{mean} and CE_{mean}, were identified. The value of L was taken in this case equal to five. $L = 5$, because only the five greatest values in both matrices were greater than 99.99%. The positions are found to be exactly the same in both matrices, that is, the highest element occurs in the same position (same row and column number) in both matrices . The same is also true for 2nd highest and so on. All of these five highest elements are found at the row corresponding to n = 9.

<u>Discussion</u>

From the simulation result, the baseline wander signal can be located perfectly at the 9th level approximation coefficients of Daubechies11 mother wavelet from a baseline-wander distorted ECG signal sampled at 1000 Hz.

Table 2. *Results obtained from the baseline simulation done on 650 artificial test signals*

Order No.	Mother Wavelet	n	mean $CE\%$	mean $CB\%$
1	db11	9	99.9924	99.9150%
2	sym12	9	99.9913	99.9011%
3	sym10	9	99.9909	99.8962%
4	db10	9	99.9906	99.8925%
5	coif5	9	99.9904	99.8894%

Depending on subband theory in DWT, the 9th level approximation coefficients of a signal sampled at 1000 Hz represents the signal in the [0 - 0.9766] Hz range. Therefore, some adaptation procedures are required for the system to handle

equivalently ECG signals with different sampling frequencies. One of these procedures is simply to resample the signal under study to 1000 Hz. This procedure is actually a time-demanding solution, especially in the case of multi-channel ECG or long-time ECG.

The second possible solution is to calculate the frequency band for all possible approximation coefficients decomposition levels of Daubechies11 mother wavelet, and then choose the frequency band nearest to the one obtained with the simulation, namely the [0-0.9766] Hz range. The corresponding decomposition level to that chosen band is indeed the level whose approximation coefficients need to be canceled. This method is able to eliminate the baseline drift without any distortion of ST segment as observed with conventional high pass filters, namely the second order Butterworth filter with 0.5 Hz cut off frequency (see figure 24). Moreover, it can be applied equally well to short and long duration ECG signals. This filtered ECG shows around 97% similarity to the noise-free ECG. [130]
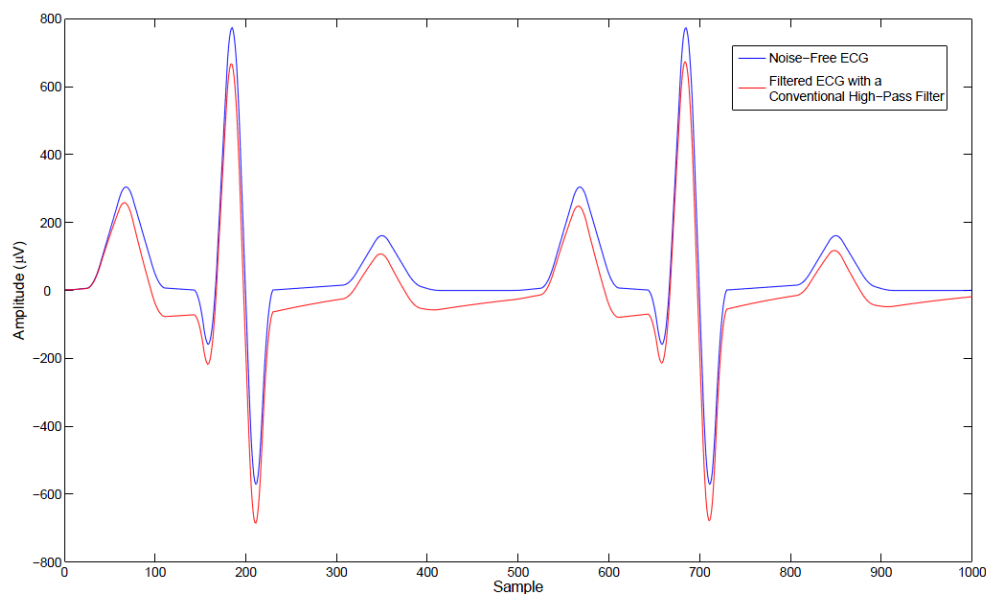
Figure 24. *The influence of using a high-pass filter to remove the baseline wander on the ECG morphology and ST segment: In blue: the original noise-free ECG signal sampled at 1kHz and added to artificial 0.1 Hz baseline wander sin signal. In red: the filtered ECG obtained using the second order Butterworth filter with 0.5 Hz cut off frequency. The similarity (percentage correlation coefficients) between the noise-free and the filtered ECG signals is equal to 96.9 % and a large distortion in ST segment and the ECG morphology is noticed.[135]*

3.11. Non-linear and scale-invariant analysis of the Heart rate

The heart rate of healthy subjects fluctuates in a complex manner. These nonstationary and nonlinear fluctuations are related mainly to a nonlinear interaction between competing neuroautonomic inputs: parasympathetic input decreases and sympathetic stimulation increases the heart rate. Meanwhile, heart pathologies may decrease the responsiveness of the heart and lead to a failure to respond to the external stimuli. Evidently, such pathologies lead to an overall reduction of the heart rate variability (HRV). Understanding the diagnostic and prognostic significance of the various measures of HRV has a great importance for the cardiology as a whole, because unlike the invasive methods of diagnostics, the required measurements are low-cost and are harmless for the patients. A particularly important application is the prognostics of the patients with increased risk of sudden cardiac death. While the "linear measures" of HRV are nowadays widely used in clinical practice, the importance of more complicated measures has been hotly disputed in the scientific literature during the recent decades.

3.11.1. Scale-independent measures

Recent studies have shown that scale-invariant characteristics can be successfully applied to the analysis of the heart rate variability (132-135). However, this conclusion has been disputed and certain scale-dependent measures (particularly, the amplitude of the wavelet spectra at specific time-scale) have been claimed to provide better results [137]. The scale independent methods have been believed to be more universal, subject-independent, and to reflect directly the dynamics of the underlying system, unlike the scale-dependent methods which may reflect characteristics specific to the subject and/or to the method of analysis [138]. Opposing argument has been that certain heart disorders affect the heart rate variability at a

specific scale or range of scales; owing to this circumstance, at the properly chosen time-scale, scale-dependent measures may provide a useful information [137].

The simplest relevant scale-independent measure is the Hurst exponent H, which has been introduced to describe statistically self-affine random functions $f(r)$ of one or more variables [139]. Such a function is referred to as fractional Brownian function and satisfies the scaling law

$$\langle [f(r1) - f(r2)]^2 \rangle \propto |r1 - r2|^{2H}.$$

Note that $H = 1/2$ is a special case of ordinary Brownian function — the increments of the function are delta-correlated, and $f(r)$ can be thought to be the displacement of a Brownian particle as a function of time r. Therefore, in the case of $H < 1/2$, there is a negative longrange correlation between the increments of the function. Analogously, $H > 1/2$ corresponds to a positive correlation. Note that the early scale-invariant studies of HRV were based on power spectra [44, 47], an aspect closely related to the scaling exponent H.

Many phenomena in nature exhibit this kind of scale-invariance, and lead to fractional Brownian time-series [139]. The same is true for the heart rate variability: after filtering out short-scale components with $\tau < 30s$ (corresponding to the respiratory rhythm, to the bloodpressure oscillations, and to the pathological Cheyne-Stokes respiration), the fluctuation function $F(n)$, defined as

$$F(v) = \langle |t_n - t_{n+v}| \rangle \qquad (3.41)$$

revealed a good scaling behavior $F(v) \propto v^H$[140]. While for healthy patients, the increments of the heart rhythm were found to be significantly anticorrelated resulting in $H < 1/2$, the heart rhythm of the patients with dilated cardiomyopathy was essentially Brownian with $H \approx 1/2$ [132]. In the case of the patient groups, there was no significant correlation between the diagnosis and the Hurst exponent, and there were many healthy subjects with $H \approx 1/2$, see Figure 25 Finally, various techniques, such as detrended fluctuation analysis [141], detrended time series analysis [142], and wavelet amplitude analysis [143] have been proposed to fine-tune the Hurst-exponent-based approach.
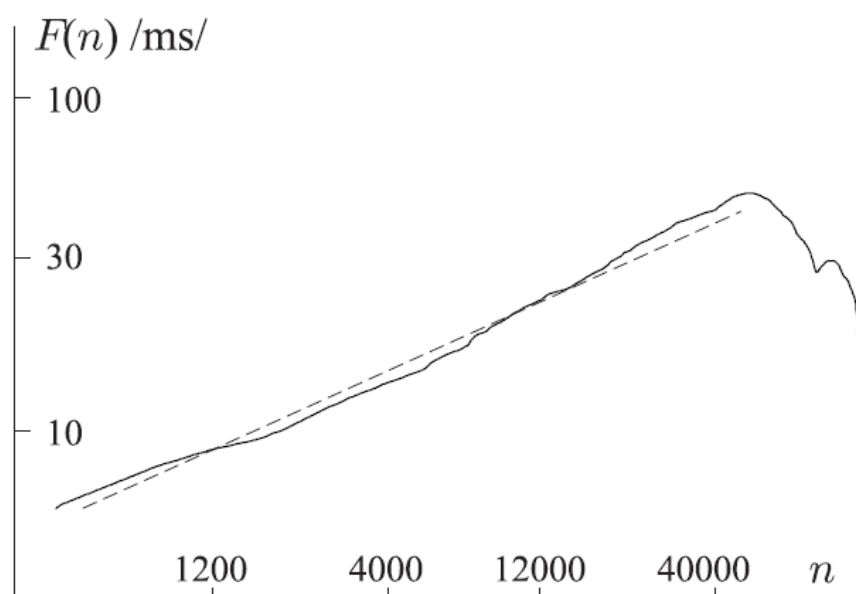
Figure 25. *The fluctuation function F(v) is plotted versus the time lag _. Almost straight line indicates a good scaling behavior $F(v) \propto v^H$ (here with $H = 0.50$).[135]*

Complex non-stationary time-series cannot be described by a single scaling exponent H. Indeed, simple scaling behavior is expected if there is a Gaussian distribution of increments. However, even in the case of Gaussian functions, the scaling exponent is not necessarily constant over the whole range of scales. Instead, it can be a slow (eg. logarithmic) function of the scale, so that other descriptions (such as stretched exponentials) may be required. Physiological time-series are typically non-Gaussian. For such functions, scale-invariance can be very complicated. A non-exhaustive way to describe such behavior is to calculate the multifractal spectrum of Hurst exponents [144]. Therefore, it is not surprising that the human heart rate signal was found to obey a multi-affine structure [145,138].

Qualitatively, a multifractal time-series behaves as follows. If the whole time-series is divided into short segments, each segment can be characterized by its own Hurst exponent h (referred to as the Lipschitz-Holder exponent). Then, the distribution of segments of fixed values of h is self-similar, and is described by a

fractal dimension $f(h)$. Technically, the spectrum $f(h)$ can be calculated by the means of wavelet transform, cf. [138]. This scheme includes the calculation of the scaling exponents $\tau(q)$ (referred to as the mass exponents), which describe, how the $q - th$ moment of the wavelet transform amplitude scales with the wavelet width. The scaling exponents $\tau(2)$ and $\tau(5)$ have been found to have a significant prognostic value (for the post-infarction prognosis) [138]. The wavelet transform amplitudes, calculated for a specific wavelet width ($\approx 5\,min$) have been claimed to be of even higher prognostic value [137]. However, independent studies have shown that the scale-invariant measures seem to be superior tools [146]. It should be also noted that the wavelet transform amplitude at a fixed time-scale is closely related to the linear measure SDANN. Substituting the robust standard deviation by a wavelet transform amplitude is a technical fine-tuning which cannot be expected to result in a qualitatively new information.

The multifractal structure of the heart rate signal has several consequences. Thus, the $q - th$ order structure function (a concept borrowed from the theory of the fully-developed turbulence) of the heart rate interval has a scaling behavior, with the scaling exponent $\zeta(q)$ being a function of q [147]. Note that this spectrum of exponents is very closely related to the above-mentioned $\tau(q)$ spectrum (both describing the same physical phenomenon, differences being of a technical kind). However, the wavelet-transform-based technique makes a more complete utilization of the underlying data and therefore, $\tau(q)$ spectrum can be expected to yield somewhat superior prognostic and/or diagnostic results.

Another aspect related to the multifractal nature of the heart rhythm, is the multiscale entropy (MSE) [148]. While the single-scale entropies (approximate entropy, Shannon entropy) are related to the short-time dynamics of the heart rhythm and to the probability distribution function of points in the reconstructed phase space, the multiscale entropy extends these concepts to longer time-scales. MSE is not directly reducible to the multifractal spectra $f(h)$ [or $\tau(q)$]; however, both techniques address the question of how wide is the range of dynamics for the mean heart rate (averaged over a time T), depending on the time-scale T. The clinical usefulness of the MSE is still unclear (apart from the fact that it has been claimed to distinguish between healthy subjects and patients with congestive heart failure [148])

3.11.2. Intermittency of the HRV

Multifractal spectrum addresses only one aspect of the non-Gaussianity of the time-series increments by revealing the possible range of scaling laws for the long-range [at time-scale of many ($\gg$ 1) heartbeat intervals] dynamics of mean heart rhythm. However, the short time variability of heart rhythm is also fluctuating in a complex manner. It has been pointed out that the NN-sequences of healthy subjects consist of intertwined high- and low variability periods [149]. This conclusion can be easily verified by a simple visual observation of the NN-sequences, see Figure 26. The quantitative analysis of such a behavior is based on the distribution law of the low variability periods [150],
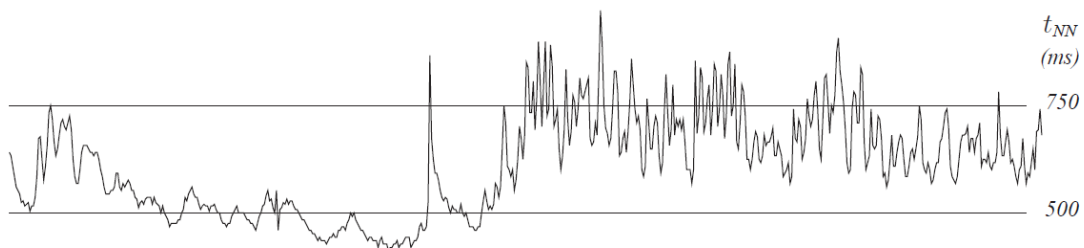
Figure 26. *For healthy patients, the high- and low-variability periods of the heart rhythm are intertwined.[135]*

which will be discussed below. Another aspect of such an intertwining is the clustering of the periods of similar mean heart rate: the heart rate signal can be divided into segments of different mean heart rate, with distinct boundaries between these segments; there is a power-law segment-length distribution of the segments [151].

In order to analyze quantitatively the intertwining of high- and low-variability periods, distribution of low-variability periods and showed that typically was studdied, it follows a multi-scaling Zipf's law. Originally, the Zipf's law has been formulated by G. K. Zipf for the frequency of words in natural languages [52]. For a given language (e.g. English), the frequency (the number of occurrences divided by the total number of words) of each word is calculated on the bases of a large set of

texts. The ranks are determined by arranging the words according to their frequency f: the most frequent word obtains rank $r = 1$, the second frequent — $r = 2$ etc. It turns out that for a wide range of ranks (starting with $r = 1$), there is a power law $p(r) \propto r^{-a}$, where $a \approx 1$. This law is universal, it holds for all the natural languages and for a wide variety of texts [152]. Furthermore, similar scaling laws describe the rank-distribution of many other classes of objects, as well. Thus, when cities are arranged according to their population s, the population of a city $s \propto r^{-a}$_, with $a \approx 1$ [152]. Another example is the income-rank relationship for companies; here again $a \approx 1$ is seen[152]. In the most general form, the law can be formulated as $p \propto (r + r0)^{-a}$, and a is not necessarily close to unity [144]. This more general form of the law can be applied to the distribution of scientists according to their citation index, to the distribution of internet sites according to the number of visitors etc. The Zipf's law is characteristic to such dynamical systems at statistical equilibrium, which satisfy the following conditions: (a) the system consists of elements of different size; (b) the element size has upper and lower bounds; (c) there is no intermediate intrinsic size for the elements. The human heart rate, when divided into the low-variability periods, satisfies all these requirements. The duration of these periods varies in a wide range of scales, from few to several hundreds of heart beats. Thus, one can expect that the rank-length distribution r follows the Zipf's law,

$$r \propto \tau^{-\gamma}. \tag{3.42}$$

First a definition of the local heart rate variability as the deviation of the heart rate from the local average has to be made,

$$\delta(n) = [t_{NN}(n) - \langle t_{NN}(n) \rangle] / \langle t_{NN}(n) \rangle;$$

the local average is calculated using a narrow ($\approx$ 5-second-wide) Gaussian weight-function. Then, the low-variability regions are defined as consecutive sequences of intervals with $|\delta(n)| < \delta 0$; the length τ of such a region is measured as the number of beats in the sequence. Further, all the low-variability regions are numbered (to identify them later), and arranged according to their length; regions of equal length are ordered randomly. In such a way, the longest observed region obtains rank

$r = 1$, second longest — $r = 2$, etc. Typically, the length-rank relationship reveals multiscaling properties, i.e. within a certain range of scales, the scaling law (2) is observed, the scaling exponent being a (non-constant) function of the threshold level, $\gamma = \gamma(\delta 0)$; see Fig. 2.13.
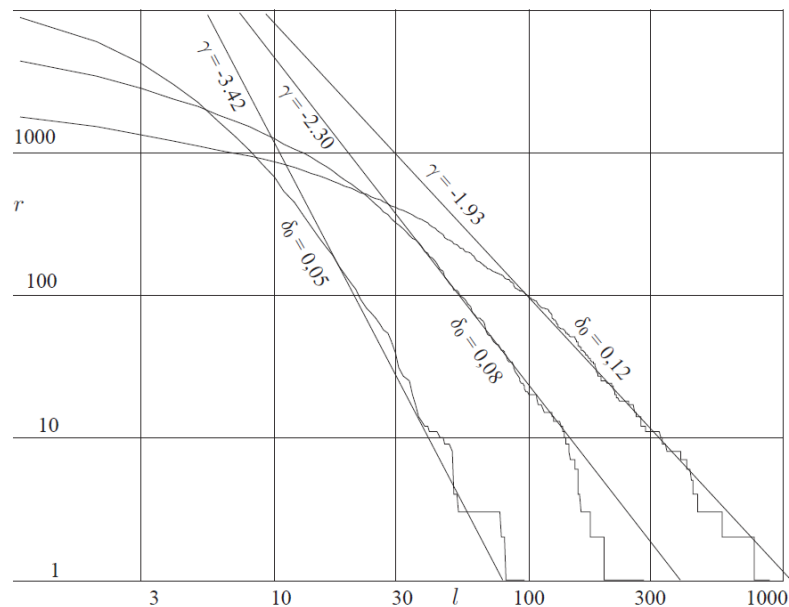
Figure 27. *Multi-scaling behavior: the rank of low-variability intervals is plotted against the length of the intervals. The scaling exponent depends on the threshold value $\delta 0$.[135]*

It is not surprising that the scaling behavior is not perfect. Indeed, the heart rhythm is a non-stationary signal affected by the non-reproducible daily activities of the subjects. The non-stationary pattern of these activities, together with their time-scales, is directly reflected in the rank-length law. This distribution law can also have a fingerprint of the characteristic time-scale (10 to 20 seconds) of the blood pressure oscillations (which modulate the level of HRV, cf. [21, 61]). It should be emphasized that the problem of the non-reproducible daily activities affects also the reliability of the other scale-invariant measures and is probably the main obstacle preventing the clinical application of the seemingly extremely efficient diagnostic and prognostic techniques. Finally, there is a generic reason why the Zipf's law is non-perfect at small rank numbers: while the Zipf's law is a statistical law, each rank length curve is based only on a single measurement. In particular, there is only one longest low-

variability period (likewise, only one most-frequent word), the length of which is just as long as it happens to be, there is no averaging whatsoever. For large ranks, the relative statistical uncertainty can be estimated as $1/\sqrt{r}$. The distribution function of the low-variability periods as a whole contains a significant amount of diagnostically valuable information, which is not covered by any other (linear or nonlinear) measure of HRV. The most part of this information seems to be reflected (according to the Student test analysis using the test groups of Table 1) by the parameters $r100$ (the rank of the interval with $r = 100$), $rmax$ (the maximal observed rank), and τend (the scale at which the scaling law breaks; for a precise definition [150]). These measures allow a clear distinction between the healthy subjects and the IHD, VES, and PCI groups [142], see also Table 3.

TABLE 3: *p-values of the Student test. Data in the topmost triangular region (with label A) are calculated using the parameter ln τend. Triangular region B corresponds to the parameter ln rmax [64]. Gray background highlights the tests with the adjusted significance p′ < 3%. The control parameter value $\delta_0 = 0.05$ has been used.*

p (%)	Healthy	IHD	SND	VES	PCI	RR	FSK
Healthy	B ⟍ A	0.06	17.21	0.02	0.07	1.59	1.55
IHD	0.36		2.85	96.79	97.62	21.93	20.05
SND	2.99	59.10		2.10	3.04	25.77	25.57
VES	0.08	91.60	63.79		94.18	17.59	16.20
PCI	25.27	21.61	46.37	22.89		22.50	20.62
RR	0.14	73.57	77.69	80.49	28.90		98.20
FSK	46.48	5.20	8.72	5.52	20.06	6.45	

3.12. Common heart rhythms and arrhythmias

Above the ways an ECG should be performed in general were referred, next follows the most common heart rhythms and arrhythmias as presented in an ECG graph. The electrical impulses generated in the SA node control the rhythm of the heart. Any disturbance of the normal sinus rhythm is called arrhythmia. In general, arrhythmia may occur in the heart either when depolarization is initiated by other pacemaker cells exhibiting accelerated automaticity as compared to the SA node, or when the conduction of the electrical impulses is altered, that is, when the conduction of the cardiac cells is partially or completely blocked causing a propagation delay of the impulse or conduction failure [153, 154, 155, 156]. Arrhythmia can be classified regarding the site of its origin.

3.12.1. Sinus Rhythm

SA node is the original source for the normal sinus rhythm with a rate between 50 and 100 beats per minute at rest. Sinus bradycardia and sinus tachycardia are defined as a rhythm below 50 and above 100 respectively. The heart rate is influenced by external perturbations like physical and mental stress and it is influenced by the continual variation of the balance between the parasympathetic and the sympathetic activities of the autonomic nervous system. Numerous studies on analyzing the dynamics of spontaneous heart rate variability has been done during the recent years. This research aimed for diagnosing and predicting cardiovascular diseases and life-threatening arrhythmias [157, 158, 159].

3.12.2. Premature Beats

The normal sinus rhythm is sometimes interrupted by a beat occurring before the expected time of the next sinus beat and is therefore referred to as a premature beat. In addition the terms 'ectopic beat' and 'extrasystole' are frequently used synonyms [155]. When the ectopic beat is originated from the atria, it is called supraventricular premature beat (SVPB) and when its origin is from the ventricles, it

is called ventricular premature beat (VPB). Ventricular premature beats, also known as premature ventricular contraction (PVC) or heart palpitations, are characterized by a premature broad QRS complex with duration greater than 120 ms, and without preceding P wave, see figure 28.
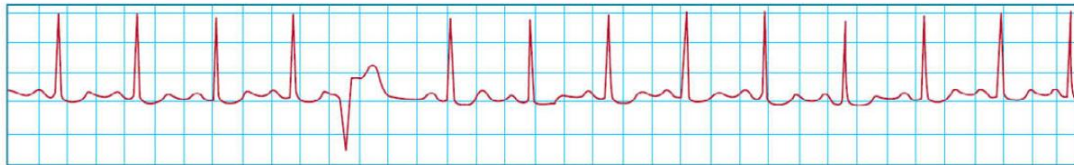
Figure 28. *The premature ventricular contraction (PVC).[160]*

Bigeminy, Trigeminy and Quadrigeminy are defined as every normal beat is followed by one, two and three premature beats respectively, see figure 29. as an example of Bigeminy.

Figure 29. *An example of Bigeminy[160]*

Whereas, if a premature beat occurs after one, two, or three normal beats, they will be defined as (1:1 extrasystole), (2:1 extrasystole) and (3:1 extrasystole) respectively. Two consecutive VPBs are called a couplet, see figure 30; three consecutive VPBs are called a triplet. Three or more consecutive VPBs are called a salvos or ventricular tachycardia. In VPBs the ventricular impulses are conducted retrogradely to the atria, at least partially. Therefore about 50% of them are discharging the sinus node. Monomorphic VPBs are called also unifocal because they generate from the same focus. Whereas, Polymorphic VPBs generate from the several focus. Most of the VPBs have a right bundle-branch block (RBBB)-like pattern or right bundle-branch block (RBBB)-like pattern.
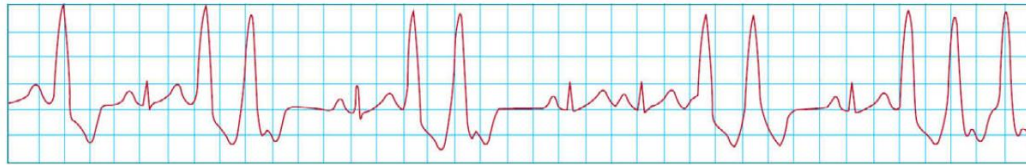
Figure 30. *An example of Couplet.[160]*

3.12.3. Atrial Arrhythmia

One or multiple atrial ectopic foci are responsible for many of the various rhythm disturbances causing atrial arrhythmias. If the ectopic focus is located between SA node and AV node, the P wave will be abnormal and sometimes negative in the ECG. When the ectopic focus is located near to the AV node the atria and the ventricles will be depolarized at the same time making P wave coincide with QRS complex in the ECG.

3.12.3.1. Atrial Tachycardia

Increasing the automacity in the pacemaking cells of one or multiple foci within the atria, atrial tachycardia will increase the heart rate. The P wave sometimes appears in the ECG coinciding with the previous T wave or even the previous QRS complex [149155

3.12.3.2. Atrial Flutter and Atrial Fibrillation

In these kinds of atrial tachyarrhythmias, the atria and the ventricles are not synchronized. The cause of both arrhythmias is a continuous reentry of an electrical impulse in the atria. The reentry mechanism starts when an impulse depolarizes receptive myocytes neighboring an area of relatively longer refractory periods. When the originally inactive area becomes activated, the impulse may propagate back towards the area which was initially depolarized. If the latter has had time to recover and to depolarize again, the reentry circle will be repeated. The high rate of atrial contraction will lead to a slow blood inflow through the atria increasing the chance for a clot to be produced [155]. The clot afterwards might cause a stroke or severe

damage to any other part of the body. In case of atrial flutter, the atria beat regularly at a rate of around 300 beats per minute. The ventricles are protected from this high rate by a refractory AV node. In the ECG, a sawtooth-like regular waveform, also called F waves or flutter waves, appears, see figure 31. Atrial fibrillation is a faster and more chaotic rhythm than atrial flutter. This kind of arrhythmia is produced by multiple reentry circuits within the atria producing a high rate of atrial contraction between 400 and 700 beats per minute in a chaotic fashion. Fibrillation waves, f waves, are multiform and irregular, see figure 32.
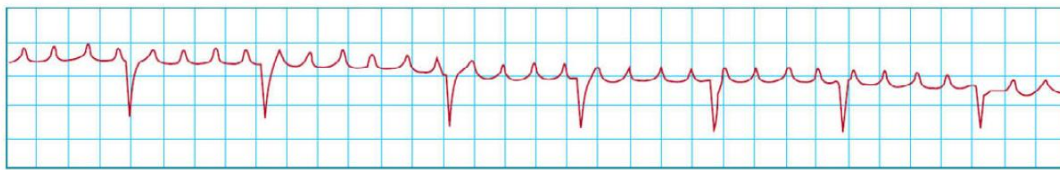
Figure 31. *Atrial Flutter.[160]*
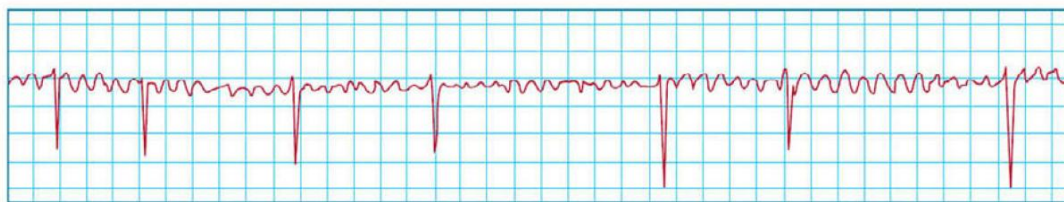
Figure 32. *Atrial fibrillation.[160]*

3.12.4. Ventricular Arrhythmia

Reentry mechanisms within the ventricles are responsible for establishing the ventricular arrhythmia which include ventricular tachycardia, ventricular flutter, and ventricular fibrillation.

3.12.4.1. Ventricular Tachycardia

Ventricular Tachycardia (VT) defines the case of having in the ECG three consecutive Premature Ventricular Complexes (PVCs) or more. VT is a severe arrhythmia that often impairs heart function considerably and may be a precursor of

ventricular fibrillation. The QRS duration of the PVCs in case of VT should be 0.14 *sec* or greater and the heart rate should be between 100 and 240 beats per minute. VT may be sustained, that is it can last seconds, minutes or hours. It may be also non-sustained when it lasts less than 30 seconds. There are three type of VT that differ in morphology, clinical significance and often in etiology:

1. **Monomorphic VT** : It is the most frequent type which can be sustained or nonsustained. It is called 'Ventricular flutter' with a rate above 200 beats per minute. The most current etiology of monomorphic VT is a coronary heart disease (CHD). The prognosis of VT generally depends on the type and severity of the heart disease.

2. **Polymorphic VT of type ' Torsade de Pointes'** : Torsade de points VT is characterized by a special ECG morphology, where QRS complexes change their polarity around the isoelectric line. This type of VT will usually terminate spontaneously after several seconds or will degenerate into ventricular fibrillation in relatively rare cases. This type of VT will be presented in details later in this chapter.

3. **Polymorphic VT without 'Torsade de Pointes'** : Polymorphism of QRS complexes without Torsade de Pointes is occasionally seen in patients with severe myocardial damage. Degeneration into ventricular fibrillation is quite common.

3.12.4.2. Ventricular Flutter

It is an organized rapid rhythm of the ventricles. QRS complex as well as T wave and P wave cannot be seen in the ECG, see figure 33. Ventricular flutter can develop into ventricular fibrillation.
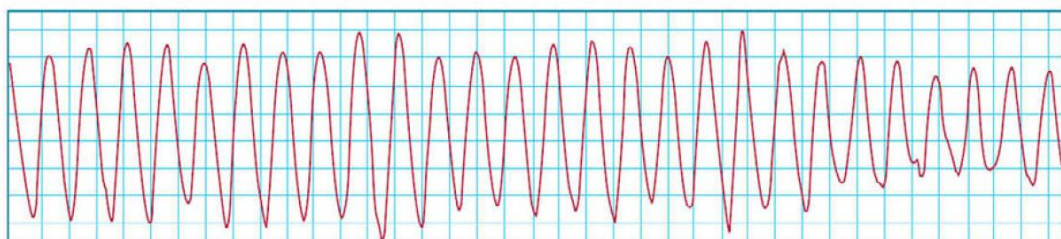
Figure 33. *An example of ventricular flutter. [160]*

3.12.4.3. Ventricular Fibrillation

It is much more chaotic rhythm than the ventricular flutter which can lead to cardiac arrest and loss of consciousness, see figure 34. The condition can often be reversed by the electric discharge of DC current from a defibrillator.

3.12.5. Wolff-Parkinson-White Syndrome

This syndrome is characterized by the presence of an accessory atrioventicular pathway located between the wall of the right or left atria and the ventricles, known as the Bundle of Kent. This pathway allows the impulse to bypass the AV node and activate the ventricles prematurely. Consequently, an initial slur to the QRS complex, known as a delta wave may be observed. The QRS complexes are wide, more than 0.11 sec, indicating that the impulse did not travel through the normal conducting system. The PR is shortened, to less than 0.12 sec, because the delay at the AV node is bypassed. Treatment would involve surgical removal or ablation of one of the pathways [161].
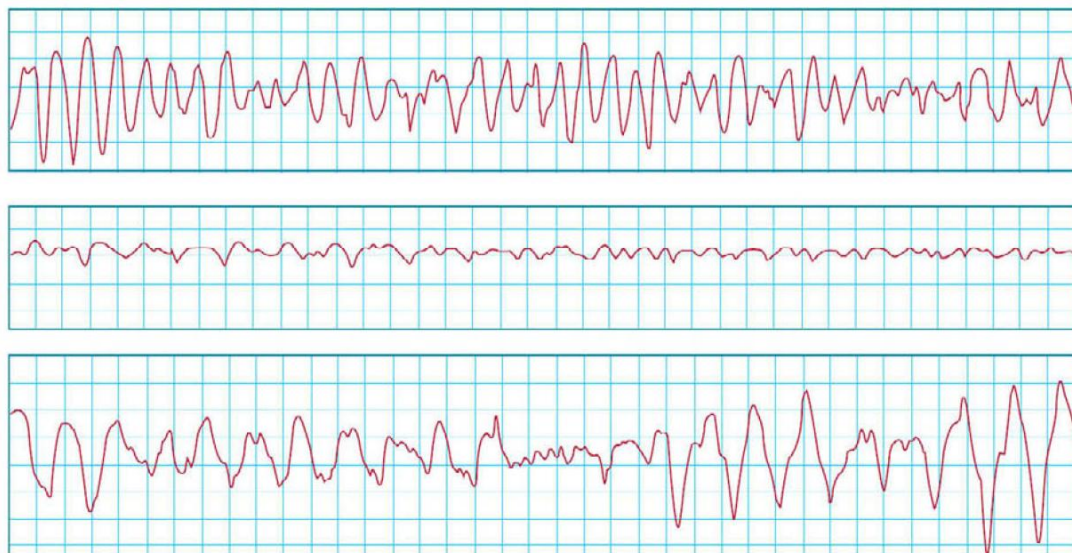
Figure 34. *An example of ventricular flutter. [160]*

3.12.6. Heart Conduction Blocks

A heart conduction block is defined as a blockage of the electrical conduction system of the heart at any level. Blocks that occur within the sinoatrial node (SA node) are described as SA nodal blocks. Blocks that occur within the atrioventricular node (AV node) are described as AV nodal blocks. Blocks that occur below the AV node are known as infra-Hisian blocks [162].

3.13. Heartbeat Morphologies

Abnormal heartbeat morphologies can be seen in many arrhythmic cases. Morphological abnormality of the heartbeat can be reflected also by the abnormal structural conditions of the heart, such as ischemia and myocardial infarction as well as atrial and ventricular hypertrophy (mass enlargement) and pericarditis (inflammation of the pericardium). Furthermore, abnormalities in beat morphology can be due to the mutations in ion channels controlling cellular repolarization of the heart, such as Long QT Syndrome, Brugada Syndrome. Other important arrhythmias, which are sometimes linked to mutations in ion channels, are T wave alternans and polymorphic VT type Torsade de 'Pointes', etc...

3.13.1. Ischemic Heart Disease

Ischemic Heart Disease (IHD), also known as Coronary Artery Disease (CAD), is a disease characterized by reduced blood supply to the heart. It is usually felt as angina, especially if a large area is affected [163]. Due to the deposition of cholesterol plaques on their walls, the blood vessels will be narrowed or even blocked. This will reduce or stop providing oxygen and nutrients to the myocytes leading to the death of that area of heart tissue and causing a possible heart attack. Electrocardiography (ECG) may be normal in several patients at rest between the episodes of pain with a possibility for a depression or an elevation of the ST segment and a T wave inversion in several leads. In cases of infarction, there will be ST segment elevation in the ECG, which may gradually evolve. An exercise testing (Treadmill Test-TMT) is often

indicated in patients who have symptoms of IHD but have normal ECG patterns [164].

3.13.2. Myocardial Infarction

Acute myocardial infarction (AMI or MI), also known as a heart attack, is a serious, sudden heart condition. It causes sometimes loss of consciousness. It occurs when the blood supply to a part of the heart is interrupted, causing death of the local heart tissue. The severity of heart attacks can vary relating to the size the affected area, which disturbs the normal propagation pathways and causes abnormal direction of the electrical impulse. ECG waves of an individual with MI differ significally from the normal ECG waves. There are many morphological varieties of infarction ECG waves depending on the position and size of the infarction in the myocardium.

3.13.3. Long QT Syndromes

An abnormally long delay between the depolarization and the repolarization of the heart ventricles is a disease defined as long QT syndrome (LQTS). Specific mutations in ion channels controlling cellular repolarization underlie the various congenital forms of long- QT syndrome [165, 166, 167]. Individuals with LQTS have a prolongation of the QT interval in the ECG. The two most common types of LQTS are genetic and drug-induced. Mutations to one of several genes, which are tending to prolong the duration of the ventricular action potential (APD) and lengthening the QT interval, is the cause of genetic LQTS. These LQTS can be inherited in an autosomal dominant or an autosomal recessive fashion. The autosomal recessive forms of LQTS tend to have a more severe phenotype, with some variants having associated syndactyly or congenital neural deafness [168, 169]. A number of specific genes loci have been identified that are associated with LQTS. Because exogenous factors such as antiarrhythmic drugs causing the acquired form of LQTS operate on the same ion channels implicated in congenital LQTS, both forms of the disease may share common electrophysiological mechanisms [170]. Drug induced LQT is usually a result of treatment by anti-arrhythmic drugs such as amiodarone or a number of other drugs that have been reported to cause this problem. Some anti-psychotic drugs, such

as Haloperidol and Ziprasidone, have a prolonged QT interval as a rare side effect. Because Long QT syndrome can lead to ventricular arrhythmias, it can cause ventricular fibrillation which is sometimes associated with syncope (loss of consciousness) and sudden cardiac death (SCD) [171, 169].

1. **LQT1**: It is the most common type of long QT syndrome, making up about 40 to 55 percent of all cases. The LQT1 gene KCNQ1 has been isolated to chromosome 11p15.5. KCNQ1 codes for the voltage-gated potassium channel KvLQT1 that is highly expressed in the heart. It is believed that the product of the KCNQ1 gene produces an alpha subunit that interacts with other proteins (particularly the mink beta subunit) to create the IKs ion channel, which is responsible for the delayed potassium rectifier current of the cardiac action potential [169]. Homozygous mutations in KVLQT1 leads to severe prolongation of the QT interval (due to near-complete loss of the IKs ion channel), and is associated with increased risk of ventricular arrhythmias and congenital [172, 169].

2. **LQT2**: It is the second most common gene location that is affected in long QT syndrome, making up about 35 to 45 percent of all cases. It involves a mutation of the human ether-a-go-go related gene (HERG) on chromosome 7. The HERG gene (also known as KCNH2) is part of the rapid component of the potassium rectifying current (IKr), That is, the IKr current is mainly responsible for the termination of the cardiac action potential and therefore the length of the QT interval. The normally functioning HERG gene allows protection against early after depolarization (EADs). Most drugs that cause long QT syndrome do so by blocking the IKr current [172, 169].

3. **LQT3**: It involves a mutation of the gene that encodes the alpha subunit of the Na+ ion channel. This gene is located on chromosome 3p21-24, and is known as SCN5A (also hH1 and NaV1.5). This mutation slows down the inactivation of the Na+ channel, causing prolongation of the Na+ influx during depolarization.

4. **LQT4**: It involves a mutation in an anchor protein Ankyrin B which anchors the ion channels in the cell. This kind of LQT occurs very rarely.

5. **LQT5 & LQT6**: LQT5 involves a mutation in the gene KCNE1 encoding for the potassium channel beta subunit MinK. In the same manner, LQT6 involves a mutation in the gene KCNE2 which encodes for the potassium channel beta subunit MiRP1.

6. **LQT7**: It is also called Andersen-Tawil syndrome. It involves a mutation in the gene KCNJ2 encoding for a potassium channel protein Kir 2.1. [173, 169].

7. **LQT8**: Also called Timothy's syndrome. It is due to a mutation in the calcium channel Cav1.2 encoded by the gene CACNA1c.

3.13.4. Brugada Syndrome

Brugada syndrome is due to a mutation in the gene that encodes for the sodium ion channel in the cell membranes of the myocytes. Gain-of-function mutations in this gene lead to elongation of the cardiac action potential [100, 102] The pattern seen on the ECG is persistent ST elevations in the electrocardiographic leadsV1-V3 with a right bundle branch block (RBBB) appearance with or without the terminal S waves in the lateral leads that are associated with a typical RBBB. A prolongation of the PR interval is also frequently seen [174, 175]. The cause of death in Brugada syndrome is ventricular fibrillation. The treatment is done via implantation of an implantable cardioverter-defibrillator (ICD) continuously monitoring the heart rhythm and defibrillating an individual if ventricular fibrillation is detected [174,175].

3.13.5. T-Wave Alternans

T-Wave alternans (TWA) is an ECG phenomenon characterized by beat-to-beat alternation or oscillations of the morphology, amplitude, and /or polarity of the T wave, see figure 35. TWA is commonly observed in the acquired and congenital and long-QT syndromes (LQTS). Moreover, it is very important prognostic indicator in that it is commonly observed just preceding episodes of Torsade de Pointes [176, 177, 178]. The study in [179] examines the cellular and ionic basis for TWA induced by rapid pacing under condition of mimicking the LQT3 from the congenital LQTS in an arterially perfused canine left ventricular wedge preparation. They recorded transmembrane action potentials from epicardial, M, endocardial cells and 6 to 8 intramural unipolar electrograms simultaneously together with transmural ECG and isometric tension development.
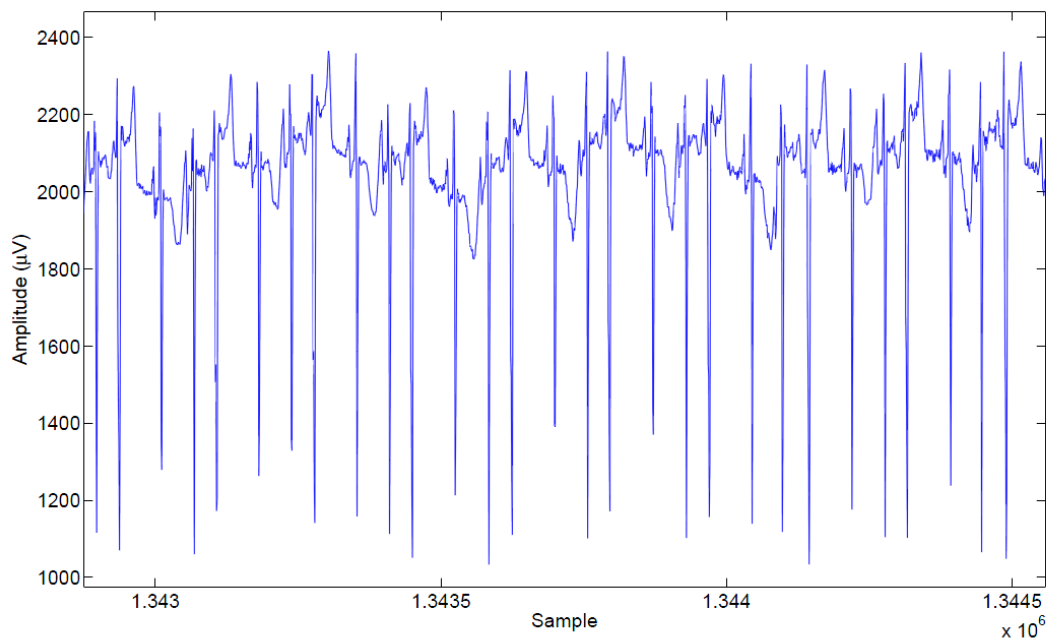
Figure 35. *An example of T-wave alternans taken from an ECG tape (Pfizer Inc.).*

[160]

A wide spectrum of T-wave and mechanical alternans is produced by increasing the pacing rate from cycle length (CL) of 500 to 400 to 250 ms in presence of sea anemone toxin. Acceleration to CLs of 400 to 300 ms produced mild to moderate beat-to-beat TWA of cells in M region. Acceleration to CLs of 300 to 250 ms caused more pronounced beat-to-beat TWA and APD of the M region, leading to a reversal repolarization sequence across the ventricle wall and thus to alternation in the polarity of T-wave. Torsade de Pointes occurred after an abrupt acceleration of CL associated with marked TWA. In almost all cases, electrical and mechanical alternans were concordant. Both ryanodine and low [Ca2+] completely suppressed alternans of the T wave and shortened APD, suggesting a critical role for intracellular Ca2+ cycling in the maintenance of TWA. T wave alternans, observed at rapid rates under long-QT conditions, is caused by the alternation of the M-cell action potential duration (APD), leading to exaggeration of transmural dispersion of repolarization during alternate beats, and thus the potential for development of Torsade de Pointes. The pathologic states with TWA are long QT syndrome, myocardial ischemia and infraction, heart failure, sudden infant death syndrome and drug-induced Torsade de Pointes [180].

There is some evidence that TWA is linked to alternations in cellular calcium homeostasis, which significantly influences the action potential duration (APD) [181]. Potassium channels may also play an important role in ischemia-induced TWA. The different sensitivity of KATP channel activation during ischemia between epicardium and endocardium may be linked to TWA at the cellular level [182, 183, 184, 185]. Macroscopic TWA has been reported in patients with the long QT syndrome [177, 186, 187, 179]. Prolongation and unstable state of the ventricular action potential may produce the macroscopic TWA and result in the polymorphic VT known as Torsade de Pointes. The prognostic value of microscopic TWA has not yet been assessed in patients with the long QT syndrome. In patients with the Brugada syndrome, some reports have revealed that intravenous administration of class Ic antiarrhythmic drugs induced macroscopic TWA and resulted in VF [188, 189]. These results suggest that in the Brugada syndrome class Ic antiarrhythmic drugs may accentuate the underlying sodium channel abnormalities, produce an unstable state of repolarization, increase the triggering of PVC, and induce VF. On the other hand, Ikeda et al. [190] reported a low prognostic value of microscopic TWA in patients with the Brugada syndrome. Elevated levels of spatial heterogeneity of repolarization as assessed by second central moment analysis in [191] appear to underlie the progression from elevated TWA levels to more complex patterns and increased risk for VF. Detection of T-wave heterogeneity (TWH) could prove useful in elucidating and clarifying mechanisms of VF. TWH monitored in precordial leads could contribute to stratifying risk for life-threatening arrhythmias, such as Torsade de Pointes.

3.14. Torsade de Pointes

The original name of Torsade de Pointes (TDP) comes from French language and means 'twisting of the points', since QRS complexes wing up and down around the isoelectric axis periodically and in a chaotic fashion changing their morphology from beat to beat, see figure 36, reminding the original author of the Torsade de Pointes movement in ballet. It is also referred to as torsade or cardiac ballet [176, 177, 178], TDP is a life-threatening arrhythmia closely linked to abnormal cardiac repolarization [192, 193, 194]. The typical initiation of TDP in ECG signal is after, so-called short-long-short (SLS) cycle sequences, see figure 36.

TDP is associated normally with marked prolongation of QT interval to 600 ms or greater. The etiology and management of torsade are quite different from generic VT cases including polymorphous VT, which are not associated with a prolonged QT interval. Therefore, it is critically important to differentiate between these entities. The delay in phase III of the action potential, which is mediated by the HERG potassium channel, is the underlying basis for the rhythm disturbance. The dysrhythmia is allowed to emerge because of the prolonged period of repolarization and the inhomogeneity of repolarization time among myocardial fibres. Although the precise mechanism of Torsade de Pointes has not been established, recent in vivo studies [195, 196], prefused wedge studies [197, 170, 198], and clinical observations made with monophasic AP recordings [199, 198] have presented evidence in support of the hypothesis that an early after depolarization-induced, triggered response
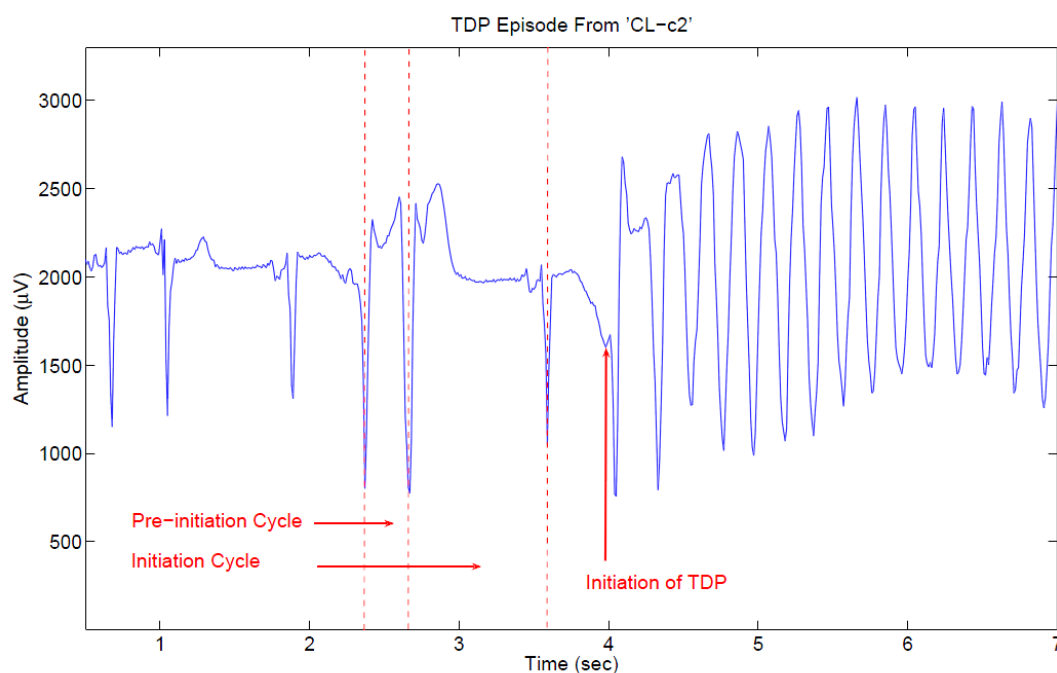

Figure 36. *The typical initiations of TDP in ECG signal after short-long-short cycle sequences. The morphology of QRS complexes during its episode is also illustrated. [160]*

initiates Torsade de Pointes but that the arrhythmia is maintained by a re-entrant mechanism. TDP is also characteristic of the congenital long QT syndrome, one form

of which is caused by mutations in the HERG gene which encodes the major repolarizating potassium channel Ikr. Furthermore, HERG appears to be the main molecular target for drugs which cause QT prolongation. Cardiac safety is now a major issue in new drug development, because there is increasing awareness that many nonantiarrhythmic drugs can prolong the QT interval and provoke TDP [126]. Moreover, TWA is very important prognostic indicator in that it is commonly observed just preceding episodes of Torsade de Pointes [176, 177, 178]. The mechanisms by which dysfunction at the molecular level translates into functional electrical instability leading to torsade de points (TDP) in LQTS are poorly understood [165]. Previous clinical [177] and experimental [200, 196] observations suggest two hypotheses regarding the electrophysiological basis of TDP. One theory states that TDP arises from triggered activity in competing ventricular foci. Evidence for the triggered activity hypothesis stems from experimental observations [200, 186] and computer models [201] demonstrating an enhanced propensity of cardiac myocytes to generate early after depolarizations (EADs) in response to factors that prolong the action potential duration (APD). Because TDP observed in patients is associated with conditions favoring the development of EADs experimentally, TDP was attributed to EAD-induced triggered activity. This mechanism, however, was challenged because rapid rates accompanying the onset of TDP abruptly shorten repolarization, thereby eradicating the prerequisite condition for EAD-mediated TDP. The second proposed mechanism is based on the association between dispersion of repolarization (DOR) and TDP, suggesting involvement of reentrant excitation. For example, patients with congenital LQTS manifest increased dispersion of QT interval. Moreover, recent observations from surrogate models of LQTS suggest a role for reentrant activity involving relatively large circuits around the cardiac chambers [195, 195]. However, focal (ie, nonreentrant) patterns of activation were also observed in these models, raising additional uncertainty regarding the underlying cellular mechanisms. Because the Iks current density of the midmyocardial cells (M cells) is relatively weak, they are more sensitive to many APD prolongation conditions than epicardial and endocardial cells [202] and they can play an important role in arrhythmias which are dependent on delayed cardiac repolarization, such as LQTS. Therefore, a transmural optical mapping system was developed to demonstrate a specific role of M cells in generating functional heterogeneities of repolarization that support intramural reentry in LQTS [165]. This system is able to measure electrical

heterogeneities between hundreds of cells spanning the ventricular wall, so that a functional topography of M cells as well as their role in promoting transmural DOR and arrhythmias in the presence of cell-to-cell electrotonic interactions can be established. Their data clearly implicate reentry as the mechanism for sustenance of TDP. It has been found that M-cell zones produced discrete refractory borders, which were directly responsible for conduction block and reentry that underlie TDP. It has been exhibited that M cells can express markedly different APDs from neighboring cells even on multicellular tissues under conditions of normal cell-to-cell coupling, and that M cells are not necessarily distributed uniformly across each transmural layer [165]. Despite relative normalization of the M-cell APD on subsequent beats, reentry persisted as the leading edge of the wavefront propagated into the recovering tail of the circuit. Such dynamic M-cell APD adaptation undoubtedly accounted for the rapidly changing trajectories of the reentrant circuit producing the characteristic polymorphic ECG morphology of TDP. The presence of uniform propagation on the epicardium may explain the appearance of a monomorphic waveform configuration in certain ECG leads but not others. Taken together, these findings suggest the existence of a single rotor during TDP that initially forms in the transmural wall and subsequently meanders into deeper layers of myocardium [91]. *Reentrant Mechanism of TDP* : The mechanism underlying TDP in this model is shown in a representative example in figure 37. After a single premature stimulus (S2), the impulse blocked in the region of most delayed repolarization (Figure 37 A, cells c, d, m1, and m2). The S2 wavefront, however, successfully propagated in the orthodromic direction (along the axon direction) (Figure 37 A, sites a' through e'), circumventing (surrounding) the region of delayed repolarization (Figure 37 A, hatched area). The zone of block of the premature beat (Figure 37 A) coincided with the region of most delayed repolarization after the S1 beat (Figure 37 R). When the former sites of block (sites c and d) regained excitability, the orthodromic impulse conducted from site e back to site a (Figure 37 B), thereby completing the first beat of reentry. A broad area of functional conduction block was present during the initial beats of reentry; however, because of pronounced rate adaptation of M cells, these refractory islands rapidly collapsed and were replaced by functional lines of block on subsequent beats (Figures 37 C through F). The polymorphic ECG characteristics of TDP were attributable to the fact that lines of block and trajectory of the reentrant circuit varied from beat to beat, initially

within the mapped transmural surface and subsequently meandering into deeper myocardial depths. Similar reentrant mechanisms were observed in all experiments.
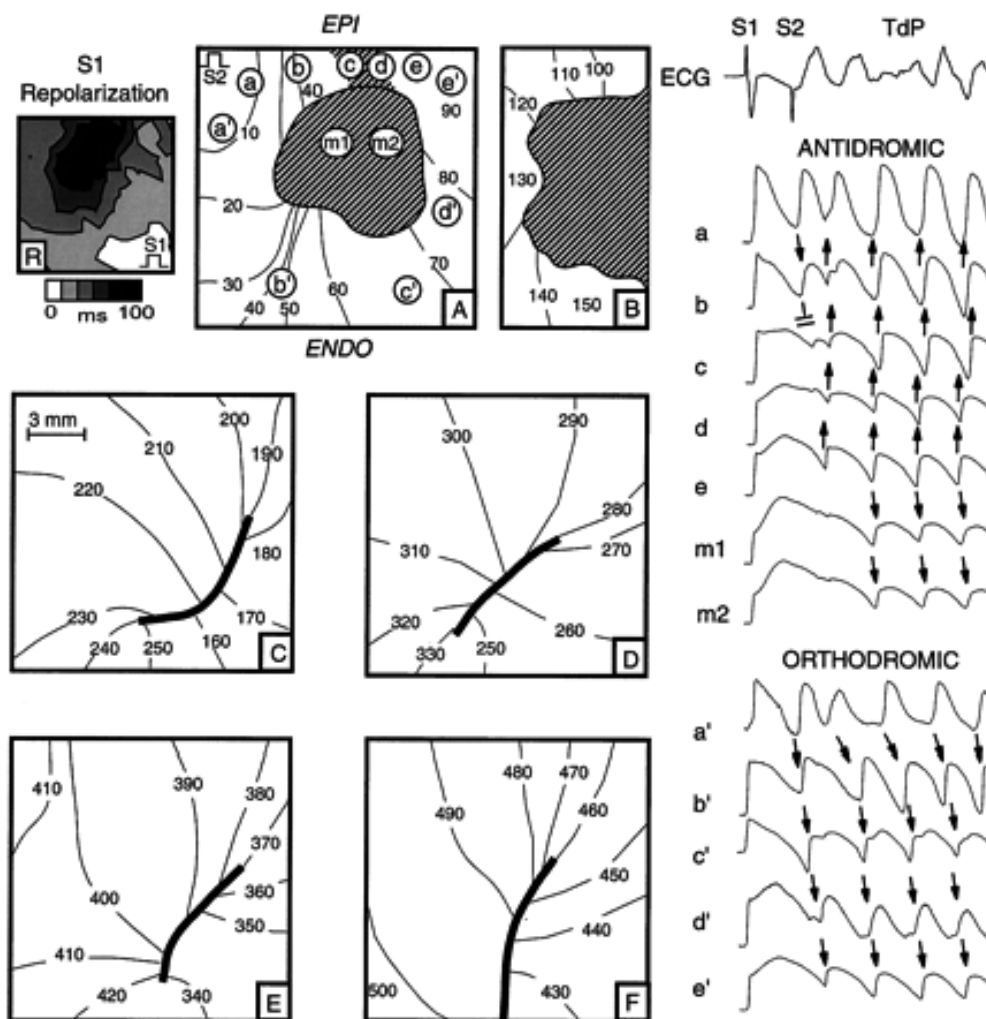
Figure 37. *Repolarization map during drive train S1-S1 pacing (R) and depolarization maps during single premature S2 (A) and ensuing TDP caused by transmural reentry (B through F). S2 was applied on the epicardial surface in the wake of the refractory barrier (R) produced by the island of M cells extending from the mid-wall to the epicardial surface. The S2 beat failed to propagate into the region of prolonged refractoriness (cells c, d, m1, and m2), causing block of the antidromic impulse while propagating in a counter clockwise (orthodromic) fashion around the refractory region formed by M cells [165].*

4. Methods of investigation

4.1. ECG hardware

Taking cardiac data requires a recognition system as simple as possible (in order to avoid high noise from the measurement itself and of course to keep the cost of the retail reproduction low etc). A construction of a system where the output can lead to a simple sound card of an average personal computer was created. The construction is portable and simple as possible, but in the same time very accurate and reliable.

4.1.1. ECG

ECGs are normally displayed with 25 mm on the horizontal axis representing one second, or 40 ms/mm. The vertical axis is usually 10 mm per mVolt. This means that a 1 mm square on the plot represents 0.04 s in time and 0.1 mV in voltage. There are conventions for labeling certain characteristic points on the ECG curve with letters. The distance from one of the prominent 'R' peaks to the next represents exactly the time between two heartbeats: this lets us readily determine the pulse rate (figure 38). This rate, expressed in beats per minute (or BPM) is displayed by the computer, and the pulse itself can optionally be output as an audio signal.
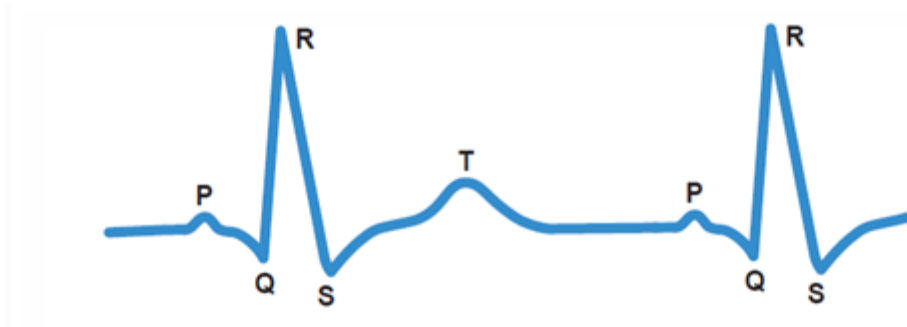

Figure 38. *The interval between two consecutive points marked 'R' in the ECG trace gives the time between heartbeats*

4.1.2 Signal processing

Measuring an ECG using a computer requires demanding real-time processing, most of which is carried out in software. The hardware takes the form of an instrumentation amplifier (**Figure 39**) and has the job of amplifying the weak signal from the sensor (which has an amplitude of approximately 1 mV) by a factor of around 1,000, and attenuating DC, common-mode, and high-frequency components. To obtain an (at least relatively) clean ECG signal it is necessary carefully to filter out any interference. This was done in software using a biquad infinite impulse response filter. The filter can be configured for any of the required responses: low-pass, high-pass, band-pass and notch. A 50-Hz rejection filter removes interference originating from the mains, and other interference is attenuated using a further high-pass filter. Since the signal is obtained from electrodes on the skin it is possible that there will be a slowly-varying offset voltage: this is removed using a DC blocking filter. The main pulse of the ECG could be extracted using a band-pass filter, giving a signal from which it is straightforward to measure the pulse rate. The Java program allows display of either the original signal or the filtered version. The various filter functions can be selected and configured by the user, and the effect on the processed signal can be clearly seen. The pulse rate is calculated from its autocorrelation function, determining the period by comparing the signal against itself with a time offset.
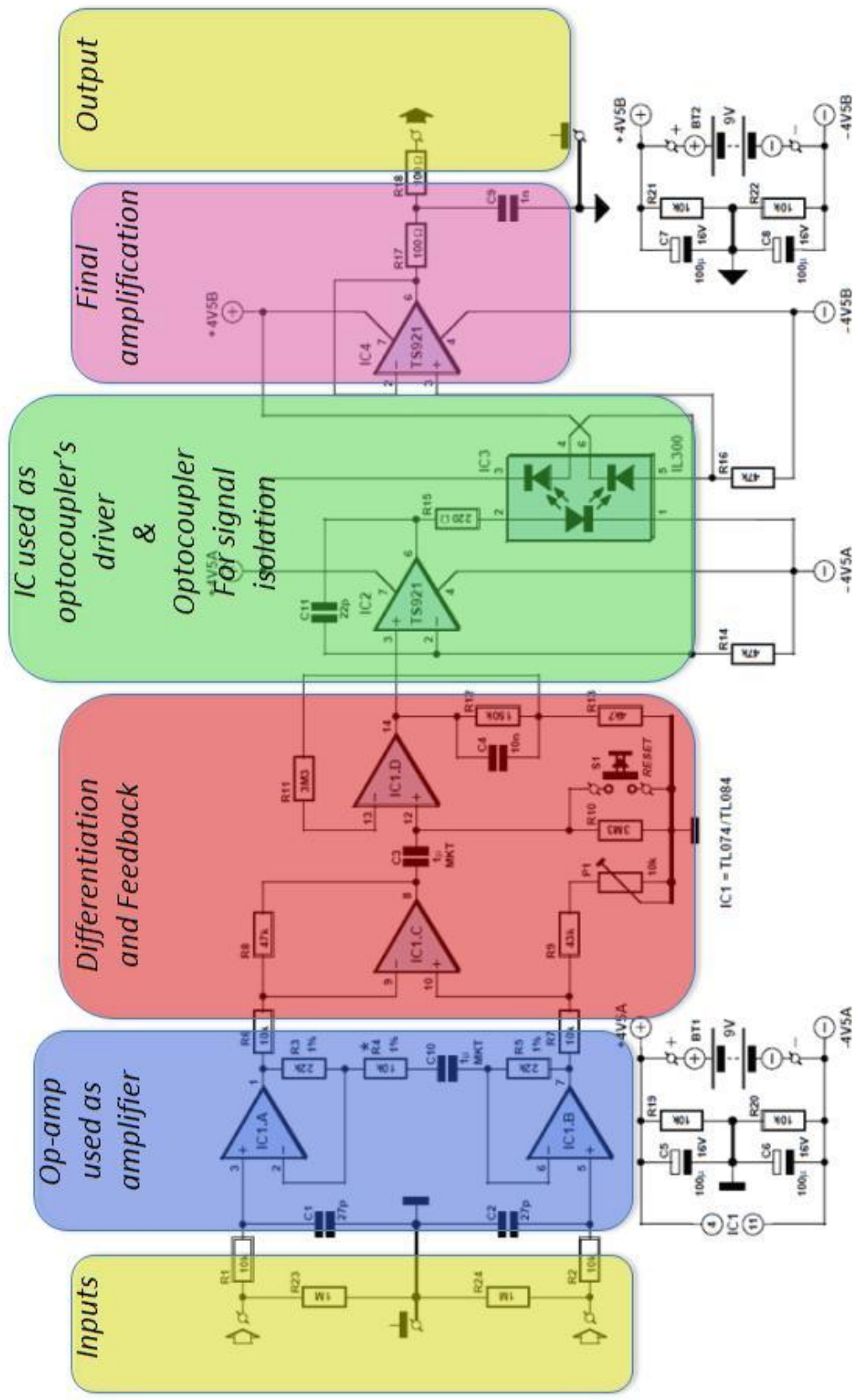
Figure 39. *Circuit of the instrumentation amplifier, with galvanical isolation between input and output provided by an optocoupler.*

4.1.3 Instrumentation amplifier

The circuit (Figure 39) can be divided into two blocks: the instrumentation amplifier itself at the input and the optocoupler isolation amplifier at the output. The signal is amplified biquad operational amplifier IC1, type TL084 (or the lower-noise TL074). IC1.A and IC1.B are non-inverting amplifiers, feeding the inputs of differential amplifier IC1.C. This arrangement is known as an 'instrumentation amplifier'. P1 allows adjustment to obtain best common- mode rejection. Coupling capacitor C3 at the input to the next stage, built around IC1.D, blocks the DC component of the output of the instrumentation amplifier. To minimize the effect on low-frequency signals the time constant of the RC network formed by C3 and R10 is more than three seconds. This means that it will take at least this long for the voltage across the capacitor to stabilize when power is applied: this delay can be avoided by pressing reset button S1. Optocoupler IC3 is driven by IC2. The type TS921 used is a 'rail to rail' opamp, which means that it can be driven to either extreme of its supply voltage range. Its output can deliver up to 80 mA, although only approximately 2.2 mA is needed to drive the transmit LED in the optocoupler.
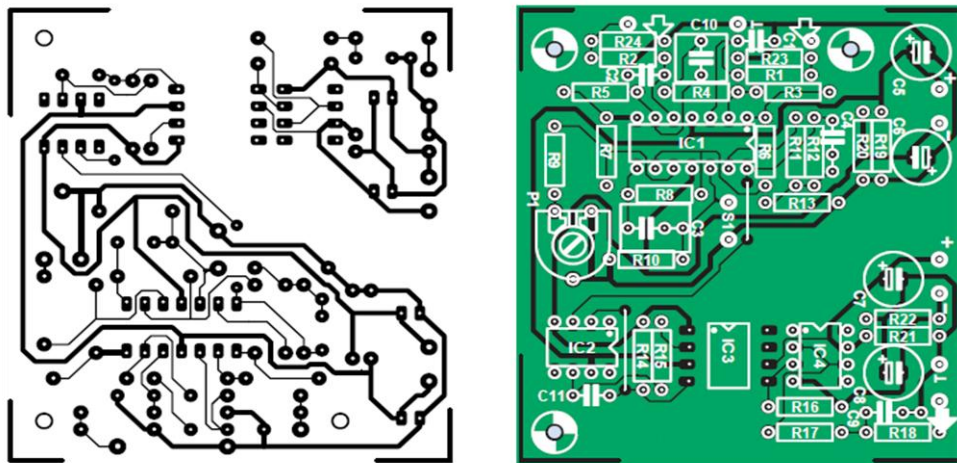

Figure 40. *There are no SMDs on the single-sided printed circuit board, and so assembly is straightforward.*

The current through the transmit LED is controlled using feedback from one of the receiver diodes in the optocoupler fed in to the inverting input of the operational amplifier. The result is that the voltage across R16 (the bias resistor for the second receiver diode) is equal to that across R14 and hence to the voltage at the non-inverting input to IC2. In other words, the voltage at the output of IC1.D appears across R16, but with galvanic isolation. C11 prevents high-frequency oscillation of the driver. The final opamp at the output of the circuit acts as a buffer amplifier. This makes for a low-impedance output, which is also short-circuit proof thanks to the 100 Ω resistors R17 and R18, forming a low-pass filter at the output in combination with C9. The complete galvanic isolation between input and output of the circuit provides for extra safety. The instrumentation amplifier and the output stage should be powered from separate batteries.

4.1.4. Components and construction

For resistors R3, R4 and R5 low-noise metal film types were used. C10 provides DC decoupling for the input amplifiers, which prevents weak muscle signals from swamping the signal from the heart. Instead of the tube, disposable self-adhesive ECG electrodes can be used. In order to do so, the capacitor would be replaced by a wire link.
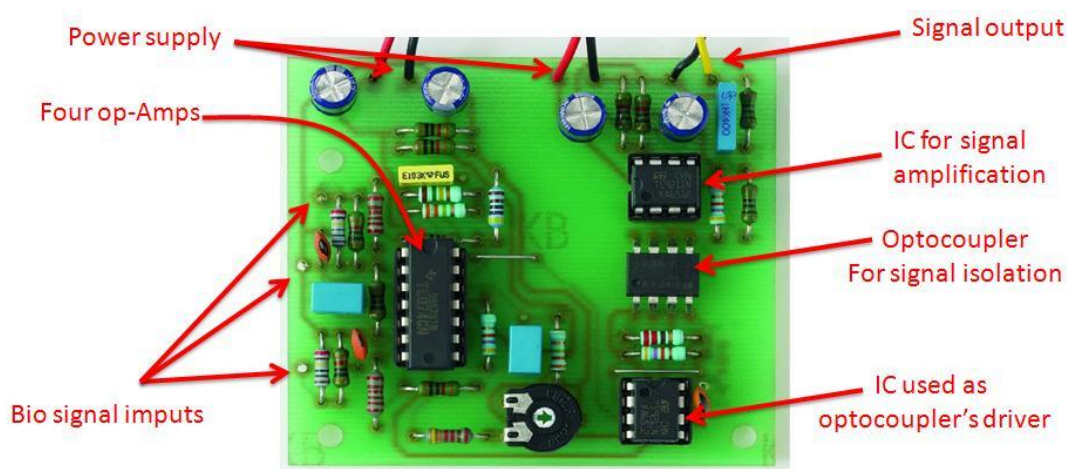

Figure 41. *The populated prototype board explained.*

If the TS921 should prove hard to obtain, a type TL071 can be substituted at the cost of reducing the dynamic range of the circuit somewhat. The 43 kΩ resistor (value from the E24 series) can also be replaced by a different value, adjustment of P1 compensating for the difference. IC3 is supplied with its pins bent at a right angle. To fit the circuit board they needed be bent apart (**Figure 41**): this was necessary in order to guarantee the necessary isolation gap. P1 can be adjusted for best common mode rejection. For best results a connection of the inputs of the instrumentation amplifier and adjustment of P1 to minimize the amplitude at the output of the 50 Hz signal picked up by the circuit was necessary. This measurement can be done using the Matlab program as will be seen later on. The heart signal sensor used for the tests consists of two adapters that can grab naked cables or metallic tips of patches like the ones used for measuring ECG signals onto humans. This is more convenient and makes the device portable with minimum loss of signal and minimum input of undesired noise that could jam the measurements. The same grabbers were used to connect the audio cable that connects the PC to the audio line (or microphone input). Most computers use a 3.5 mm stereo jack.

4.2. Matlab as a tool for creating new ECG analysis program

Now that the ECG board is complete, the only thing needed to be done is the software, e.g. the programs that not only reads the signals, but also processes them. For this purpose Matlab was chosen for creating the necessary software. Matlab (which is an abbreviation of the words MATrix LABoratory) is a particularized program, optimized to perform calculations in the field of mechanics and in general to resolve scientific matters. It started as a program for calculations between mathematical tables, but in time it evolved into a program capable to resolve any scientific issue.

Matlab implements the language of Matlab and provides a wide library of special functions so the user can program them and have the solution in his matters, much easier and with greater accuracy. This extensive library of the predefined functions helps resolve complex issues much easier in MATLAB than in other computer languages like Fontran or C. Here, while proceeding, it will be clear that a

wider use of these tools and functions which leads to the creation of new equations and programs. All these will help to creating different parameters in ECG and in general they will help in the process.

Matlab is the appropriate tool for the creation of this research since it can perform multitasking analysis from a combination of mathematical models, signal analysis models and simulation analysis. It is compatible with a computers soundcard in order to use it as an input for the signals extracted from the ECG device. It has the capability to perform digital signal processing thru a variety of internal predefined functions for modeling. MATLAB comes complete with an extensive library of predefined functions that provide tested and prepackaged solutions to many basic technical tasks. MATLAB includes tools that allow a program to interactively construct a graphical user interface (GUI) for his or her program. With this capability, the programmer can design sophisticated data analysis programs that can be operated by relatively-inexperienced users.

4.3. New functions created for this research (to read files ECG of ECG hardware)

The first program created to Matlab was about the need to read the signals that are leaded from the output of the construction, to the input of the sound card. This program is consisted from the following lines:

```
Fs=11025;
Signal=wavrecord(10*Fs,Fs);
```

These lines are used to read a healthy cardiac signal from the simulator (Rate: 72Bpm) and the output is shown in figure 42. The variable Fs is the waveform rate (11025 KHz) and the 10*Fs are the seconds measured, which are 10 (**figure 43**).
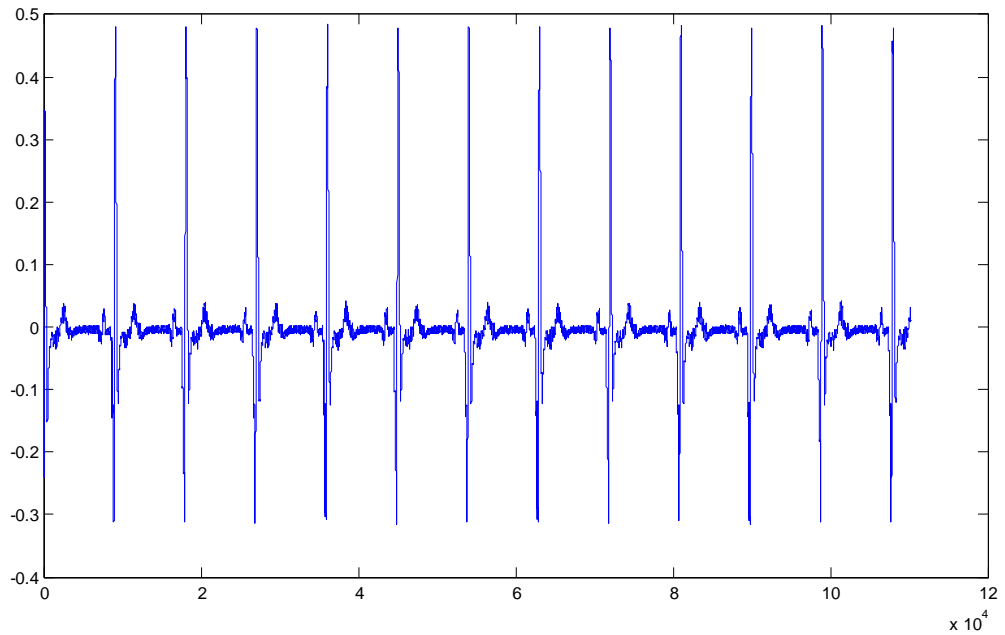
Figure 42. *Output of an SNR*

As seen in figure 43, in 10 seconds the simulated heart gave 12 beats. If the measurement is expanded in 60 seconds, the simulator would give 72 heartbeats, which is confirmed from the user manual of the simulator.
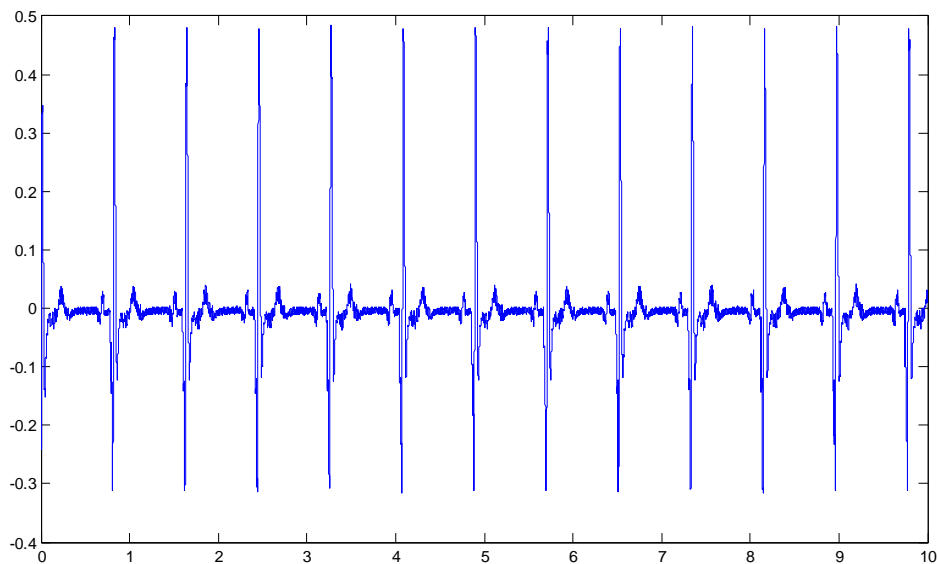
Figure 43. The *110250 spots are divided with the waveform rate which was 11.025 KHz and the graphical now is in seconds.*

This is the basic command that will be used in the program in the graphical interface, so checking and reading of the board is made.
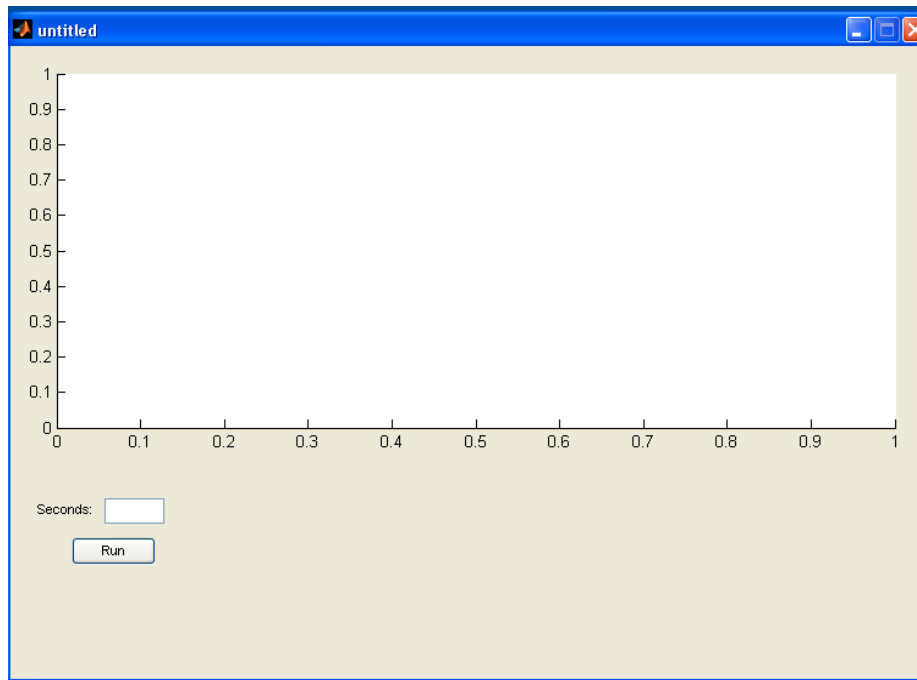
Figure 44. *The starting page of the program in which only the drawing output and the box where the insertion of the seconds measured are shown. The "run" button performs the original routine.*
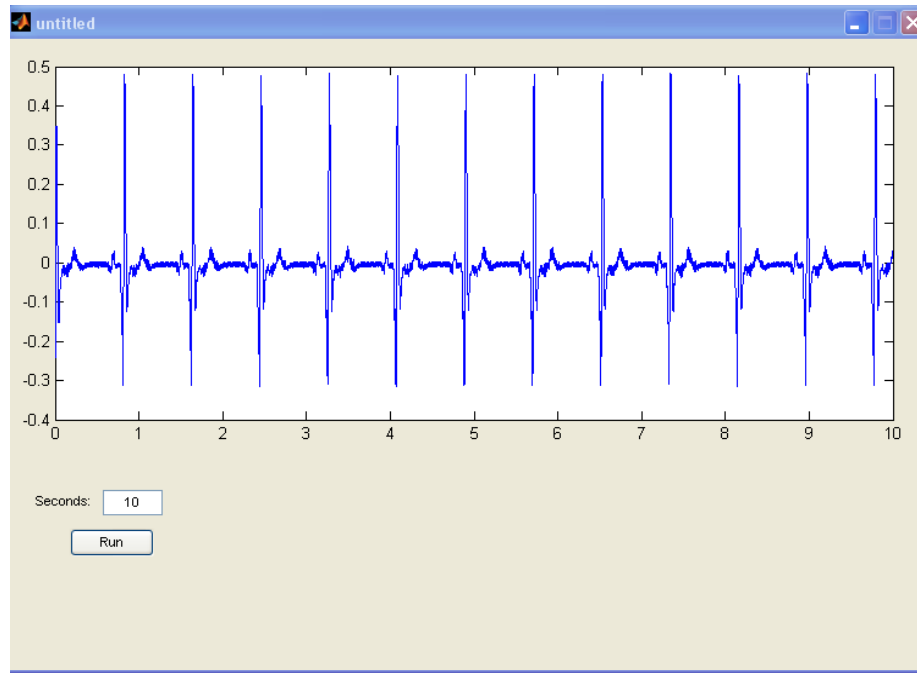
Figure 45. *Figure 43 as shown in the graphical interface of the program.*

Next step on the analysis and process of the heart signals is the calculation or the heart rate. In order to do so, a measurement of how many times a higher state in

the signal in 10 seconds time is seen, had to be done. Then an escalation of it to 60 seconds is followed. From figure 43 it became obvious that in 10 seconds time the construction measured 12heart beats, thus 72 heart beats per minute (hbpm). For the needs of a fast measure of the heart rate a program that is consisted from the following lines was created:

```
clc
clear a % to clear a
clear b % to clear b
clear n1 % to clear n1
clear x1 % to clear x1
clear n % to clear n1
clear x % to clear x1

john=0;

x=signal; % x equals our signal

xx=x/max(x); % normalizing amplitude by divide signal
with its maximum value

nn=[1:length(xx)]'/11025; % axis x is the length divided
by the waveform rate

b=0; % we equal b to zero

a=imextendedmax(xx,1);

for i=2:length(a)-1
    if a(i)==1 & a(i-1)==0 & a(i+1)==1
        amin=(i);
    end
    if a(i)==1 & a(i-1)==1 & a(i+1)==0 %
        amax=(i);
        v(i)=max(xx(amin:amax)>0.85); % we record the
max variable of the temporary xx which corresponds to the
top states

    end
end

n1=nn(a);
```

```
x1=xx(a);

plot(nn,xx,n1,x1,'r.') %  we plot our signal and the top
states it calculated

peaksno=sum(v~=0); % we calculate all of the peaks

Rhythm=(peaksno*60)/length(nn) % we calculate the rate,
based on the minutes it recorded.
```

With the above program calculation of the heart rate and the coding works is made as follows. At first all the variants equals to zero. Then the variable x is stated as the signal and that variable `xx` is the normalized signal. Next, `nn` are the numbers of the horizontal axis that define time, in seconds because earlier all of the numbers were divided to 11025 which is the waveform rate (Hz). 1 Hz is 1 circle per second, so 11025Hz are 11025 circles per second, so since the signal has measured 110250 spots, it has counted 10 seconds. Then with command `imextendedmax(xx,1);` the program equals 1 with all the values that are around the top. In this way, a board (board a) that is consisted by 1 and 0 is created. With commands "for" and "if", isolation of the entire areas one by one and search the `max xx` for each one follows. This way "board V" which is consisted by "xx" and "0" is created (where there is not a tag due to non existence of peak, 0 is inserted). Next with command `sum(v~=0)` all the max values are measured. With `Rhythm=(peaksno*60)/length(nn)` all the max values from the seconds which the construction measured in 60 in order to define the rate per minutes are escalated. This code was installed to the program in figure 45 along with the capability of the manual calculation of the heart rate. This function was installed due to some cases the heart disorder is so great that the earlier and standard thresholds couldn't help. Also this capability to manually calculate the heart rhythm in case someone would want to double check the output of the program (**figure 46**).
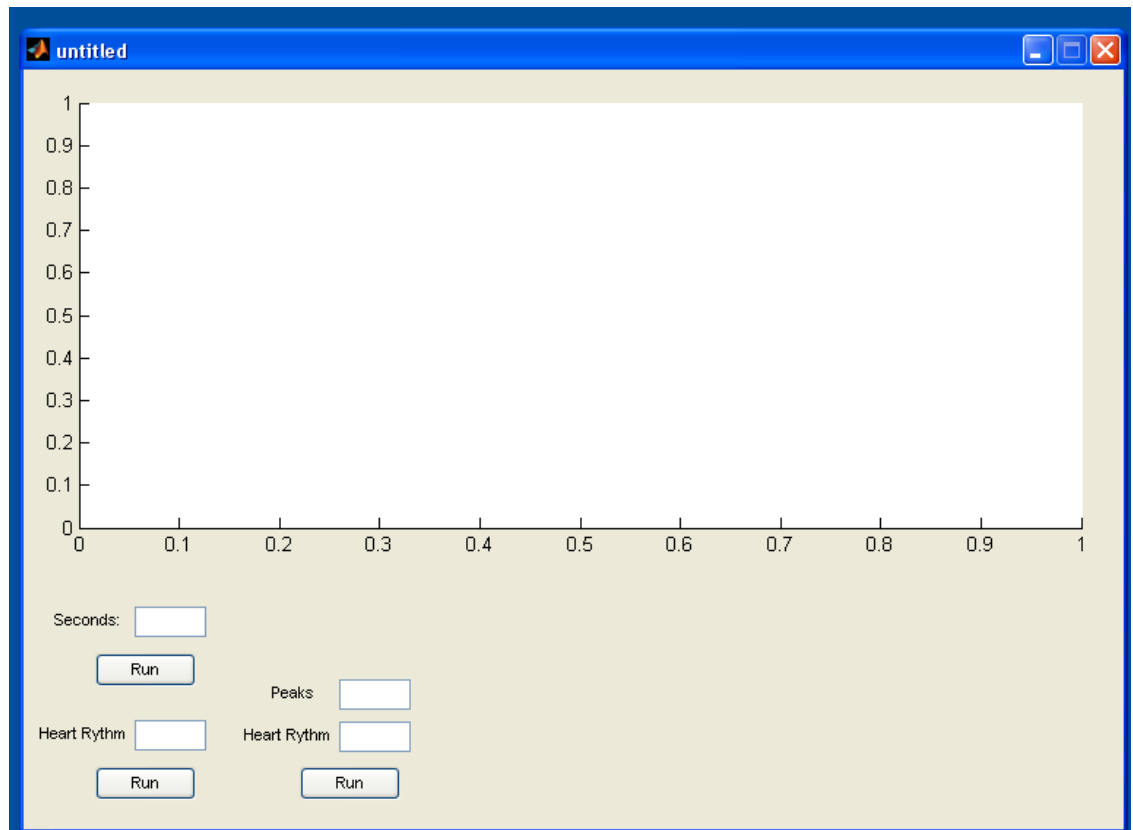
Figure 46. *The program*

Matlab is consisted by a variety of equations and functions in its libraries which are used to insert in any created program in order to process measurements much easier. Another function which borrowed from the Matlab library is fitting using the "spline" method. The spline fitting is a method of data intepolaration.

4.4 Cubic Splines

It is well known that interpolation using high-order polynomials often produces ill- behaved results. There are numerous approaches to eliminating this poor behavior. Of these approaches, cubic splines are very popular. In MATLAB, there are basic cubic spline, ppval, mkpp, and unmkpp. Of these, only spline appears in the MATLAB documentation. However, help text is available for all these functions. In the following sections, the basic, feature of cubic splines as implemented in these M-file functions is demononstrated. In addition, an alternative to cubic splines, called a

piecewise cubic Hermite interpolating polynomial is considered. This piecewise polynomial is computed by the function pchip and returns a piecewise polynomial just as spline does.

4.4.1 Basic features

In cubic splines, cubic polynomials are found to approximate the curve between each pair of data points. In the language of splines, these data points are called breakpoints. Since a straight line is uniquely defined by two points, an infinite number of cubic polynomials can be used to approximate a curve between two points. Therefore, in cubic splines, additional constraints are placed on the cubic polynomials to make the result unique. By constraining the first and second derivatives of each cubic polynomial to match at the breakpoints, all internal cubic polynomials are well defined. Moreover, both the slope and curvature of the approximate polynomials are continuous across the breakpoints. However, the first and last cubic polynomials do not have adjoining cubic polynomials beyond the first and last breakpoints. As a result, the remaining constraints must be determined by some other means. The most common approach, which is the default for the function spline, is to adopt a not-a-knot- condition. This condition forces the third derivative of the first and the second cubic polynomials to be identical, and likewise for the last and second-to- last cubic polynomials.

Based on the above description, one could guess that finding cubic spline polynomials required solving a large set of linear equations. In fact, given n breakpoints, there are n-1 cubic polynomials to be found, each having 4 unknown coefficients. Thus, the set of equations to be solved involves 4(n-1) unknowns. Thus, if there are 50 breakpoints, there are 50 equations in 50 unknowns. Luckily, these equations can be concisely written and solved using sparse matrices, which is what the function spline uses to compute the unknown coefficients.

4.4.2 Piecewise Polynomials

In its most simple use, spline takes data x and y and desired values xi, finds the cubic spline interpolation that fit x and y, and then evaluates the polynomials to find

the corresponding yi values for each xi value. This matches the use of $yi = interpl\,(x, y, xi,\,'spline')$. Consider the example:
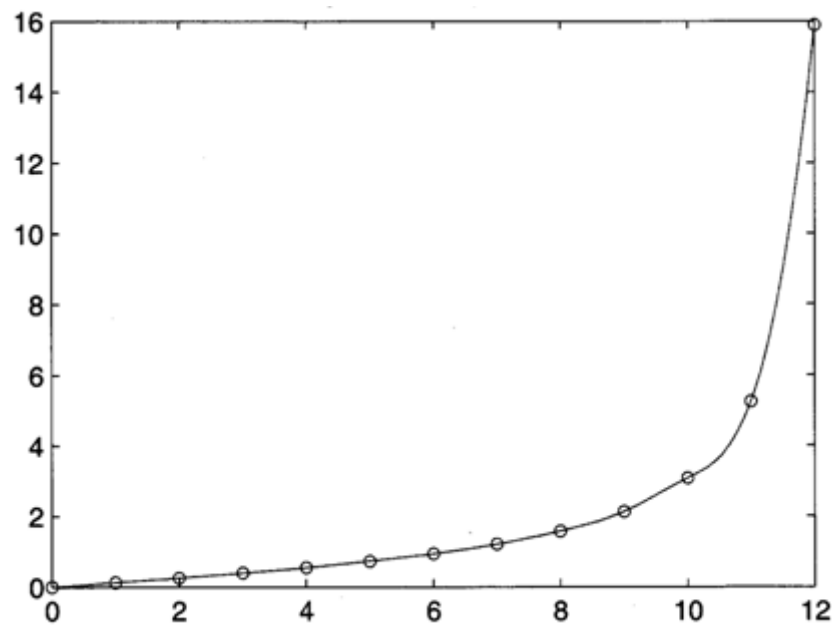
Figure 47. *Spline Fit*

```
>> x=0:12;
>> y= tan (pi*x/ 25);
>> xi =linspace (0,12);
>>yi=spline (x, y, xi);
>>plot (x, y, 'o', xi, yi)
>>title ('Figure 20.1: Spline Fit'
```

This approach is appropriate if only one set of interpolated values is required. However, if another set is needed from the same set of data, it doesn't make sense to recompute the same set of cubic spline coefficients a second time. In this situation, one can call spline with only the two arguments, for example,

```
>>pp=spline(x,y)
pp=
      form : 'pp'
      breaks   : [0 1 2 3 4 5 6 7 8 9 10 11 12]
      coefs    : [12x4 double]
      order    : 4
      dim      : 1
```

When called in this way, spline returns a structure containing the $pp-form$, or piecewise polynomial form, of the cubic splines. This structure contains all the information necessary to evaluate the cubic splines for any set of desired interpolation. The $pp-form$ structure is also compatible with the optional Spline Toolbox available with MATLAB. Given the pp-form, the function $ppval$ evaluates the cubic splines. For example

```
>>yi=ppval(pp.xi):
```

Computes the same yi values computed earlier. Similarly,

```
>>xi2=linspace (10, 12);
>>yi2=ppval (pp.xi2);
```

uses the pp-form again to evaluate the cubic splines over a finer spacing restricted to the region between 10 and 12.

```
>> xi3=10:15;
>> yi3=ppval (pp.xi3)
>> yi3=
     3.0777    5.2422    15.8945    44.0038    98.5389
188.4689
```

shows that cubic splines can be evaluated outside the region over which the cubic polynomials were computed. When the data appears beyond the last or before the first breakpoint, the last and first polynomials are used respectively to find interpolated values.

The cubic splines pp-form given above, stores the breakpoints and polynomial coefficients, as well as other information regarding the cubic splines representation. This form is a convenient data structure in MATLAB since all information is stored in a single structure. When a cubic spline representation is evaluated, the various fields in the pp-form must be extracted. In MATLAB this process is conveniently performed by the function unmkpp. Using this function on the above pp-form gives

```
>> [breaks. Coefs. Npolys. Ncoefs. Dim] = unmkpp (pp)


    Breaks=
        columns 1 through 12
        0    1    2    3    4    5    6    7    8    9
        10   11
        Column 13
        12
        coefs=
        0.0007    -0.0001         0.1257         0
        0.0007    0.0020          0.1276         0.1263
        0.0010    0.0042          0.1339         0.2568
        0.0012    0.0072          0.1454         0.3959
        0.0024    0.0109          0.1635         0.5498
        0.0019    0.0181          0.1925         0.7265
        0.0116    0.0237          0.2344         0.9391
        -0.0083   0.0586          0.3167         1.2088
        0.1038    0.0336          0.4089         1.5757
        -0.1982   0.3542          0.7967         2.1251
        1.4948    -0.2406         0.9102         3.0777
        1.4948    4.2439          4.9136         5.2422
        Npolys=12
        Ncoefs=4
        Dim=1
```

Here `breaks` contains the breakpoints, `coefs` is a matrix whose ith row is the ith cubic polynomial, `npolys` is the number of polynomials, `ncoefs` is the number of coefficients per polynomial, and `dim` is the spline dimension. Note that this pp-form is sufficiently general that the spline polynomials need not be cubic. This fact is useful when the spline is integrated or differentiated.

In prior versions of MATLAB, the pp-form from was stored in a single numerical array rather than a structure. As a result, `unmkp` was valuable in separating the parts of the pp-form from the numerical array. Given the simplicity of the structure form, one can easily address the fields directly and avoid using `unmkpp` entirely. However, `unmkpp` continues to support the prior numerical array pp-form, thereby making process of extracting the parts of a pp-form transparent to the user.

Given the broken-apart form above, the function `mkpp` restores the pp-form, for example:

```
>> pp=mkpp (breaks, coefs)
 pp= form: 'pp'
 breaks: [0 1 2 3 4 5 6 7 8 9 10 11 12]
 coefs: [12 x 4 double]
 pieces: 12
 order: 4
 dim: 1
```

since the size of the matrix `coefs` determines `npolys` and `ncoefs` they are not needed by `mkpp` to reconstruct the pp-form.

By using the spline for data interpolaration, the goal for the program is to calculate, for the n seconds of measurement, the exact polynomials needed. The idea of heart signals comparison is based in the deviation of the factors of the polynomials, which will be discussed further in the analysis and process section.

4.5. Routine creation

For the spline functionality, during command input of the program at first the necessary routines in the system were created, so that each signal being inserted automatically calculates spline and shows the outcome in figure 48.
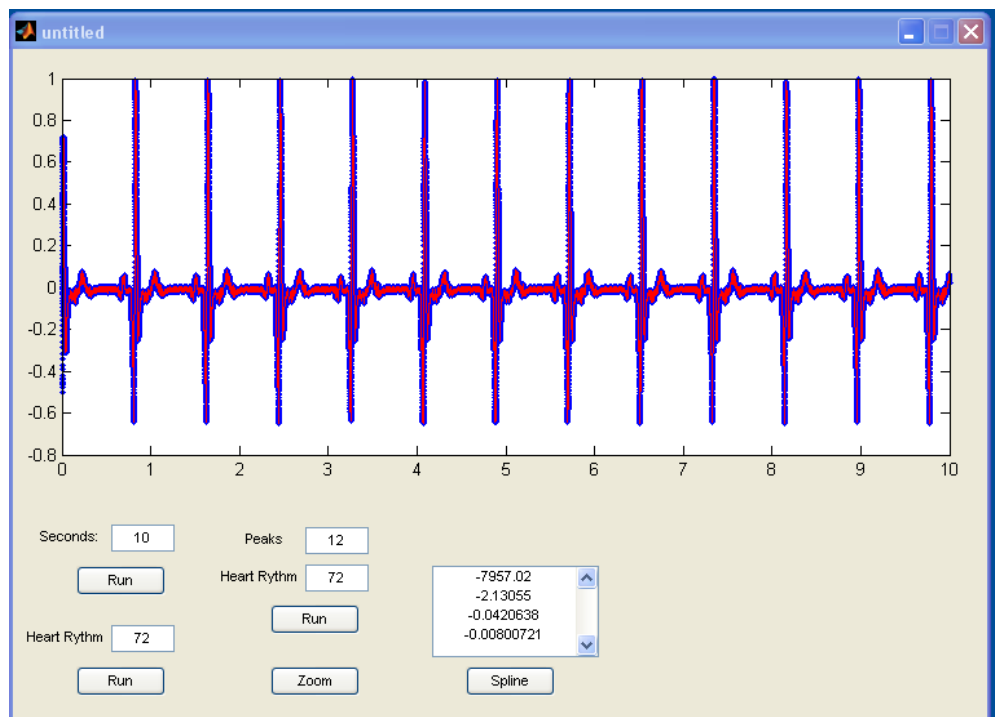
Figure 48. *Spline fit in program*

Also a box in which the user can see the standard deviation of the 4 factors was added. In the program all the necessary commands are inserted in order to show in an extra graph outside of the program the plot of pp.coefs of the spline fit (**figure 49**).
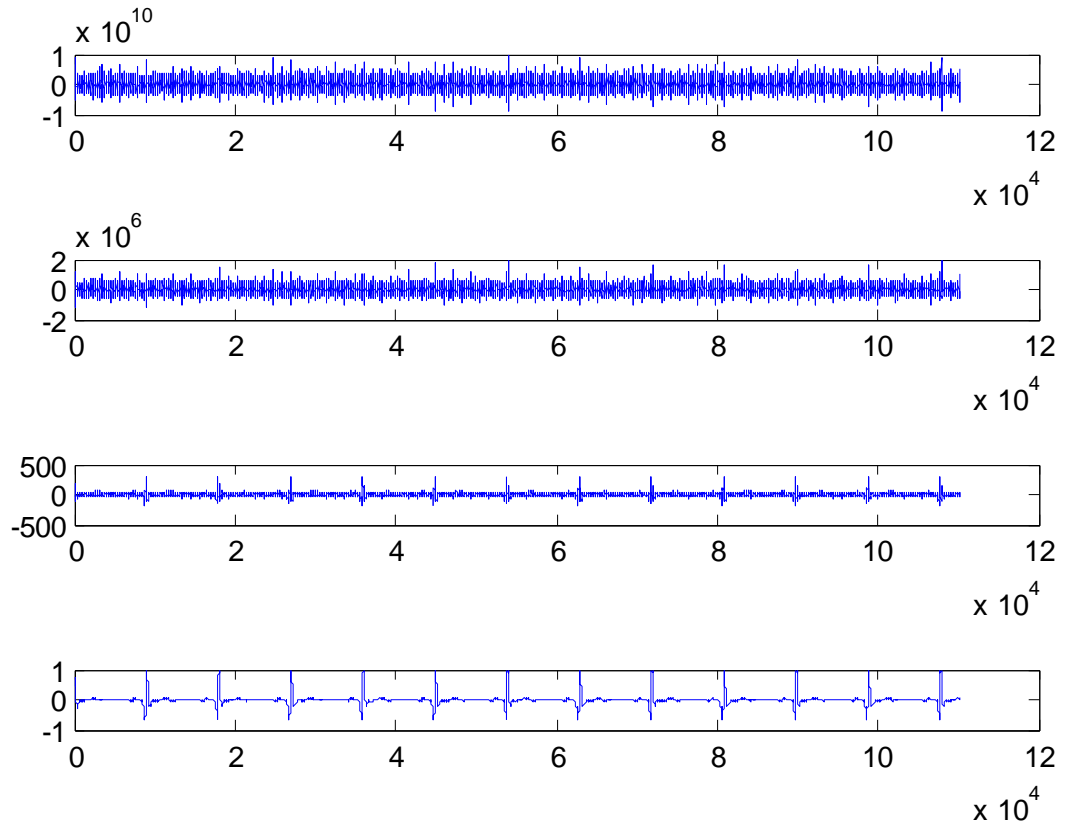
Figure 49. *pp.coef of the spline fit*

Another function added to the program so that can help in the diagnose, the user himself will perform, is the function of the calculation of the parameters set (standard deviation of 4 spline coefs) as a reference samples from various conditions. Figure 50 displays the user interface of the program after this install. The pop-up menu includes reference samples measured from the specific equipment and are the following:

- NSR
- VTpoly
- VF
- AFIB
- SVT
- ASYS

In the box above the pop-up menu the factor elements are displayed, as set for the specific signals. In the next box the heart rhythm for the specific signal/disease is also seen.
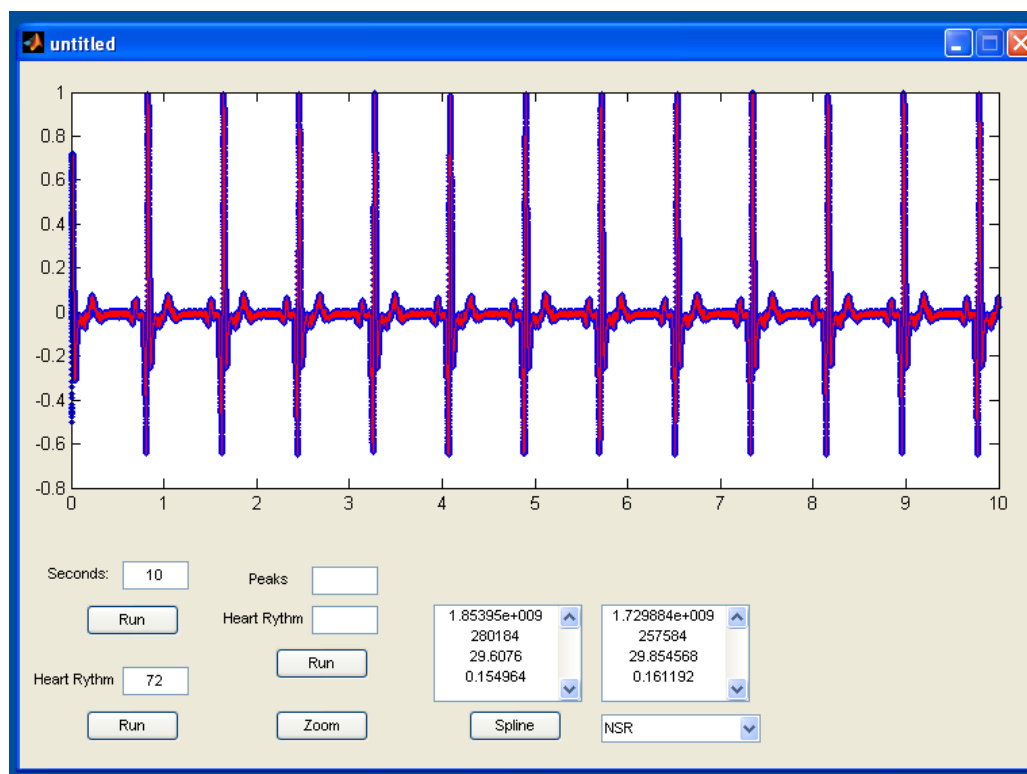
Figure 50. *Standard deviation of 4 coefs*

4.6. Acquisition

In order to perform a correct ECG, users ought to follow a raw of rules. All the cable equipment should be in good condition and, if possible, not crooked. The user should be aware of the full potential of the ECG and all the necessary tools for the procedure must be in place. The environment is necessary to be clean, sorted and quiet for the patient so that he can feel comfortable.

Helping the patient to lie down comfortably on the examination bed is the first thing to do. The inner part of the ankles and wrists must be wet before any cables can be attached. Then the sticky pads are applied.

Figure 51. *Patients performing ECG. A patient must be calm in order the ECG has reliable readings.[203]*

For children there are special sticky pads of smaller size of that of the adults. Even smaller ones are used for infants. The patient should stay as calm and still as possible and he shouldn't talk or be scared during the procedure or this would show an undesirable reading on the ECG. The ECG is a simple procedure that lasts in only a few minutes. In the most cases it does not cause pain and does not disturb the patient.

4.6.1. Usual difficulties during the procedure

It is not always easy for an ECG to take place despite it is a very easy procedure. Lots of factors can leverage the results of the ECG. Age, patience, mental condition, physical condition, fatigue and anxiety are some of them. How cooperative a patient can be is the first and foremost factor. It is very important for the patient to remain calm, relaxed and to retain fear or panic of his thoughts.

The most uncooperative patients are kids that, as all, do not trust strangers, and cannot stay still long enough for the procedure to take place. They usually feel fear because they can't understand what will happen in the next moments.

Figure 52. *Children are often the most demanding patients; they should be distracted so that they remain calm throughout the process.[204]*

They feel queer because they must take of their clothes in front of strangers. Depending to the patients age they sometimes get scared that something bad is about to happen or even start speculating on their condition. They can be tired from previous tests taken part earlier in the day and do not have enough patience for "another test". Children are the most demanding patients and it is not easy to persuade them to stay calm during an ECG. Adults on the other hand are not easy to relax, due to stress, fatigue and pressed schedule, or even fear that something wrong is happening to them. So the best thing to do is to explain with simple words the procedure of the test in order to calm the patient. It is highly advised to take the pressure and pulse of the patient for a more complete picture of the cardiac function.

4.6.2. Factors that influenced the readings and ways of confrontation

From all the ECG examinations, the most demanding ones are usually the ones that involves children. It is difficult to approach and persuade a child and to discipline it in the needs and rules of the procedure. The trick is to carry it out like it is a game in order to let it go and to get calm. In adults another type of problems is usually involved. For instance, intense hairy bodies or even strong sweat can interfere in the

reading of the ECG due to the not good appliance of the sticky pads. A long lasting dermatologic situation in the area of the thorax, a deep trauma or a burn could cause pain and worry the patient. The use of mobile phones is strictly restricted during the test, because the interference they cause can alter the efficiency of the ECG, or even the output data of the test. Another factor is the level of communication and consciousness of the patient. The way he reacts can difficult the reading of the ECG. A bad mental condition or stress can increase the heart beats and give the wrong impression during the test. Finally, intoxicated patients do not get reliable readings due to the rhythmic disorders they may indicate.

5. Simulation techniques

It has been obvious from scientists from the past years, and mentioned earlier in this research, that the heart signals tend to show a repetition if they compare their shape and data for the same functions between individual persons.
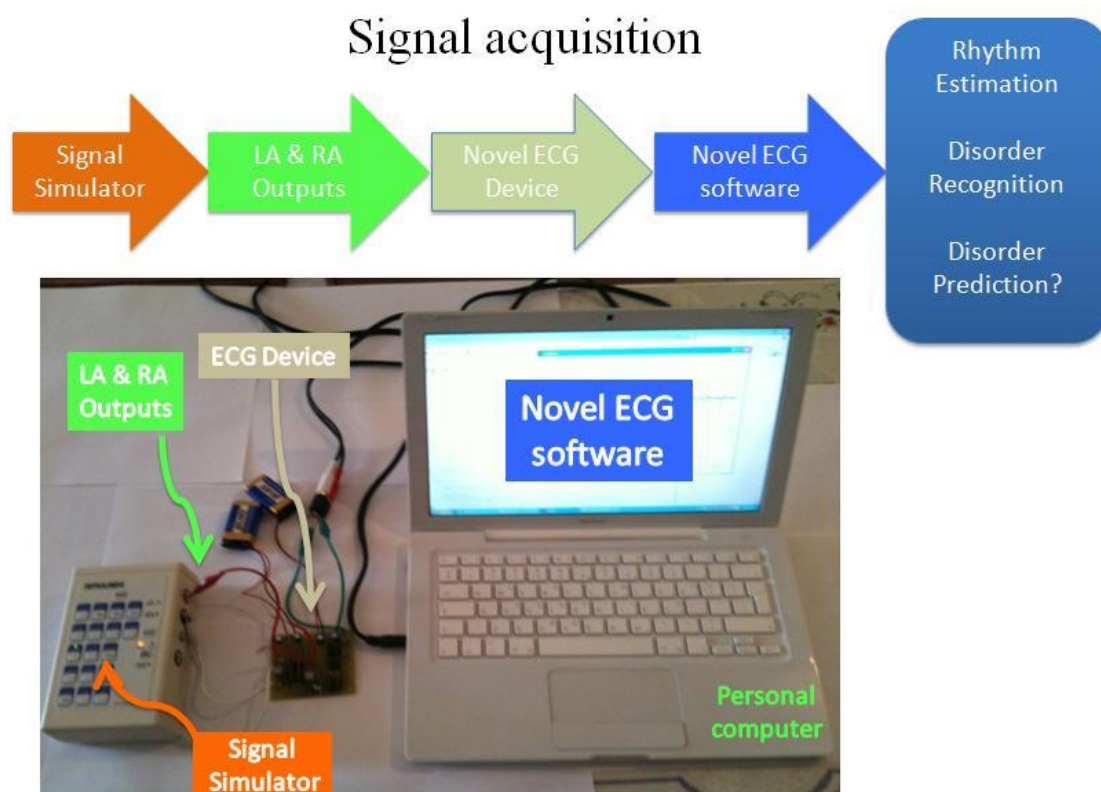
Figure 53. *The main tools for data collection, measurement and process.*

For the needs of not only diagnose, but also prediction as explaining later, a use of a heart beat signal simulator is needed in order to create a reference database of signals that will be used for analysis. This database is needed so that with the proper process a comparison of them with the readings extracted from a patient is applicable.

5.1. Simulating device

In this research, The Simulaids® ECG generator™ was used (figure 54). This particular device is a very useful, reliable and easy to use generator. It has the ability

to simulate 17 arrhythmias in both adult and pediatric rates. It can perform both three and four lead monitoring and obtain rhythm and defibrillate directly through paddles with optional manual adaptors.
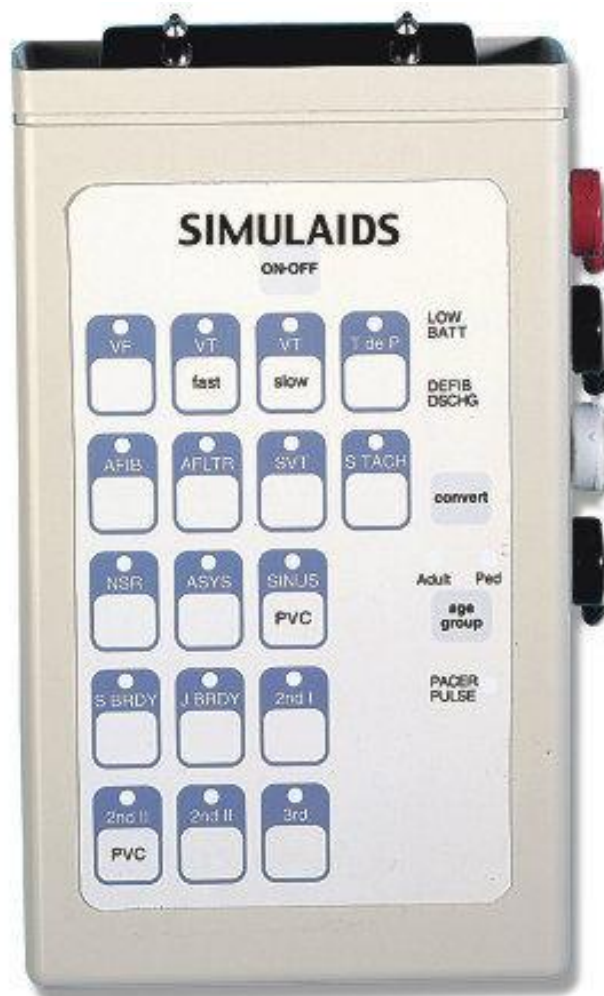
Figure 54. *The Simulaids interactive ECG simulator*

It has the ability to simulate the below heart conditions and combined variations of them.

- V. Fib
- V. Tach (Fast)
- V. Tach (Slow)
- V. Tach (Polymorphic)
- Fib
- Flutter

- SVT
- Sinus Tach
- Sinus with PVCs
- Asystole
- NSR
- Junctional Brady
- Sinus Brady
- 2nd degree type I A-V block
- 2nd degree type II A-V block
- 2nd degree type II A-V block with PVCs
- 3rd degree A-V block
- Generate realistic 3-lead or 4-lead ECG rhythms. The RA, LA, and LI signal morphologies create accurate representations of the QRS, P, and T axes.

5.2. Simulated signals

In the figures bellow, the reference signals measured with the simulator and the program are presented. All the signals have been measured for 10 seconds with waveform frequency at 11025Hz and have been normalized based in the maximum state.
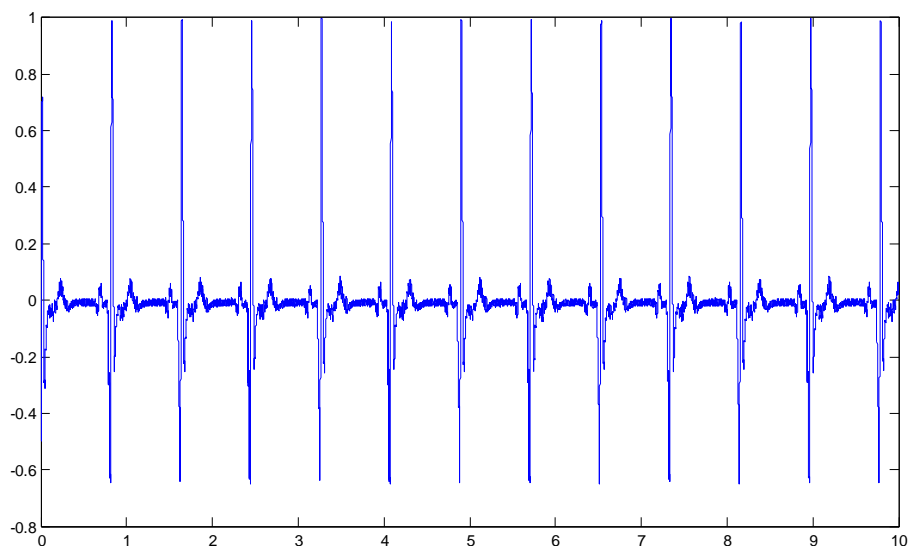
Figure 55. *NSR*
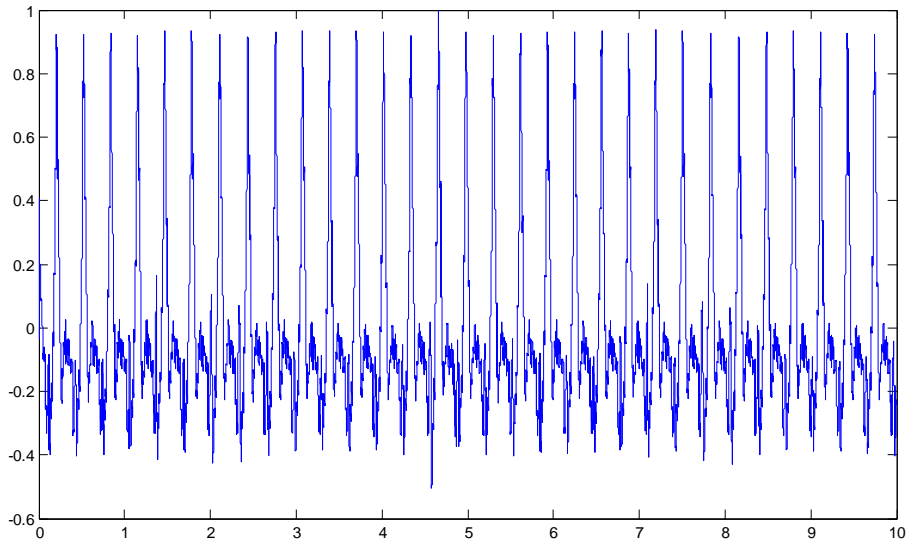
Figure 56. *VTfast*
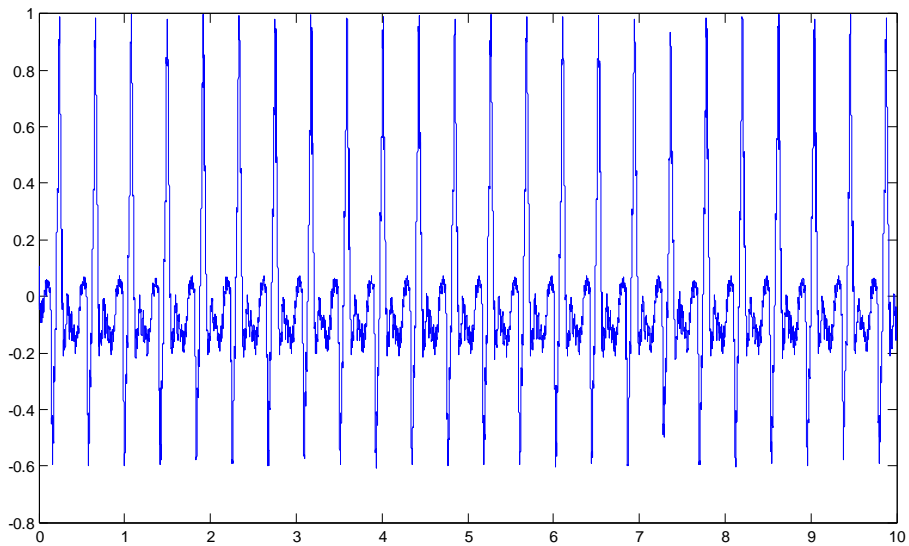
Figure 57. *VTslow*
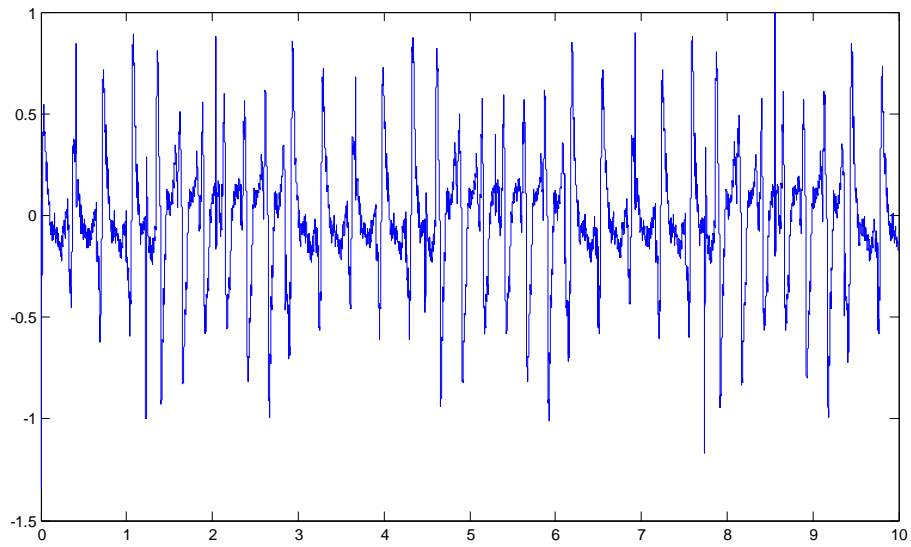
Figure 58. *VTpoly*
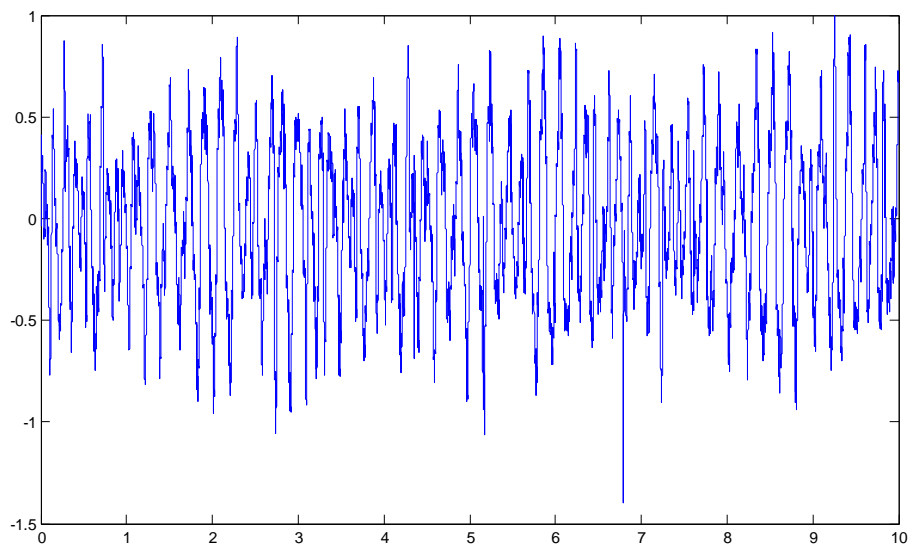
Figure 59. *VF*
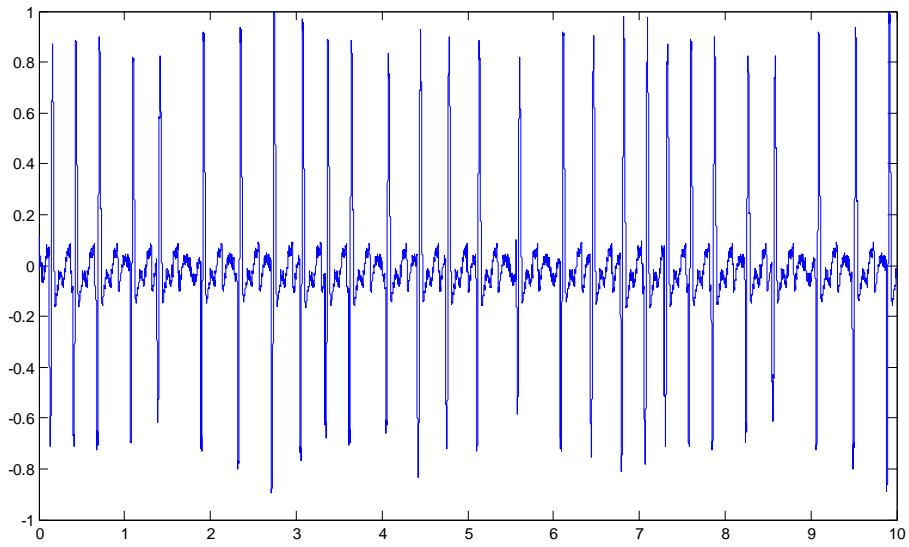
Figure 60. *AFIB*
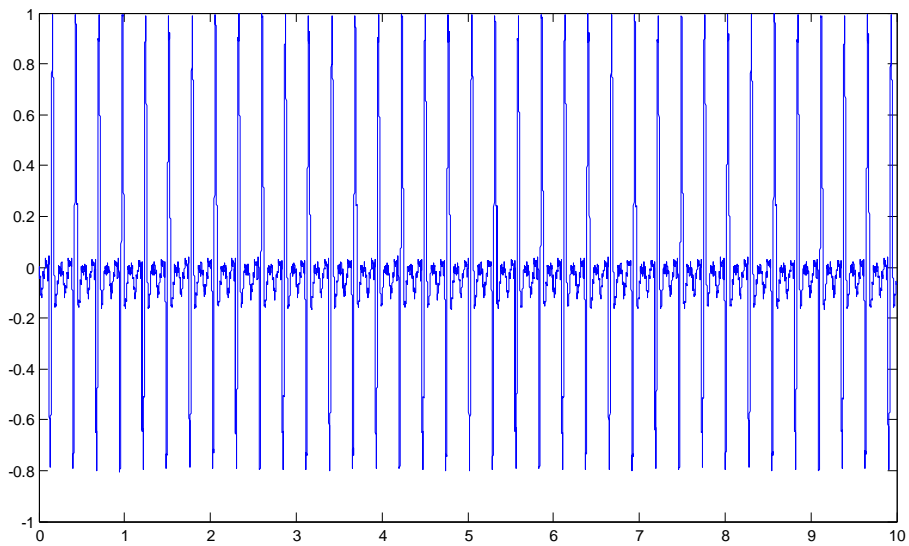
Figure 61. *SVT*
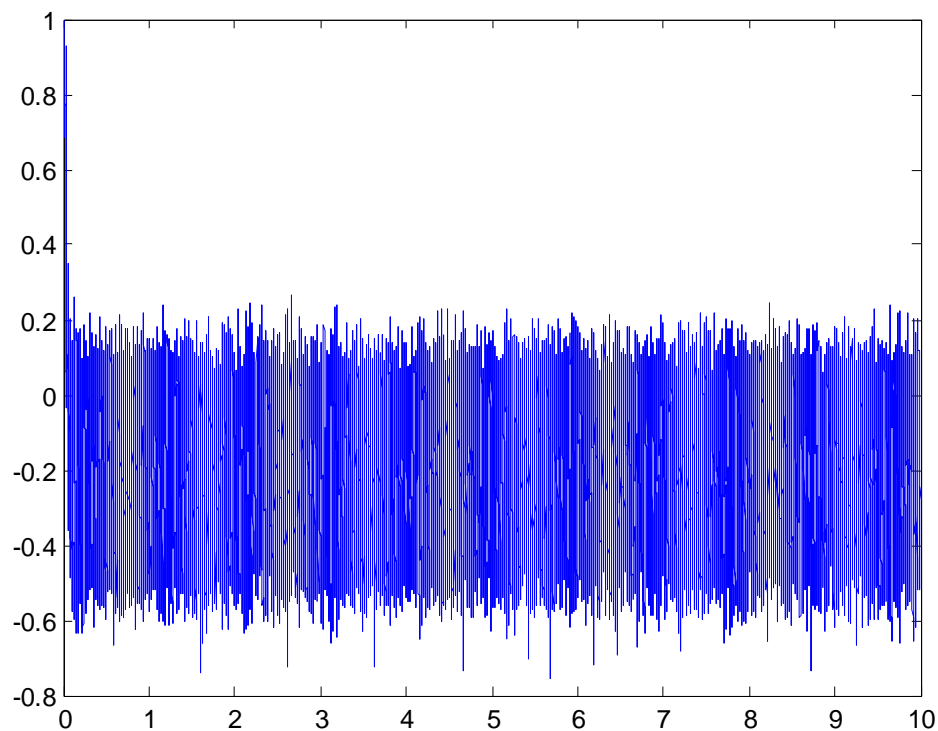
Figure 62. *ASYS*

5.3. Heart rhythm estimation

In chapter 4.3, the new functions created in Matlab for the calculation of the heart rate were introduced and a detailed analysis of the way of performed calculations was presented. This procedure is based on the calculation of the max states located in the final graph of the measurement.

In order to do so, as mentioned, all the top states are written down after normalization of them with max state. In many cases it is possible for the measurement of the max states to be proven inaccurate, because the program will measure all the max states, regardless which condition is the graph referred to.

Thus it is obvious that the basic given data in calculation of the heart rate is the visual recognition from the user. It is up to the user himself to understand whether the observed reading is, not only decease, but also that its heart rhythm reading has a meaning of existence. This happens due to the fact that the simulator isn't built to

perform a continuous 24/7 observation of a patient, but to perform a single, time based reading, for a dedicated amount of time given.

In Table 4 are values the program calculated for various types of heart conditions and the values that should be based in the bibliography.

Table 4: *Comparison between measured BPM and actual BPM based in bibliography*

SIGNAL	Measured	bibliography
NSR	72	60 - 100
VTfast	186	100 - 240
VTslow	144	100 - 240
AFIB	132	110 - 300
AFLTR	156	130 - 180
SVT	222	175 - 250
Pedi NSR	90	75 - 120
Pedi VTslow	144	100 - 240

5.4. Heart rhythm disorders

In chapter 4.3, there was a reference about the new functions. The use of spline fit for the heart signals analyze was chosen and the standard deviation of each particular signal was defined as representative factors. In case of asystole, as mentioned earlier, a factor has not been calculated, due to the reason that, only during optical recognition of the heart signal, one can conclude that there is no pulse in the heart.

In order to better study the disorders and possible correlations, the final program developed in chapter 4.3 was used in order to do repeated measurements in the Simulaids® ECG generator™ studied in chapter 3.7.1. More specifically, around 50 measurements in each heart condition studied, was performed. By doing so, a reasonably large enough data pool for statistic reasons was created.

In each measurement, the program calculated the standard deviation from each one of the four factors. These four factors (four standard deviation outputs) were recorded for each of the fifty measurements performed, per each heart condition. Next follows the calculation of the average expected value the four factors have, in each heart condition individually. In the following table, the average value of these four factors of spline coef, for the above reference signals, for 50 simulations following by their respective graphs is presented.

Table 5: *The four factors of spline fit which are given from the average values of 50 measurements*

	1st coef	2nd coef	3rd coef	4th coef
NSR	1,729884E+09	257584,24	29,854568	0.1611928
VTpoly	2,13E+09	324286,74	42,401066	0,25210052
VF	3,86E+09	573317,08	57,513844	0,34683454
AFIB	1,82E+09	272227,38	41,018404	0,22626798
SVT	1,79E+09	270306,88	44,918436	0,2476587

As it is being clear from Table 4, between the heart conditions forms some differences that lead to the conclusion that there might be able to interpret the results and perform a diagnose for the disorder or not of the heart.

After a lot of repetitive measurements and various calculations and graph plotting, it is concluded that the best and more secure way to study heart conditions and find the possible correlations they might have, is a bipolar plot of coef No 4 VS coef No3, that is consisted from the fifty repeated measurements per heart condition, for all heart conditions (Figure 63).
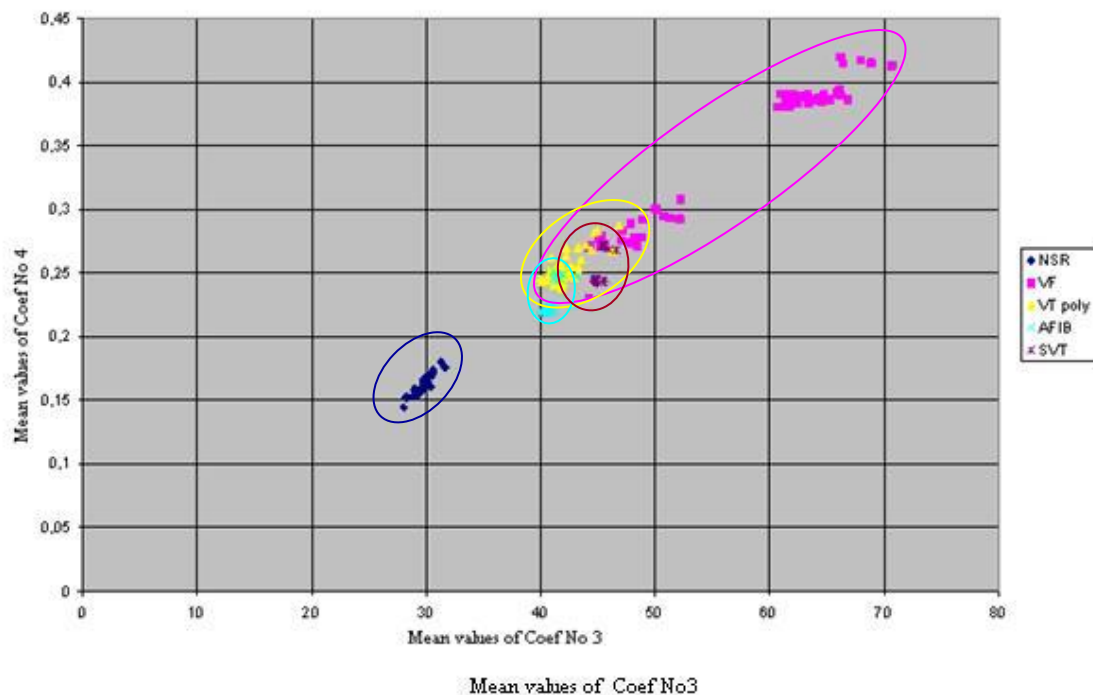
Figure 63. *Data with the necessary groups.*

An important conclusion can be exported while possessing figure 63. It is the capability to mathematically separate the actual heart disorders from the healthy signals. Secondly, there is an opportunity to evaluate the condition of a patient. To further evaluate and get a safer conclusion, further study of the rest of the factors, may occur. The only exception is where the measured factors are as followed: Factor No 3 around 60 to 70 and factor No4 to be around 0.4. There, it is pretty obvious that VF is the referred disease.

In an effort to better separation of the heart disorders with the help of the factors calculated, a 3D graph of factors 2, 3 and 4 was plotted.

In Figure 65, it is seen that the values that represent the NSR are in lower levels than any other value from any other signal. The VF conditions factors are righter and extend higher than the other signals. The VT condition is at the left of VF and NSR, but can differ than AFIB and SVT conditions because it is higher and on the right of them. AFIB condition differ than SVT because it is lower and on the left of it. So with the help of figure 64 it is now brighter than ever that mathematically, a separation of heart conditions with these 3 factors can be made.
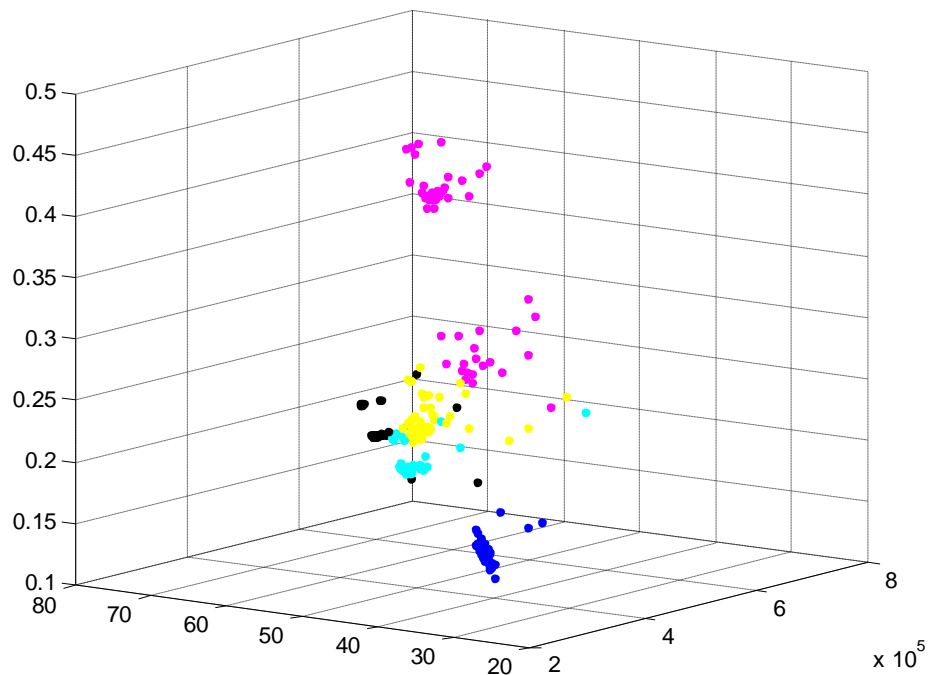
Figure 64. *3D graph of factors 2, 3 and 4.*

By moving further the study, a better understanding whether there is any linear relationship between the 3 factors needed to be done. So a linear fit for these 3 factors was done and discovered that factors 3 and 4 are linearly connected with an equation of R^2 equal to 0.96.
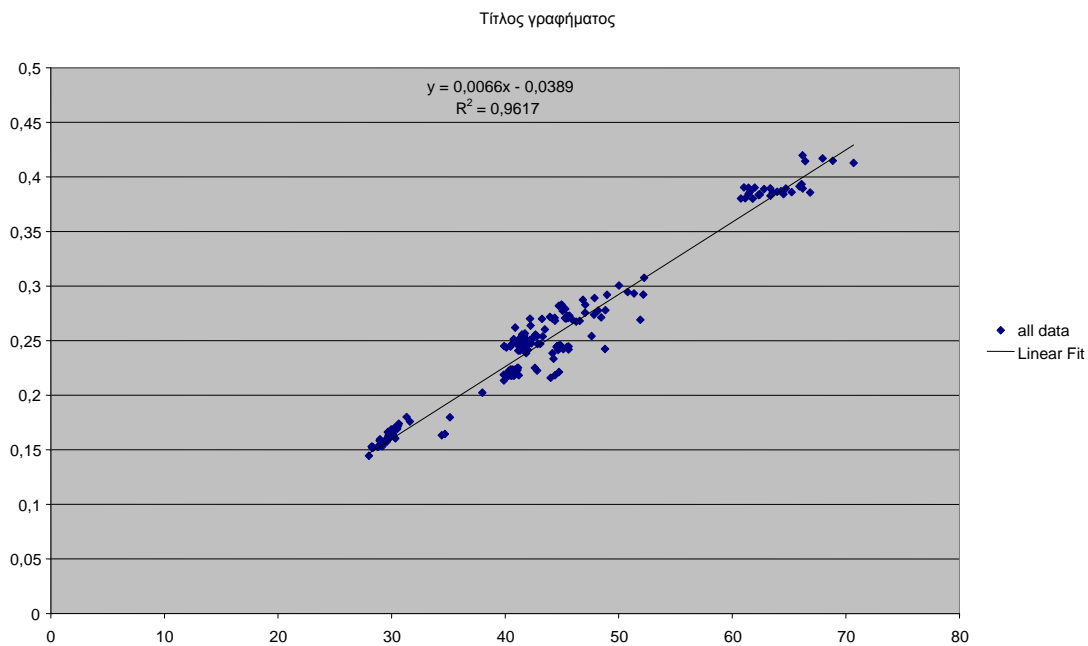
Figure 65. *Linear fit with all its parameters.*

5.5. Real Heart Signals

As this research continues, the first group of recorded data of real subjects is at the stage of comparison with the theoretical model. This group includes 35 volunteers, 12 of them are supposed to be NSR. The rest 23 patients have already been diagnosed with heart disorder and receive the appropriate medical treatment by their doctors. These patients were used in order to evaluate the accuracy of the theoretical model. All of the 35 characteristic values of the volunteers are shown in figure 66 while figure 67 represents the necessary grouping. Again, as it is obvious from Figure 68, these subjects are scattered through the area of the theoretical model that represents all the diseases. As shown in figures 68, 69, 70 and 71 the values are gathered inside the groups of each heart disorder.
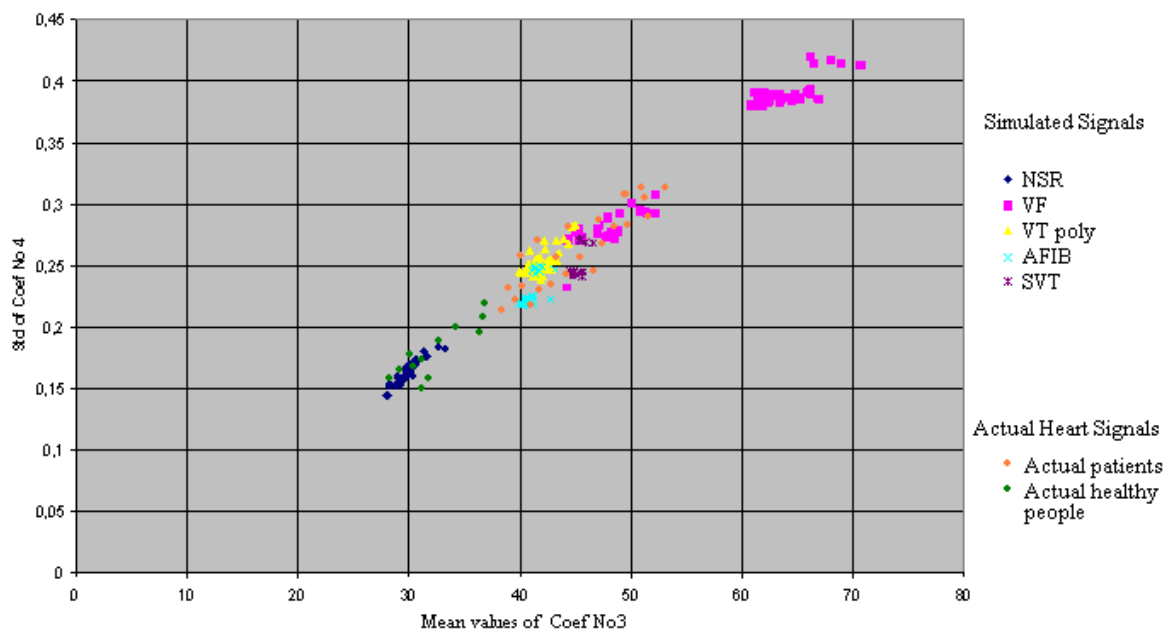
Figure 66: *Figure 64 including the actual heart signals*

All of the subjects have these pre mentioned heart disorders and are already taking medication from their attending doctor. The first conclusion that can be exported from the following figures is the verification of the theoretical model as the actual signals took their place in the expected positions.
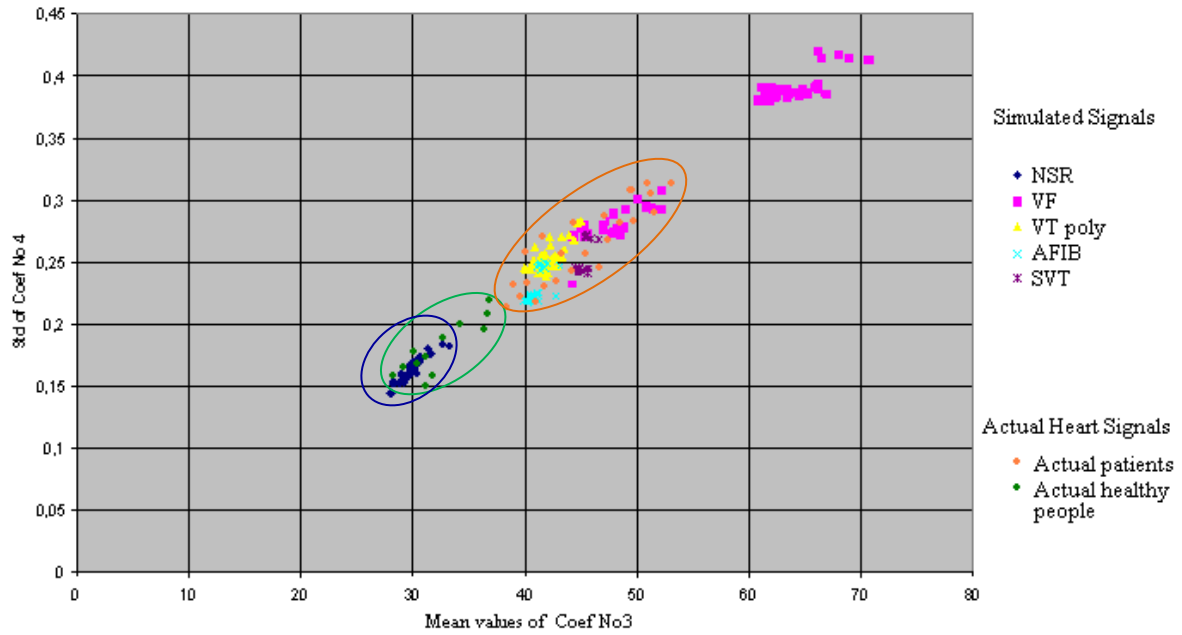
Figure 67: *Figure 66 with groups in the actual heart signals and simulated NSR*

Figure 68 shows the simulated VF signals and the actual subjects that are diagnosed with VF, all the actual patients are located in the same area with the simulated VF.
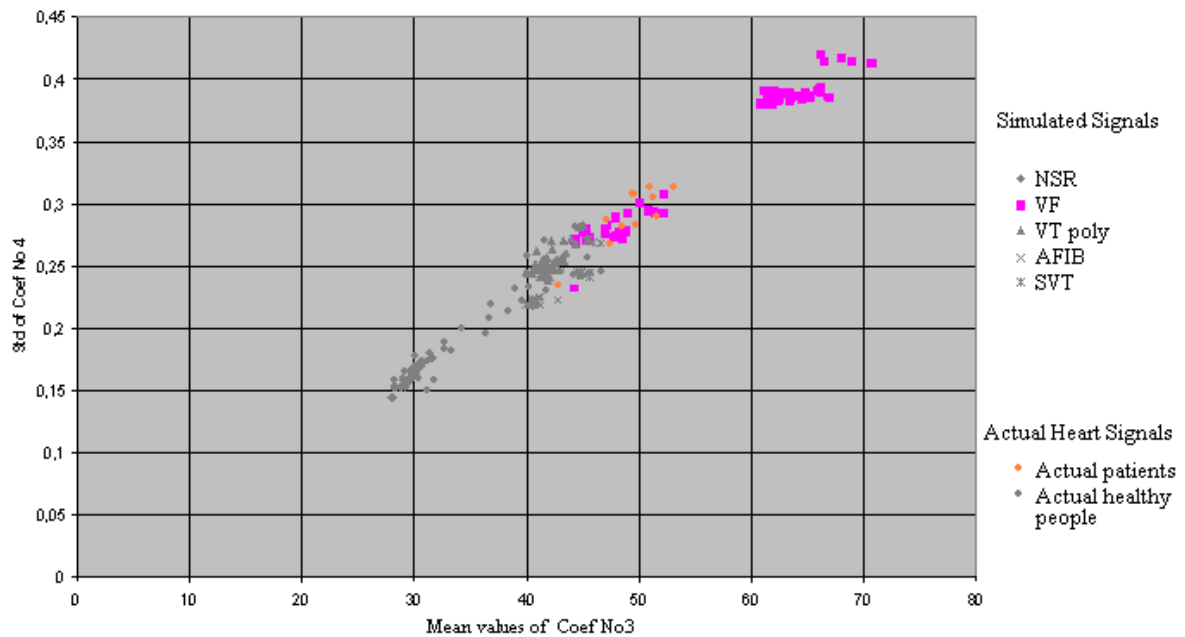
Figure 68: *VF simulated signals with the actual VF patients*

In figure 69 there is the same comparison but this time with the VT poly signals and at the same time the actual patients that are diagnosed with VT poly.
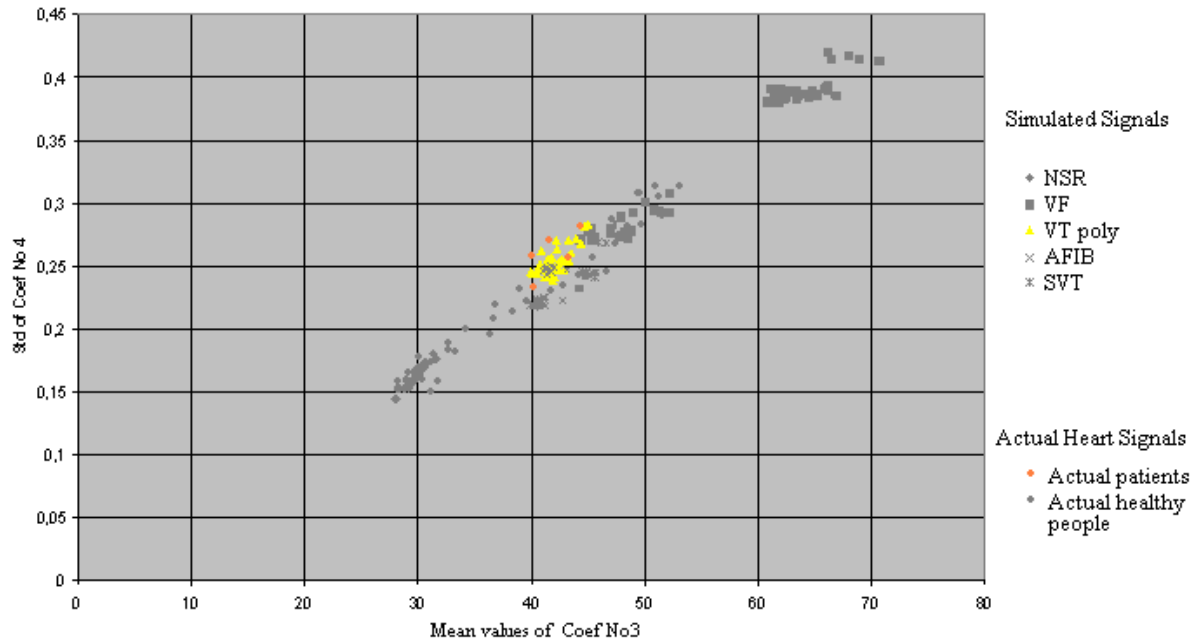
Figure 69: *VT poly simulated signals with the actual VT poly patients*

SVT simulated signals comes next in figure 70, again followed by the actual patients with SVT.
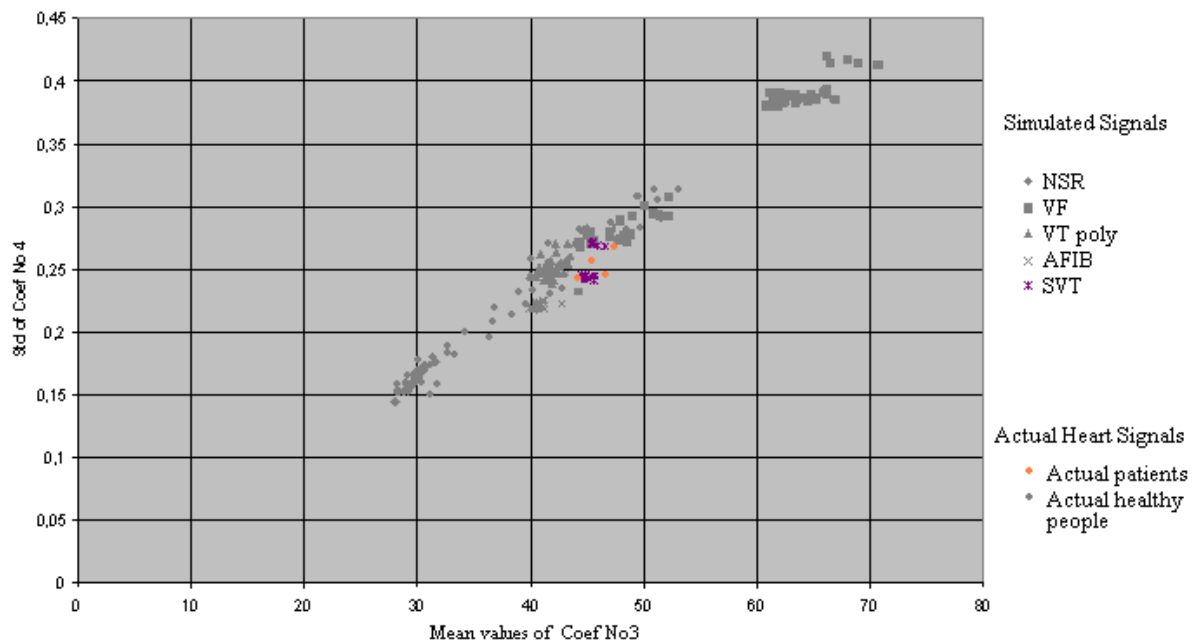
Figure 70: *SVT simulated signals with the actual SVT patients*

Figure 71 shows the simulated AFIB signals and the Actual patients that are diagnosed with AFIB, all the actual patients are located in the same area with the simulated AFIB.
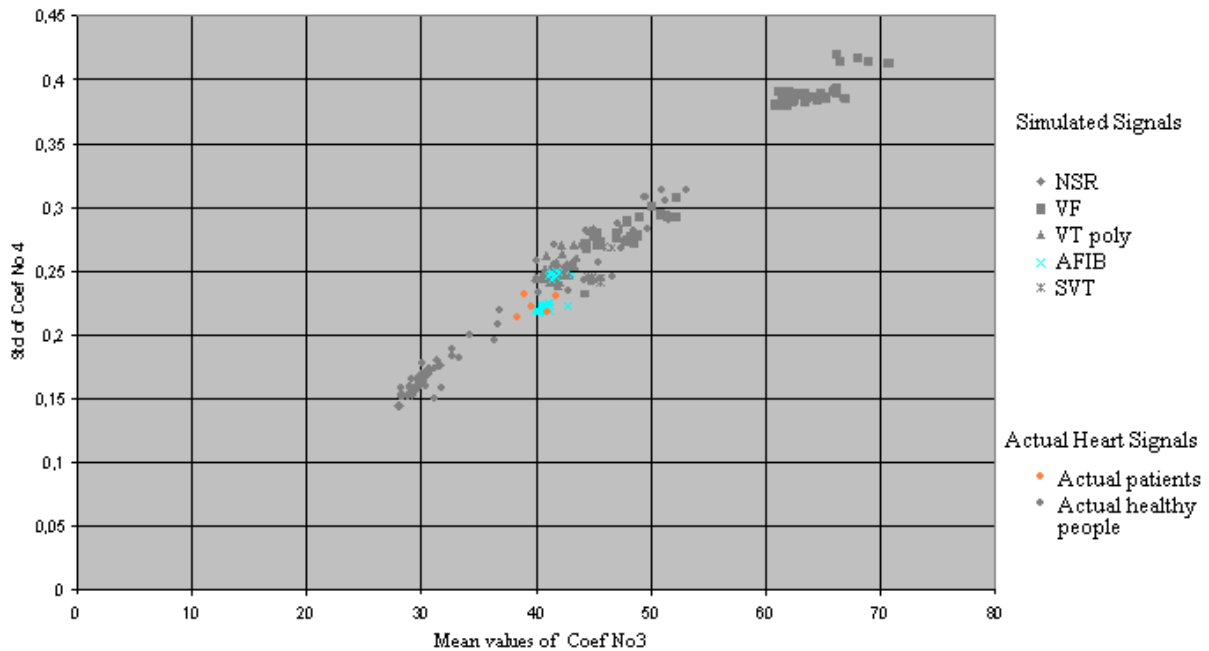
Figure 71: *AFIB simulated signals with the actual AFIB patients*

In figure 72 there are the NSR signals including all the healthy persons.
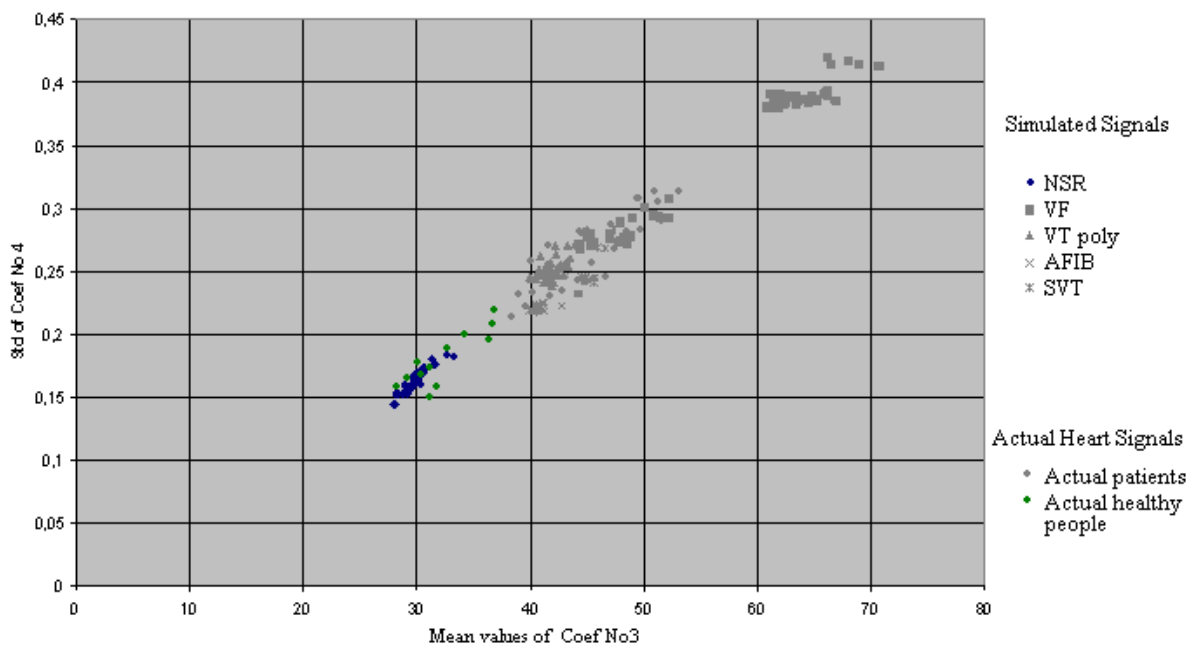
Figure 72: *NSR simulated signals with the actual healthy people.*

While processing and plotting their characteristic values in the theoretical model, as it is obvious from Figure 72 and better isolated in figure 73, four of them tend to show a high risk of heart defect since they are separating from the located NSR area.
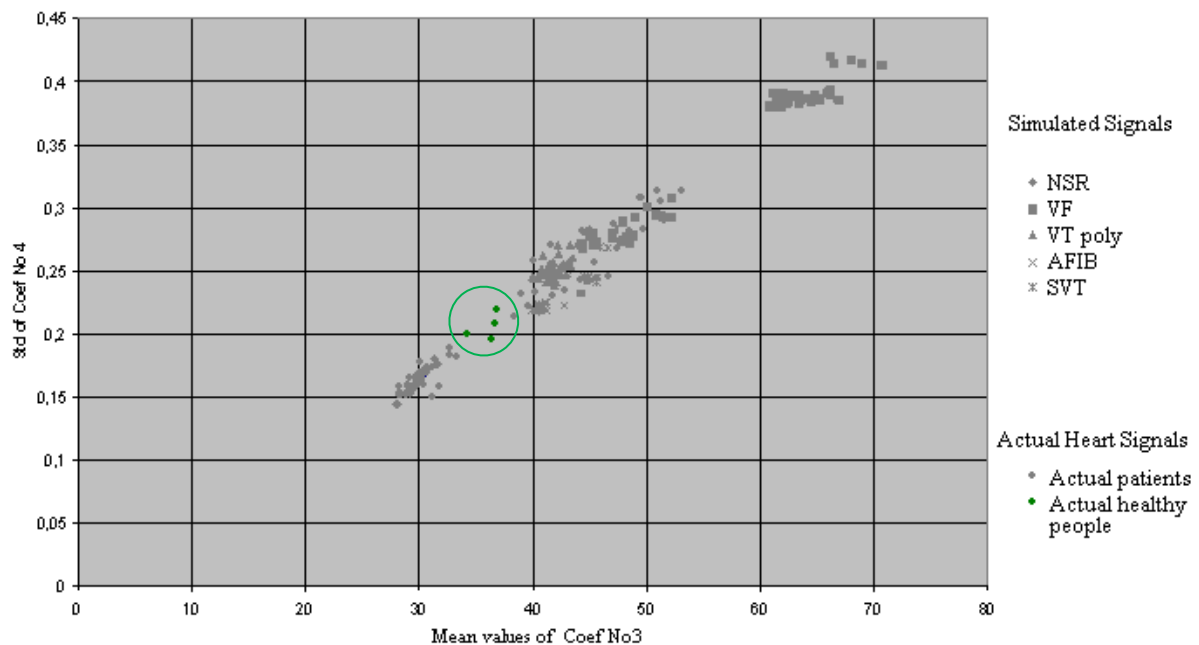
Figure 73: *The four actual healthy people that are instructed to further investigate their health.*

These persons were later interviewed; some of them confirmed that they experienced some sort of heave, or tachycardia after stress. They were suggested to further investigate these symptoms.

5.6. Differences between the theoretical model and various others

Through the years, in cardiac signal analysis are applied various methods of approach to both study of the heart and the analysis to explore the possibility of segregation of heart disorder and possible prediction. But in all these methods, extensive use of multiple equations and mathematical models is required, which they demand powerful dedicated servers. At the same time they are unreachable for scientists with lower mathematical profile where they require a simpler and specific

pattern for recognition and further study of various heart disorders. In the following paragraphs some of the most widely spread cases with various and complex models and approximates are presented.

In 2006 Neascu et all, study two forms of signals, from healthy and stressed people, in various approaches, like Power spectrum, Correlation, wavelet maps, return maps etc. Their results does not exceed from the already known, that the function of the heart is complex enough, but in they end up in the conclusion that though the semi-quantitative tests applied to the ECG signal analysis are not able to provide specific information regarding the intrinsic mechanisms of the heart, they might lead to a more "colored" picture of the modifications induced by the physiological condition of stress [205]. In the approach studied by this research, the use of multiple equations is not used; on the contrary the obvious is being modeled. In figure 75 the ECG of a calm person and a stressed one is shown. Without the need to further get to the internal mechanisms that produce these differences, simply the diversity is being modeled and represented with the created bi-plot program. Later it is possible to notice whether different stress factors affect differently in the morphology of the signal, but for the time being, the differentiation can be done with the suggested simple approach. Nevertheless as shown in figure 74, artificially stressed persons were differentiated from the healthy group of subjects without approaching the patients group.
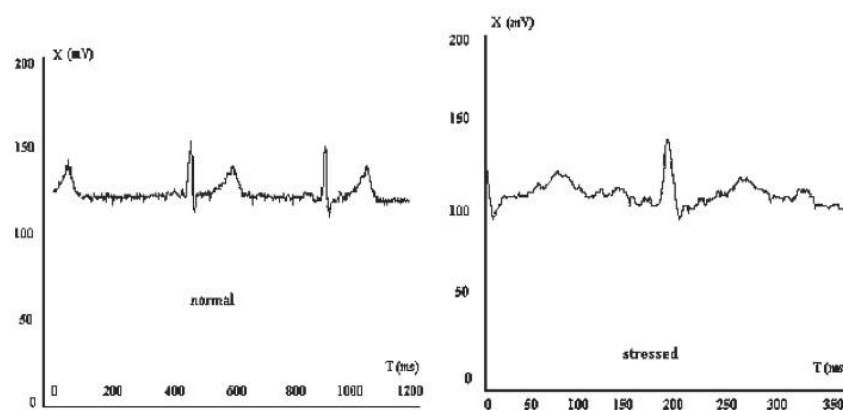
Figure 74: *Left ECG: a "normal" ECG VS a "stressed" ECG of the same individual person [205].*

In 2005, Zhang et all, studied cardiac signals with the use of Principal component Analysis and Support Vector Machines. They conclude in the already

known fact that under circumstances, PCA and SVM can give some elements to evaluate ECG [206]. But in his case as well as other papers [207] the need of complex dedicated servers are needed for a simple diagnose, so when it comes to prediction, that is even more complex. Considering the fact that the main purpose of this research was to study ECG and approach them through a simplified methodology, both PCA, as well the use of neural networks was out of the question.

From the current study it has been obvious that the simple separate of diseases with 3D plot (figure 64) is totally safe and can directly incorporate as a subprogram of the main computing software through commands "if then else". These commands in each new measurement, examine the factors of coefs 2, 3, 4 and cubic spline to decide in which group the measured signal is part of.

The use of SVM could complete the safe separation of the specific group in case the research required could not easily be separated. Its use was not considered necessary to apply, and foremost it was not applicable in the timeframe of this research, due to the fact that the main disadvantage of SVM is that if the number of features is much greater than the number of samples, the method is likely to give poor performances. In this part of the research the analysis was made with mainly simulated signals as reference signals of each heart disorder since the amount of real signals is not in the same analogy. From the simulated signals it is obvious that the 3D plot diagram (Figure 64) was enough for the separation. However, from a practical point of view perhaps the most serious problem with SVMs is the high algorithmic complexity which preferably should be avoided since, as mentioned earlier, it uses part of the ECG signal and not the entire form of it.

In conclusion, there is a wide variety of studies and papers that use SVM and PCA for ECG analysis. In all these cases the methodologies are based in specific attributes of the signals, such as the width, or the amplitude of the QRS area. Yet there are methodologies that use the method of cubic spline in order to correct ECG from baseline drift or to model some of its areas like QRS.

This methodology approach in the contrary to all the pre-mentioned models does not examine some areas of ECG, but through modeling the entire ECG and configures it as an equation with specific factors. These factors are unique for each ECG signal, so if a manual change of them appears then the original ECG signal will be altered. But, in any time of the research, when the groups of patients are completed

with the theoretical model and an extra analysis in a specific group is essential, then SVM method can be applied to analyze parts of the ECG signals database.

6. Conclusions and further development of the research

6.1. Conclusions

In conclusion, through this research it is proven that the evaluation of a heart signal can be done with mathematical equations or with specific algorithms. In these algorithms there is a capability to evaluate a heart signal and analyze with safety whether it belongs to a healthy heart or not. It can even clarify with relative ease, in case of a non healthy heart, the heart condition it suffers.

As for the capability to predict the appearance of a disorder, the results were very promising. A group of 35 individual persons were used in order to apply their characteristic patterns in the theoretical model. As mentioned earlier, 22 persons are actual patients that have diagnosed heart disorders and are already taking medication from their attending doctors. The values from these patients are located not only inside the general group of the simulated non-healthy ECGs (figure 70), but also in the dedicated groups of the simulated ECGs, as seen in Figures 68 - 72. The rest 13 persons don't have any history related to heart diseases. As expected, these data signals are plotted in the same group of the simulated NSR signals (figure 72). In figure 73 there are 4 persons that their characteristic values tend to show a distance from the rest NSR signals, simulated and real, and tend to approach the ones with various diseases. This tendency was expected in order to prove whether the theoretical model is correct regarding the capability to predict the appearance of a disorder. These individual persons were later interviewed and confirmed that they experience some short of heave or tachycardia after stress. They were suggested to further investigate those symptoms by visiting a doctor. So, figure 73 exports great expectations that there is a possibility a heart condition may occur when a signal of a healthy heart diverges from the limits of a SNR signal. Then a more systematic monitoring should take part, in order to see if this speculation is correct. Increased chances of occurrence of heart disorder has a heart in which its values go way beyond the values of a NSR and get closer to the values indicating heart malfunction. They

appear in the "pre heart disorder area" which is the area between the two main groups (figure 73).

All the results presented in this research, lead to a breakthrough methodology as the comparison of coefficient factors and heart disorder groups measured, shows continuity as seen in the linear fit graph (figure 63). Based to all the above, the novel methodology, as well as the theoretical novel applied are highly accurate, not only for heart disorder categorization, but also for heart disorder prediction analysis.

6.2. Further development

To further develop the research; more human data is needed especially from people with no history of heart diseases but with the characteristic patterns alike the ones of figure 73. These people tend to show a distance from the rest NSR signals, simulated and real, and are included in the "pre heart disorder area".

Next step is the comparison of the groups and also the individual readings collected, with the theoretical model. Notable attention needs the affect of age and sex in the rates of the model. It is highly important to understand how the advance (of each heart disorder) factor affects the theoretical model. It is significant to observewhetherthisfactordecreasesorincreasesthedispersionofthepoints in the areas where the theoretical model limits the disorder.

At this point, a further research is required, that deals with the monitoring of this group with continuous measurements in order to check whether the prediction model is totally accurate. Meaning, if the future group of subjects located in the "pre heart disorder area" like the 4 people in this research, who despite not having a recorded heart disorder history, their measurements excluded them from the "NSR" group, confirms a heart abnormality through future clinical tests, then can be said that the heart disorder prediction model, presented in this research is totally accurate. The separation of the patient readings should be divided into groups, and the grouping could be based onto age or sex. This research should need one attending doctor in order to examine persons on a monthly basis, not necessarily in hospitals or medical departments since measurements will be taken only from the novel signal analyzer presented in this research. Also repeated tests every 3 months in hospital units are to take place, that include: Stress test, ECG, blood samples, cholesterol and triglycerides.

Chapter 6: Conclusions and further development

If during the research someone from the group proves to evolve a heart disorder, then the subject should automatically be removed from the monitoring group since is characterized as "patient" and is moved to a different database. The goal of this post research is to observe the transition of the particular subject readings as they progress though time, how its factors change and how they evolve in the theoretical model. In case of correlation of the movement rate to the areas with heart disorders in time, this wills outcome a different version of the prediction model which could include a time prediction parameter.

As for the novel ECG analyzer that is developed for the needs of this research, mild updates are needed in order to become a more user friendly device. The improvement of the external appearance which includes the appropriate casing and documentation will make it more elegant and help it find its way in the retail market. Secondly and most important is the development a communication accessory that cooperates with the device and can transfer the readings directly to the computer as raw data without the use of the sound card. This could be done by sending the data with some form of wireless communication from the existing technology such as Bluetooth and Wi-Fi; after all, they are widely spread to the market. Alternatively, redesign of the device and installation of a wireless input-output controller compatible with one, if not all, of the previously mentioned technologies. In this way each individual patient could perform a simple test to himself and send the data after collecting them from device directly to the doctor via his mobile phone or PC by email, without even having to visit him.Finally all this future research will contribute to a further investigation of the heart physiology and of course, to predict a human heart disorder.

References

1. Gray, H., and Lewis, W. H. Anatomy of the human body, 20th ed. Lea and Febiger, Philadelphia ; New York, 1918.Coumel P, Fayn J, Maison-Blanche P & Rubel P (1994) Clinical relevance of assessing QT dynamicity in Holter recordings. J Electrocardiology 27S: 62-66.
2. http://en.wikipedia.org/wiki/Image:Diagramfheumaneart28cropped%29.svg
3. Stein, W. D. Channels, Carriers and Pumps: An Introduction to Membrane Transport. Academic Press, San Diego, 1990.
4. Z. Ihara, "design and performance of lead systems for the analysis of atrial signal components in the ECG", École Polytechnique Federale De Lausanne, 2006.
5. Plonsey, R., and Barr, R. C. Bioelectricity, a quantitative approach, 2 ed. Kluwer Academic / Plenum Publishers, New York, 2000.
6. E. Marbán, "Cardiac channelopathies" Nature 415, 213-218, Jan 2002.
7. Waller, A. D. On the electromotive changes connected with the beat of the mammalian heart, and of the human heart in particular. Phil Trans R Soc B 180 (1889), 169–194.
8. http://4.bp.blogspot.com/_rSjy2FkXvWo/R741av8FlpI/AAAAAAAAAAo/nKLOh6 bG5F8/s400/Willem_Einthoven_ECG.jpg
9. Einthoven, W. Die galvanometrische Registrierung des menschlichen Elektrokardiogramms, zugleich eine Beurtheilung der Anwendung des Capillarelektrometers in der Physiologie. Pflugers Archiv f˙ur die Gesamte Physiologie des Menschen und der Tiere 99, 472-480 (1903).
10. Baselli G, Cerutti S, Civardi S, Lombardi F, Malliani A, Merri M, Pagani M & Rizzo G (1987) Heart rate variability signal processing: A quantitative approach as an aid to diagnosis in cardiovascular pathologies. Int J Bio Med Comput 20: 51-70.
11. http://en.wikipedia.org/wiki/Actionotential.
12. http://www.cvphysiology.com/Arrhythmias/A007.htm.
13. http://www.mfi.ku.dk.
14. Malmivuo J & Plonsey R (1995) Bioelectromagnetism. Oxford University Press, New York.
15. L. Sornmo and P. Laguna, Bioelectrical Signal Processing in Cardiac and Neurological Applications. Linacre House Jordan Hill Oxford OX2 8DP United Kingdom: Elsevier, 1 ed., 2005.
16. http://www.cvphysiology.com/Cardiac%20Function/CF022.htm
17. http://www.cvphysiology.com/Cardiac%20Function/CF022.htm .
18. Eckberg D (1983) Human sinus arrhythmia as an index of vagal cardiac outflow. Respirat Environ Exercise Physiol 54(4): 961-966.
19. Akselrod S, Gordon D, Madved J, Snidman N, Shannon D & Cohen R (1985) Hemodynamic regulation: investigation by spectral analysis. Am J Physiol 249: H867-H875.
20. VanRavenswaaij-Arts C, Koll_ee L, Hopman J, Stoelinga G & VanGeijn H (1993) Heart rate variability, review. Ann Intern Med 118(6): 436-447.
21. Kitney R & Rompelman O (eds) (1987) The Beat-by-Beat Investigation of Function. Clarendon Press, Oxford.
22. Pagani M, Lombardi F, Guzzetti S, Rimoldi O, Malfatto G, Cerutti S & Malliani A (1984) Power spectral density of heart rate variability as an index of sympatho-vagal interaction in normal and hypertensive subjects. J Hypertens 2(suppl. 3): 383-385.
23. Pomeranz B, Macaulay R, Caudill M, Kutz I, Adam D, Gordon D, Kilborn K, Barger A, Shannon D, Cohen R & Benson H (1985) Assessment of autonomic function in man by heart rate spectral analysis. Am J Physiol 248(Heart Circ. Physiol. 17): H151-H153.

References

24. Hainsworth R (1995) The control and physiological importance of heart rate. In: Malik M & Camm A (eds) Heart rate variability. Futura Publishing Company Inc., Armonk, p 3-19.
25. Kamath M & Fallen E (1993) Power spectral analysis of heart rate variability: a noninvasive signature of cardiac autonomic function. Crit Rev Biomed Eng 21(3): 245-311.
26. Merri M, Alberti M & Moss A (1993) Dynamic analysis of ventricular repolarization duration from 24-hour Holter recordings. IEEE Trans Biomed Eng 40(12): 1219-1225.
27. Task Force of ESC & NASPE (1996) Heart rate variability. Standards of measurement, physiological interpretation, and clinical use. Task Force of the European Society of Cardiology and the North American Society of Pacing and Electrophysiology. Circulation 93(5): 1043-1065.
28. Farrell T, Bashir Y, Cripps T, Malik M, Poloniecki J, Bennett E, Ward D & Camm A (1991) Risk strati_cation for arrhythmic events in postinfarction patients based on heart rate variability, ambulatory electrocardiographic variables and the signal averaged electrocardiogram. J Am Coll Cardiol 18: 687-697.
29. Casolo G, Stroder P, Signorini C, Calzolari F, Zucchini M & Balli E (1992) Heart rate variability during the acute phase of myocardial infarction. Circulation 85: 2073-2079.
30. Huikuri H, Sepp¨anen T, Koistinen M, Airaksinen K, Ik¨aheimo M, Castellanos A & Myerburg R (1996) Abnormalities in beat-to-beat dynamics of heart rate before the spontaneous onset of life-threatening ventricular tachyarrhythmias in patients with prior myocardial infarction. Circulation 93: 1836-1844.
31. Lombardi F, Sandrone G, Mortara A, Rovere ML, Colombo E, Guzzetti S & Malliani A (1992) Circadian variation of spectral indices of heart rate variability after myocardial infarction Am Heart J 123: 1521-1529.
32. Malliani A, Pagani M, Lombardi F & Cerutti S (1991) Cardiovascular neural regulation explored in the frequency domain. Circulation 84(2): 482-492.
33. Bellavere F (1995) Heart rate variability in patients with diabetes and other noncardiological diseases. In: Malik M & Camm A (eds) Heart rate variability. Futura Publishing Company, Armonk, p 507-516.
34. Pagani M, Malfatto G, Pierini S, Casati R, Masu A, Poli M, Guzzetti F, Lombardi F, Cerutti S & Malliani A (1988a) Spectral analysis of heart rate varibility in the assessment of autonomic diabetic neuropathy. J Auton Nerv Syst 23: 143-153.
35. Freeman R, Saul J, Roberts M, Berger R, Broadbridge C & Cohen R (1991) Spectral analysis of heart rate in diabetic neuropathy. Arch Neurol 48: 185-190.
36. Bernardi L, Ricordi L, Lazzari P, Sold_a P, Calciati A, Ferrari M, Vandea I, Finardi G & Frantino P (1992) Impaired circulation modulation of sympathovagal modulation of sympathovagal activity in diabetes. Circulation 86: 1443-1452.
37. Huikuri H (1997) Abnormal dynamics of ventricular repolarization - a new insight into the mechanisms of life-threatening ventricular arrhythmias. Eur Heart J 18: 893-895.
38. Selman A, McDonald A, Kitney R & Linkens D (1982) The interaction between heart rate and respiration: Part I. Experimental studies in man. Automedica 4: 131-139.
39. Adamson P, Huang M, Vanoli E, Foreman R, Schwartz P & Hull S (1994) Unexpected interaction between myocardial infarction: a longitudinal study in dogs at high and low risk for sudden cardiac death. Circulation 90: 976-982.
40. Molgaard H, Mickley H, Pless P, Bjerregaard P & Moller M (1993) E on heart rate variability in survivors of acute myocardial infarction. Am J Cardiol 71: 1357-1359.
41. Sandrone G, Mortara A, Torzillo D, Rovere ML, Malliani A & Lombardi F (1994) Effects of beta blockers (atenolol or metoprolol) on heart rate variability after acute myocardial infarction. Am J Cardiol 74: 340-345.

References

42. Zuanetti G, Latini R, Neilson J, Schwartz P, Ewing D & the Antiarrhythmic drug evaluation group (ADEG) (1991) Heart rate variability in patients with ventricular arrhythmias: Effect of antiarrhythmic drugs. J Am Coll Cardiol 17: 604-612.
43. Bigger J, Rolnitzky L, Steinman R & Fleiss J (1994) Predicting mortality after myocardial infarction from the response of RR variability to antiarrhythmic drug therapy. J Am Coll Cardiol 23: 733-740.
44. Pagani M, Somers V, Furlan R, Dell'Orto S, Conway J, Baselli G, Cerutti S, Sleight P & Malliani M (1988b) Changes in autonomic regulation induced by physical training in mild hypertension. Hypertension 12: 600-610.
45. Furlan R, Piazza S, Dell'Orto S, Gentile E, Cerutti S, Pagani M & Malliani A (1993) Early and late effects of exercise and athletic training on neural mechanisms controlling heart rate. Cardiovascular Research 27: 482-488.
46. Rovere ML, Specchia G, Mortara A & Schwartz P (1988) Baroreflex sensitivity, clinical correlates, and cardiovascular mortality among patients with a first myocardial infarct. Circulation 78: 816-824.
47. Malliani A, Pagani M, Lombardi F & Cerutti S (1991) Cardiovascular neural regulation explored in the frequency domain. Circulation 84(2): 482-492.
48. Pagani M, Lucini D, Rimoldi O, Furlan R, Piazza S & Biancardi L (1995) Effects of physical and mental exercise on heart rate variability. In: Malik M & Camm A (eds) Heart rate variability. Futura Publishing Company Inc., Armonk, p 245-266.
49. Janssen M, Swenne C, de Bie J, Rompelman O & van Bemmel J (1993) Methods in heart rate variability analysis: Which tachogram should we choose? Comput Methods Programs Biomed 41: 1-8.
50. Merri M, Benhorin J, Alberti M, Locati E & Moss A (1989) Electrocardiographic quantitation of ventricular repolarization. Circulation 80: 1301-1308.
51. Speranza G, Nollo G, Ravelli F & Antolini R (1993) Beat-to-beat measurement and analysis of the R-T interval in 24 h ECG Holter recordings. Med Biol Eng Comput 31: 487-494.
52. Merri M, Alberti M, Benhorin J & Moss A (1991) Preprocessing of Holter ECGs for analysis of the dynamic interrelations between heart rate and repolarization duration variabilities. J Electrocardiology 23S: 157-162.
53. Sapoznikov D, Luria M, Mahler Y & Gotsman M (1992) Computer processing of artifact and arrhythmias in heart rate variability analysis. Comput Methods Programs Biomed 39: 75-84.
54. Tikkanen PE, Sellin LC, Kinnunen HO & Huikuri HV "Using simulated noise to define optimal QT intervals for computer analysis of ambulatory ECG". Medical Engineering & Physics 21(1): 15-25. University of Oulu, Finland Feb 1999.
55. Sapoznikov D, Luria M, Mahler Y & Gotsman M (1992) Computer processing of artifact and arrhythmias in heart rate variability analysis. Comput Methods Programs Biomed 39: 75-84.
56. Merri M, Farden D, Mottley J & Titlebaum E (1990) Sampling frequency of the electrocardiogram for spectral analysis of the heart rate variability. IEEE Trans Biomed Eng 37(1): 99-106.
57. Pinna G, Maestri R & Sanarico M (1996) Effects of record length selection on the accuracy of spectral estimates of heart rate variability: A simulation study. IEEE Trans Biomed Eng 43(7): 754-757.
58. Kamalesh M, Burger A, Kumar S, & Nesto R (1995) Reproducibility of time and frequency domain analysis of heart rate variability in patients with chronic stable angina. PACE 18: 1991-1994.
59. Pitzalis M, Mastropasqua F, Massari F, Forleo C, Maggio MD, Passantino A, Colombo R, Biase MD & Rizzon P (1996) Short- and long-term reproducibility of time and frequency domain heart rate variability measurements in normal subjects. Cardiovasc Res 32: 226-233.
60. Berntson G, Quigley J, Jaye F & Boysen S (1990) An approach to artifact identication: Application to heart period data. Psychophysiology 27(5): 586-598.

References

61. Pahlm O & Sornmo L (1984) Software QRS detection in ambulatory monitoring - a review. Med Biol Eng Comput 22: 289-297.
62. Malik M, Farrell T & Camm A (1990) Circadian rhythm of heart rate variability with clinical and angiographic variables and late mortality after coronary angiography. Am J Cardiol 66(12): 1049-1054.
63. Dimier-David L, Billon N, Costagliola D, Jaillon P & Funck-Brentano C (1994) Reproducibility of non-invasive measurement and of short-term variability of blood pressure and heart rate in healthy volunteers. Br J Clin Pharmacol 38: 109-115.
64. Pinna G, Maestri R, Cesare AD, Colombo R & Minuco G (1994) The accuracy of powerspectrum analysis of heart-rate variability from annotated RR lists generated by Holter systems. Physiol Meas 15: 163-179.
65. Malik M, Xia R, Odemuyiwa O, Staunton A, Poloniecki J & Camm A (1993) Influence of the recognition artefact in automatic analysis of long-term electrocardiograms on time-domain measurement of heart rate variability. Med Biol Eng Comput 31(5): 539-544.
66. Mulder L (1992) Measurement and analysis methods of heart rate and respiration for use in applied environments. Biol Psychol 34: 205-236.
67. Thomas L, Clark K, Mead C, Ripley K & Oliver G (1979) Automated cardiac dysrhythmia analysis. Proc IEEE 67(9): 1322-1337.
68. Friesen G, Jannett T, Jadallah M, Yates S, Quint S & Nagle H (1990) A comparison of the noise sensitivity of nine QRS detection algorithms. IEEE Trans Biomed Eng 37: 85-98.
69. Hamilton P & Tompkins W (1986) Quantitative investigation of QRS detection rules using the MIT/BIH arrhythmia database. IEEE Trans Biomed Eng 33(12): 1157-1165.
70. http://www.ncbi.nlm.nih.gov/pubmed/16830954.
71. Malik M, Farrell T, Cripps T & Camm A (1989b) Heart rate variability in relation to prognosis after myocardial infarction: Selection of optimal processing techniques. Eur Heart J 10(12): 1060-1074.
72. Wiklund U, Akay M & Niklasson U (1997) Short-term analysis of heart-rate variability by adapted wavelet transforms. IEEE Eng Med Biol 16(5): 113-138.
73. Oetken G, Parks T & Schuessler H (1979) A computer program for digital interpolator design. In: the Digital Signal Processing Committee (ed) Programs for Digital Signal Processing. IEEE Press, New York, p 8.1.1-8.1.6.
74. Sapoznikov D, Luria M & Gotsman M (1994) Dierentation of periodic from nonperiodic low-frequency heart rate fluctuations. Comput Biomed Res 27: 199-209.
75. P. Tikkanen *"Characterization and application of analysis methods for ECG and time interval variability data "*, University of Oulu, 1999.
76. Lippman N, Stein K & Lerman B (1994) Comparison of methods for removal of ectopy in measurement of heart rate variability. Am J Physiol 267(Heart Circ. Physiol. 36): H411-H418.
77. Pinna G, Maestri R, Cesare AD, Colombo R & Minuco G (1994) The accuracy of powerspectrum analysis of heart-rate variability from annotated RR lists generated by Holter systems. Physiol Meas 15: 163-179.
78. Proakis J, Rader C, Ling F & Nikias C (1992) Advanced Digital Signal Processing. Macmillan, New York.
79. Kleiger R, Stein P, Bosner M & Rottman J (1992) Time domain measurements of heart rate variability. Ambulatory Electrocardiography 10(3): 487-498.
80. Stein P, Bosner M, Kleiger R & Conger B (1994) Heart rate variability: A measure of cardiac autonomic tone. Am Heart J 127(5): 1376-1381.
81. Öri Z, Monir G, Weiss J, Sayhouni X & Singer D (1992) Heart rate variability. Frequency domain analysis. Ambulatory Electrocardiography 10(3): 499-537.
82. Baselli G & Cerutti S (1985) Identification techniques applied to processing of signals from cardiovascular systems. Med Inf 10(3): 223-235.

References

83. Hoopen MT & Bongaarts J (1969) Probabilistic characterization of R-R intervals. Cardiovasc Res 3: 218-236.
84. Baevskij R, Kirillov O & Kletskin S (1984) Mathematical Analysis of the Changes in Cardiac Rhythm During Stress. Nauka, Moscow.
85. Casolo G, Balli E, Taddei T, Amuhasi J & Gori C (1989) Decreased spontaneous heart rate variability in congestive heart failure. Am J Cardiol 64: 1162-1167.
86. Odemuyiwa O, Malik M, Farrell T, Bashir Y, Poloniecki J & Camm J (1991) Comparison of the predictive characteristics of heart rate variability index and left ventricular ejection fraction for all-cause mortality, arrhythmic events and sudden death after acute myocardial infarction. Am J Cardiol 68: 434-439.
87. Scott D (1979) On optimal and data-based histograms. Biometrika 66(3): 605-610.
88. Willard K & Connelly D (1992) Nonparametric probability density estimation: Improvements to the histogram for laboratory data. Comput Biomed Res 25: 17-28.
89. Jaffe R, Fung D & Behrman K (1993) Optimal frequency ranges for extracting information on automatic activity from the heart rate spectrogram. J Auton Nerv Syst 46: 37-46.
90. Korhonen I (1997) Methods for the analysis of short-term variability of heart rate and blood pressure in frequency domain. PhD thesis, Tampere University of Technology.
91. Kitney R, Fulton T, McDonald A & Linkens D (1985) Transient interactions between blood pressure, respiration and heart rate in man. J Biomed Eng 7: 217-224.
92. Pagani M, Lombardi F, Guzzetti S, Rimoldi O, Furlan R, Pizzinelli P, Sandrone G, Malfatto G, Dell'Orto S, Piccaluga E, Turiel M, Baselli G, Cerutti S & Malliani A (1986) Power spectral analysis of heart rate and arterial pressure as a marker of sympathovagal interaction in man and concious dog. Circ Res 59: 178-193.
93. Bianchi A, Mainardi L, Petrucci E, Signorini M, Mainardi M & Cerutti S (1993) Timevariant power spectrum analysis for the detection of transient episodes in HRV signal. IEEE Trans Biomed Eng BME-40(2): 136-144.
94. http://en.wikipedia.org/wiki/Electrophysiology
95. Novak P & Novak V (1993) Time/frequency mapping of the heart rate, blood pressure and respiratory signals. Med Biol Eng Comput 31: 103-110.
96. Novak V, Novak P, Champlain JD, Blanc AL, Martin R & Nadeau R (1993) Influence of respiration on heart rate and blood pressure fluctuations. J Appl Physiol 74(2): 617-626.
97. Katona P & Jih F (1975) Respiratory sinus arrhythmia: noninvasive measure of parasympathetic cardiac control. J Appl Physiol 39(5): 801-805.
98. http://en.wikipedia.org/wiki/Actionotential.
99. Rienzo MD, Mancia G, Parati G, Pedotti A & Zanchetti A (eds) (1993) Blood Pressureand Heart Rate Variability. Computer Analysis and Clinical Applications. IOS Press, Amsterdam.
100. Cerutti S, Bianchi A, Baselli G, Civardi S, Guzzetti S, Malliani A, Pagani A & Pagani M (1989) Compressed spectral arrays for the analysis 24-hr heart rate variability signal. Enhancement of parameters and data reduction. Comput Biomed Res 22: 424-441.
101. Rienzo MD, Castiglioni P, Mancia G, Parati G & Pedotti A (1989) 24 h sequential spectral analysis of arterial blood pressure and pulse interval in free-moving subjects. IEEE Trans Biomed Eng 36(11): 1066-1075.
102. Furlan R, Guzzetti S, Crivellaro W, Dassi S, Tinelli M, Baselli G, Cerutti S, Lombardi F, Pagani M & Malliani A (1990) Continuous 24-hour assessment of neural regulation of systemic arterial pressure and RR variabilities in ambulant subjects. Circulation 81: 537-547.

References

103. Bianchi A, Mainardi L, Petrucci E, Signorini M, Mainardi M & Cerutti S (1993) Timevariant power spectrum analysis for the detection of transient episodes in HRV signal. IEEE Trans Biomed Eng BME-40(2): 136-144.

104. Rienzo MD, Castiglioni P, Mancia G, Parati G & Pedotti A (1989) 24 h sequential spectral analysis of arterial blood pressure and pulse interval in free-moving subjects. IEEE Trans Biomed Eng 36(11): 1066-1075.

105. Malik M, Cripps T, Farrell T & Camm J (1989a) Long-term spectral analysis of heart rate variability - an algorithm based on segmental frequency distributions of beat-to-beat intervals. Int J Biomed Comput 24: 89-110.

106. Kobayashi M & Musha T (1982) 1=f fluctuations of heartbeat period. IEEE Trans Biomed Eng 29(6): 456-457.

107. Priestley M (1981) Spectral Analysis and Time Series. Academic Press Inc., London.

108. Kay S (1988) Modern Spectral Estimation. Theory & Application. Prentice Hall, Englewood Cliffs.

109. Marple S (1987) Digital Spectral Analysis with Applications. Prentice Hall, Englewood Cliffs.

110. Johnsen S & Andersen N (1978) On power estimation in maximum entropy spectral analysis. Geophysics 43(4): 681-690.

111. Choi B (1992) ARMA Model Identication. Springer-Verlag, New York.

112. Nikias C & Petropulu A (1993) Higher-Order Spectra Analysis: A Nonlinear Signal Processing Framework. PTR Prentice Hall, Englewood Cliffs.

113. Calcagnini G, Censi F, Camera A, Lino S & Cerutti S (1996) Interference and phase locking patterns between low and high frequency rhythms of cardiovascular signals in normal subjects. Proc 18th Annual International Conference of IEEE{EMBS, Amsterdam.

114. Hlawatsch F & Boudreaux-Bartels G (1992) Linear and quadratic time-frequency signal representations. IEEE Signal Process Mag 9(2): 21-67.

115. Rioul O & Vetterli M (1991) Wavelets and signal processing. IEEE Signal Process Mag 8(4): 14-38.

116. Cohen L (1989) Time-frequency distributions - a review. Proc IEEE 77(7): 941-981.

117. Loughlin P (1996) Special issue on time-frequency analysis. Proc IEEE 84(9).

118. Basano L, Ottonello P, Poggi A, Adezati L, Semino S, Ubaldi P & Viviani G (1995) An instrument for real-time spectral estimation of heart rate variability signal. Comput Methods Programs in Biomed 47: 229-236.

119. Keselbrener L & Akselrod S (1996) Selective discrete Fourier transform algorithm for time-frequency analysis: Method and application on simulated and cardiovascular signals. IEEE Trans Biomed Eng 43(8): 789-802.

120. Lee F & Nehorai A (1992) Adaptive power spectrum estimation algorithm for heart rate variability analysis. Computers in Cardiology, 273-276.

121. Mainardi L, Bianchi A & Cerutti S (1994) On-line beat-to-beat monitoring of spectral parameters of heart rate variability signal using a pole-tracking algorithm. Methods Inf Med 33: 85-88.

122. Mainardi L, Bianchi A, Baselli G & Cerutti S (1995) Pole-tracking algorithms for the extraction of time-variant heart rate variability spectral parameters. IEEE Trans Biomed Eng 42(3): 250-259.

123. Pola S, Macerata A, Emdin M & Marchesi C (1996) Estimation of the power spectral density in nonstationary cardiovascular time series: Assessing the role of the timefrequency representations (TFR). IEEE Trans Biomed Eng 43(1): 46-59.

124. Akay M, Landesberg G, Welkowitz W, Akay YM & Sapoznikov D (1993) Carotid-cardiac interaction: Heart rate variability during the unblocking of the carotid artery. In: Sideman S & Beyar R (eds) Interactive Phenomena in the Cardiac System. Plenum Press, New York, p 365-372.

125. Cohen A & Kovacevic J (1996) Wavelets: The mathematical background. Proc IEEE 84(4): 514-522.

References

126. Hess-Nielsen N & Wickerhauser M (1996) Wavelets and time-frequency analysis. Proc IEEE 84(4): 523-540.
127. Karrakchou M, Vibe-Rheymer K, Vesin JM, Pruvot E & Kunt M (1996) Improving cardiovascular monitoring through modern techniques. IEEE Eng Med Biol 15(5): 68-78.
128. Thakor N & Sherman D (1995) Wavelet (time-scale) analysis in biomedical signal processing. In: Bronzino J (ed) The Biomedical Engineering Handbook. CRC Press, Inc., Boca Raton, p 886-906.
129. Unser M & Aldroubi A (1996) A review of wavelets in biomedical application. Proc IEEE 84: 626-638.
130. Priestley M (1996)Wavelets and time-dependent spectral analysis. J Time Series Analysis 17(1): 85-103.
131. Daubechies I (1992) Ten Lectures on Wavelets. SIAM, Philadelphia.
132. Strang G & Nguyen T (1996) Wavelets and Filter Banks. Wellesley-Cambridge Press, Wellesley.
133. Coifman R & Wickerhauser M (1992) Entropy-based algorithms for best basis selection. IEEE Trans Inform Theory 38(2): 713-718.
134. Friesen G. M. and Jannett C. T. et al. (1990). A compareison of the Noise Sensitivety of Nine QRS Detection Algorithm. *IEEE Transactions on Biomedical Engineering, 37*.
135. A. Khawaja, *"Automatic ECG Analysis Using Principal Component Analysis And Wavelet Transformation"*, Vol.3 Karlsruhe Transactions on Biomedical Engineering, Universität Karlsruhe (TH), Institute of Biomedical Engineering.
136. Khawaja A., Automatic ECG Analysis Using Principal Component Analysis and Wavelet Transformation, 2007, 117-121
137. Amaral, L.A.N., Goldberger, A.L., Ivanov, P.Ch., and Stanley, H.E., Scaleindependent measures and pathologic cardiac dynamics. Phys. Rev. Lett., 1998, 81, 2388–2391.
138. Amaral, L.A.N., Goldberger, A.L., Ivanov, P.Ch., and Stanley, H.E., Scaleindependent measures and pathologic cardiac dynamics. Phys. Rev. Lett., 1998, 81, 2388–2391.
139. Merri M, Moss A, Benhorin J, Locati E, Alberti M & Badini F (1992) Relation between ventricular repolarization duration and cardiac cycle length during 24-hour Holter recordings. Circulation 85: 1816-1821.
140. Peng C.K., Mietus, J., Hausdorff, J.M., Havlin, S., Stanley, H.E., and Goldberger, A.L., Long-range anticorrelations and non-Gaussian behavior of the heartbeat. Phys. Rev. Lett., 1993, 70, 1343–1347.
141. Peng C.K., Mietus, J., Hausdorff, J.M., Havlin, S., Stanley, H.E., and Goldberger, A.L., Long-range anticorrelations and non-Gaussian behavior of the heartbeat. Phys. Rev. Lett., 1993, 70, 1343–1347.
142. Ashkenazy, Y., Lewkowicz, M., Levitan, J., Havlin, S., Saermark, K., Moelgaard, H., and Bloch Thomsen, P. E., Discrimination of the healthy and sick cardiac autonomicnervous system by a new wavelet analysis of heartbeat intervals. Fractals, 1999, 7,85–91.
143. Ashkenazy, Y., Lewkowicz, M., Levitan, J., Moelgaard, H., Bloch Thomsen, P. E., and Saermark, K., Discrimination of the healthy and sick cardiac autonomic nervous system by a new wavelet analysis of heartbeat intervals Fractals, 1998 6, 197–203.
144. Mandelbrot, B.B., The Fractal Geometry of Nature, Freeman, San Francisco, 1983.
145. Peng C.K., Mietus, J., Hausdorff, J.M., Havlin, S., Stanley, H.E., and Goldberger, A.L., Long-range anticorrelations and non-Gaussian behavior of the heartbeat. Phys. Rev. Lett., 1993, 70, 1343–1347.
146. Saermark, K., Moellery,M., Hintzey, U., Moelgaardz, H., Bloch Thomsenx, P.E., Huikuri, H., Makikiallio, T., Levitan, J., and Lewkowicz, M., Comparison of recent methods of analyzing heart rate variability. Fractals, 2000 8, 315–322.

References

147. Lin, D. C. and Hughson, R. L., Modeling Heart Rate Variability in Healthy Humans: A Turbulence Analogy. Phys. Rev. Lett., 2001, 86, 1650–1653. 22

148. Costa, M., Goldberger, A. L., and Peng C.-K., Multiscale Entropy Analysis of Complex Physiologic Time Series. Phys. Rev. Lett., 2002, 89, 068102 (4 pages).

149. Poon C.S., Merrill C.K., Decrease of cardiac chaos in congestive heart failure. Nature, 1997, 389, 492–495.

150. Kalda, J, S¨akki, M, Vainu, M, and Laan, M, Zipf's law in human heartbeat dynamics. e-print http://arxiv.org/abs/physics/0110075 (4 pages, 2001).

151. Bernaola-Galv´an, P., Ivanov, P. Ch., Amaral, L.A.N., and Stanley, H. E., Scale Invariance in the Nonstationarity of Human Heart Rate. Phys. Rev. Lett., 2001, 87, 168105 (4 pages).

152. Zipf, G.K., Human Behavior and the Principle of Least Effort. Cambridge, Addison-Wesley, 1949.

153. H. Traberg, "Marriott's Practical Electrocardiography,"*N Engl J Med*, vol. 332, no. 10, pp. 690–, 1995.

154. E. O. Robles de Medina, "Clinical Electrocardiography : Antoni Bayes de Luna.," *Circulation*, vol. 100, no. 5, pp. 567–, 1999.

155. L. Sornmo and P. Laguna, *Bioelectrical Signal Processing in Cardiac and Neurological Applications*. Linacre House Jordan Hill Oxford OX2 8DP United Kingdom: Elsevier, 1 ed., 2005.

156. M. Jain, S. Chaturvedi, V.Mithal "Detection of abnormalities and Disseases in ECG data", Dept of Computer Science and Engineering, India Nov 2008.

157. M. Malik and A. J. Camm, "Heart Rate Variability ," *Futura, Armonk, New York*, 1995.

158. R. E. Kleiger, J. P. Miller, J. T. J. Bigger, and A. J. Moss,"Decreased heart rate variability and its association with increased mortality after acute myocardial infarction," *Am J Cardiol*, vol. 59, pp. 256–262, Feb 1987.

159. C. De Capua, Stefano De Falco, Rosario Morello, "A soft computing-based measurement system for medical applications in diagnosis of cardiac arrhythmias by ECG signals analysis", La Coruna Nov 2006.

160. R. G. Mark, "Clinical Eelectrocardiography And Arrhythmias", USA: Massachusetts Institute of Technology, 2004.

161. http://en.wikipedia.org/wiki/Heartlock

162. http://en.wikipedia.org/wiki/Ischaemiceartisease

163. http://www.webhealthcentre.com/centers/heart.asp

164. F. G. Akar, G.-X. Yan, C. Antzelevitch, and D. S. Rosenbaum, "Unique topographical distribution of M cells underlies reentrant mechanism of torsade de pointes in the long-QT syndrome," *Circulation*, vol. 105, pp. 1247–1253, Mar 2002.

165. M. E. Curran, I. Splawski, K. W. Timothy, G. M. Vincent, E. D. Green, and M. T. Keating, "A molecular basis for cardiac arrhythmia: HERG mutations cause long QT syndrome," *Cell*, vol. 80, pp. 795–803, Mar 1995.

166. J. Wei, D. W. Wang, M. Alings, F. Fish, M. Wathen, D. M. Roden, and A. L. J. George, "Congenital long-QT syndrome caused by a novel mutation in a conserved acidic domain of the cardiac Na+ channel," *Circulation*, vol. 99, pp. 3165–3171, Jun 1999.

167. P. T. Ellinor, D. J. Milan, and C. A. MacRae, "Risk stratification in the long-QT syndrome,"*N Engl J Med*, vol. 349, pp. 908–909, Aug 2003. Comment

168. http://en.wikipedia.org/wiki/LongTyndrome

169. W. Shimizu and C. Antzelevitch, "Sodium Channel Block With Mexiletine Is Effective in Reducing Dispersio of Repolarization and Preventing Torsade de Pointes in LQT2 and LQT3 Models of the Long-QT Syndrome," *Circulation*, vol. 96, no. 6, pp. 2038–2047, 1997.

170. http://en.wikipedia.org/wiki/LongTyndrome.

References

171. P. J. Schwartz, A. J. Moss, G. M. Vincent, and R. S. Crampton, "Diagnostic criteria for the long QT syndrome. An update," *Circulation*, vol. 88, pp. 782–784, Aug 1993.

172. S. J. Compton, R. L. Lux, M. R. Ramsey, K. R. Strelich, M. C. Sanguinetti, L. S. Green, M. T. Keating, and J. W. Mason, "Genetically defined therapy of inherited long-QT syndrome. Correction of abnormal repolarization by potassium," *Circulation*, vol. 94, pp. 1018–1022, Sep 1996.

173. M. Tristani-Firouzi, J. L. Jensen, M. R. Donaldson, V. Sansone, G. Meola, A. Hahn, S. Bendahhou, H. Kwiecinski, A. Fidzianska, N. Plaster, Y.-H. Fu, L. J. Ptacek, and R. Tawil, "Functional and clinical characterization of KCNJ2 mutations associated with LQT7 (Andersen syndrome)," *J. Clin. Invest.*, vol. 110, no. 3, pp. 381–388, 2002.

174. http://en.wikipedia.org/wiki/Brugadayndrome.

175. J. Brugada, P. Brugada, and R. Brugada, "The syndrome of right bundle branch block ST segment elevation in V1 to V3 and sudden death–the Brugada syndrome," *Europace*, vol. 1, pp. 156–166, Jul 1999.

176. M. Bessette and S. Jacobson, "Torsade de Pointes," *eMedicine*, vol. http://www.emedicine.com/emerg/topic596.htm , May 2006.

177. P. J. Schwartz and A. Malliani, "Electrical alternation of the T-wave: clinical and experimental evidence of its relationship with the sympathetic nervous system and with the long Q-T syndrome," *Am Heart J*, vol. 89, pp. 45–50, Jan 1975.

178. B. Surawicz and C. Fisch, "Cardiac alternans: diverse mechanisms and clinical manifestations," *J Am Coll Cardiol*, vol. 20, no. 2, pp. 483–499, 1992.

179. W. Shimizu and C. Antzelevitch, "Cellular and ionic basis for T-wave alternans under long-QT conditions," *Circulation*, vol. 99, pp. 1499–1507, Mar 1999.

180. R. L. Verrier, "T-Wave Alternans and Risk Stratification for Sudden Cardiac Death, http://www.physionet.org/events/hrv-2006/verrier.pdf ."

181. B.-R. Choi and G. Salama, "Simultaneous maps of optical action potentials and calcium transients in guineapig hearts: mechanisms underlying concordant alternans," *J Physiol (Lond)*, vol. 529, no. 1, pp. 171–188, 2000.

182. J. N. Cohn, D. G. Archibald, S. Ziesche, J. A. Franciosa, W. E. Harston, F. E. Tristani, W. B. Dunkman, W. Jacobs, G. S. Francis, and K. H. Flohr, "Effect of vasodilator therapy on mortality in chronic congestive heart failure. Results of a Veterans Administration Cooperative Study," *N Engl J Med*, vol. 314, pp. 1547–1552, Jun 1986. Clinical Trial.

183. S. Miyoshi, T. Miyazaki, K. Moritani, and S. Ogawa, "Different responses of epicardium and endocardium to KATP channel modulators during regional ischemia," *Am J Physiol*, vol. 271, pp. 140–147, Jul 1996.

184. A. G. Kleber, M. J. Janse, F. J. van Capelle, and D. Durrer, "Mechanism and time course of S-T and T-Q segment changes during acute regional myocardial ischemia in the pig heart determined by extracellular and intracellular recordings," *Circ Res*, vol. 42, pp. 603–613, May 1978.

185. S. G. Dilly and M. J. Lab, "Electrophysiological alternans and restitution during acute regional ischaemia in myocardium of anaesthetized pig," *J Physiol*, vol. 402, pp. 315–333, Aug 1988.

186. W. Zareba, A. Moss, S. le Cessie, and W. Hall, "T wave alternans in idiopathic long QT syndrome," *J Am Coll Cardiol*, vol. 23, no. 7, pp. 1541–1546, 1994.

187. S. B. Platt, J. M. Vijgen, P. Albrecht, G. F. Van Hare, M. D. Carlson, and D. S. Rosenbaum, "Occult T wave alternans in long QT syndrome," *J Cardiovasc Electrophysiol*, vol. 7, pp. 144–148, Feb 1996. Case Reports.

188. M. Takagi, A. Doi, K. Takeuchi, and J. Yoshikawa, "Pilsicanide-induced marked T wave alternans and ventricular fibrillation in a patient with Brugada syndrome," *J Cardiovasc Electrophysiol*, vol. 13, p. 837, Aug 2002. Case Reports.

189. M. Chinushi, T. Washizuka, H. Okumura, and Y. Aizawa, "Intravenous administration of class I antiarrhythmic drugs induced T wave alternans in a patient

References

with Brugada syndrome," *J Cardiovasc Electrophysiol*, vol. 12, pp. 493–495, Apr 2001. Case Reports.

190. T. Ikeda, H. Sakurada, K. Sakabe, T. Sakata, M. Takami, N. Tezuka, T. Nakae, M. Noro, Y. Enjoji, T. Tejima, K. Sugi, and T. Yamaguchi, "Assessment of noninvasive markers in identifying patients at risk in the Brugada syndrome: insight into risk stratification," *J Am Coll Cardiol*, vol. 37, pp. 1628–1634, May 2001.

191. B. D. Nearing and R. L. Verrier, "Tracking cardiac electrical instability by computing interlead heterogeneity of T-wave morphology," *J Appl Physiol*, vol. 95, pp. 2265–2272, Dec 2003.

192. F. Dessertenne, "[Ventricular tachycardia with 2 variable opposing foci]," *Arch Mal Coeur Vaiss*, vol. 59, pp. 263–272, Feb 1966. Case Reports.

193. D. M. Roden, "Acquired long QT syndromes and the risk of proarrhythmia," *J Cardiovasc Electrophysiol*, vol. 11, pp. 938–940, Aug 2000.

194. J. Ben-David and D. P. Zipes, "Torsades de pointes and proarrhythmia," *Lancet*, vol. 341, pp. 1578–1582, Jun 1993.

195. N. el Sherif, E. B. Caref, H. Yin, and M. Restivo, "The electrophysiological mechanism of ventricular arrhythmias in the long QT syndrome. Tridimensional mapping of activation and recovery patterns," *Circ Res*, vol. 79, pp. 474–492, Sep 1996.

196. S. C. Verduyn, M. A. Vos, J. van der Zande, A. Kulcsar, and H. J. Wellens, "Further observations to elucidate the role of interventricular dispersion of repolarization and early afterdepolarizations in the genesis of acquired torsade de pointes arrhythmias: a comparison between almokalant and d-sotalol using the dog as its own control," *J Am Coll Cardiol*, vol. 30, pp. 1575–1584, Nov 1997.

197. C. Antzelevitch, Z. Q. Sun, Z. Q. Zhang, and G. X. Yan, "Cellular and ionic mechanisms underlying erythromycin-induced long QT intervals and torsade de pointes," *J Am Coll Cardiol*, vol. 28, pp. 1836–1848, Dec 1996.

198. W. Shimizu and C. Antzelevitch, "Cellular Basis for the ECG Features of the LQT1 Form of the Long-QT Syndrome : Effects of í-Adrenergic Agonists and Antagonists and Sodium Channel Blockers on Transmural Dispersion of Repolarization and Torsade de Pointes," *Circulation*, vol. 98, no. 21, pp. 2314–2322, 1998.

199. W. Shimizu, T. Ohe, T. Kurita, M. Kawade, Y. Arakaki, N. Aihara, S. Kamakura, T. Kamiya, and K. Shimomura, "Effects of verapamil and propranolol on early afterdepolarizations and ventricular arrhythmias induced by epinephrine in congenital long QT syndrome," *J Am Coll Cardiol*, vol. 26, pp. 1299–1309, Nov 1995.

200. C. Antzelevitch and S. Sicouri, "Clinical relevance of cardiac arrhythmias generated by afterdepolarizations. Role of M cells in the generation of U waves, triggered activity and torsade de pointes," *J Am Coll Cardiol*, vol. 23, pp. 259–277, Jan 1994.

201. C. Luo and Y. Rudy, "A dynamic model of the cardiac ventricular action potential. II. Afterdepolarizations, triggered activity, and potentiation," *Circ Res*, vol. 74, no. 6, pp. 1097–1113, 1994.

202. S. Sicouri and C. Antzelevitch, "A subpopulation of cells with unique electrophysiological properties in the deep subepicardium of the canine ventricle. The M cell," *Circ Res*, vol. 68, pp. 1729–1741, Jun 1991.

203. Http://www.firstaidwarehouse.co.uk/pic/280x280/13/50/welch_allyn_cardioperfect_pc_based_ecg_system_cpr_ui_eb_d.jpg

204. http://www.mountnittany.org/assets/images/krames/107989.jpg

205. Cristina Neacsu, Karen Daniels "Translational Covering of Closed Planar Cubic B-Spline Curves". Computer Graphics Forum Volume 25, Issue 4, pages 743–757, December 2006

206. Hao Zhang, Li-Qing Zhang "ECG analysis based on PCA and Support Vector Machines". Department of Computer Science and Engineering, Shanghai Jiao Tong University, China, 2006

References

207. 219. Stamkopoulos, T. Diamantaras, K. Maglaveras, "ECG analysis using nonlinear PCA neural networks for ischemia detection", Signal Processing, Vol. 46 (1998) 3058-3067 K. Silipo, R. Marchesi, C., "Artificial neural networks for automatic ECG analysis", Signal Processing, Vol. 46 (1417-1425).

List of publications

I. Antonopoulos, N.Y.A. Shammas, S. Grainger, I. Taylor, Th. Ganetsos, N. Laskaris and A. Karatradou, *"New Methods for analyzing Cardio Signals",* 21st Intern. Medicine Conference, 23-26 November 2006, Thessalonica, Greece.

Konstantinos Kalovrektis⸲, Theodore Ganetsos, Evangelos Fountas ,N.Y.A. Shammas⸲ I.Taylor , John Andonopoulos, and Gkotsinas Antonios, "Development of a Wireless embedded system to reduce the influence of Gaussian noise and 50 Hz Power line noise in Electromyography (EMG)"⸲ 13th WSEAS CSCC Multiconference Rodos (Rhodes) Island, Greece, July 22-25, 2009

Konstantinos Kalovrektis⸲, Theodore Ganetsos,   N.Y.A. Shammas, I.Taylor , John Andonopoulos," Development of a novel system to analyze and detect small changes in ECG signals that indicate cardiac disorders"⸲ 4th WSEAS International Conference on CIRCUITS, SYSTEMS, SIGNAL and TELECOMMUNICATIONS (CISST '10), Harvard, Cambridge, USA, January 27-29, 2010

Konstantinos Kalovrektis⸲, Theodore Ganetsos, ,N.Y.A. Shammas , I.Taylor , John Andonopoulos, Lykas Christos." An integrated development hardware design for an advanced wireless Ag/AgCl sensor to acquiring biosignals form ornamental plants**,** 4th WSEAS International Conference on CIRCUITS, SYSTEMS, SIGNAL and TELECOMMUNICATIONS (CISST '10), Harvard, Cambridge, USA, January 27-29, 2010

Appendices

1. Circuit structure

The list of the components used to construct the ECG recording system follows:

Resistors
R1, R2, R4, R6, R7, R19-22 = 10
R3, R5 = 22kΩ 1%
R8 = 47kΩ
R9 = 42kΩ
R10, R11 = 3MΩ
R12 = 150kΩ
R13 = 4kΩ
R14, R16 = 47kΩ
R15 = 220Ω
R17, R18 = 100Ω
R23, R24 = 1MΩ
P1 = 10kΩ preset

Capacitors
C1, C2 = 27pF
C3, C10 = 1μF 63V, 5mm lead pitch (no electrolytic cap)
C4 = 100nF
C5-C8 = 100μF 16V radial
C9 = 1nF
C11 = 22pF

Semiconductors
IC1 = TL074 DIP14
IC2, IC4 = TS921 or TL071 DIP8
IC3 = IL300

2. Changes in the Third Edition of MATLAB

Some of the major changes include:
- Case-sensitive function and directory names on all platforms.
- Function handles.
- The use of an end statement at the end of functions.
- Nested functions.
- Math operations with single and integer data types.
- Major revision of the GUI code, including the addition of panels, button groups, and toolbars. The code auto- generated by guide has been totally changed. Frames have been deprecated.
- Major revisions to programming tools, such as the addition of conditional breakpoints and the mlint tool to check for poor programming practices within an M-file.

2.1. The advantages of MATLAB for technical programming

MATLAB has many advantages compared to convectional computer languages for technical problem solving. These include:

1. **Ease of Use**

MATLAB is an interpreted language, like many versions of Basic. Like Basic, it is very easy to use. The program can be used as a scratch pad to evaluate expressions typed at the command line, or it can be used to execute large prewritten programs. Programs may be easily written and modified with the built-in integrated development environment and debugged with the MATLAB debugger. Because the language is so easy to use, it is ideal for educational use and for the rapid prototyping of new programs.

Many program development tools are provided to make the program easy to use. They include an intergraded editor/debugger, on-line documentation and manuals, a workspace browser, and extensive demos.

2. **Platform Independence**

MATLAB is supported on many different computer systems, providing a large measure of platform independence. At the time of this writing, the language is supported on Windows NT/2000/XP, Linux, UNIX, and the Macintosh. Programs written on any platform and the data files written on many platforms written in MATLAB can migrate to new platforms when the needs of the user change.

3. **Pre-Defined Functions**

MATLAB comes complete with an extensive library of predefined functions that provide tested and prepackaged solutions to many basic technical tasks. For example, suppose that you are writing a program that must calculate the statistics associated with an input data set. In most languages, you would need to write subroutines of functions to implement calculations such as the arithmetic mean, standard deviation, median among others. These and hundreds of other functions are built right into the MATLAB language, making your job much easier.

4. **Device-independent plotting**

Unlike other computer languages, MATLAB has many integral plotting and imaging commands. The plots and the images can be displayed on any graphical output device supported by the computer on which MATLAB is running. This capability makes MATLAB an outstanding tool for visualizing technical data.

5.   **Graphical user interface**

MATLAB includes tools that allow a program to interactively construct a graphical user interface (GUI) for his or her program. With this capability, the programmer can design sophisticated data analysis programs that can be operated by relatively-inexperienced users.

6.   **MATLAB Compiler**

MATLAB's flexibility and platform independence are achieved by compiling MATLAB programs into a device-independent p-code and then interpreting the p-code instructions at run-time. This approach is similar to that used by Microsoft's Visual Basic Language. Unfortunately, the resulting programs can sometimes execute slowly because the MATLAB code is interpreted rather than compiled.

A separate MATLAB compiler is available. This compiler can compile a MATLAB program into a true executable that runs faster than the interpreted code. It is a great way to convert a prototype MATLAB program into an executable suitable for sale and distribution to users.

MATLAB is a huge program with an incredibly rich variety of functions. Even the basic version of MATLAB without any toolkits is much richer than other technical programming languages. There are more than 1000 functions in the basic MATLAB product alone, and the toolkits extend this capability with many more functions in various specialties.

2.2.   Disadvantages of MATLAB

MATLAB has two principal disadvantages. The first is that it is an interpreted language and therefore can execute more slowly than compiled languages. This problem can be mitigated by properly structuring the MATLAB program, and by the use of the MATLAB compiler to compile the final MATLAB program before distribution and general use.

The second disadvantage is cost: a full copy of MATLAB is five to ten times no more expensive than a conventional C of Fortran compiler. This relatively high cost is more than offset by the reduced time required for an engineer or scientist to create a working program, so MATLAB is cost-effective for businesses. However, it is too expensive for most individuals to consider purchasing. Fortunately, there is also an inexpensive Student Edition of MATLAB, which is a great tool for students wishing to learn the language. The Student Edition of MATLAB is essentially identical to the full edition.

A graphical user interface (GUI) is a pictorial interface to a program. A good GUI can make programs easier to use by providing them with a consistent appearance, and with intuitive controls such as pushbuttons, edit boxes, list boxes, sliders, and menus. The GUI should behave in understandable and predictable manner, so that a user knows what to expect when he or she performs an action. For example, when a mouse click occurs on a pushbutton, the GUI should initiate the action described on the label of the button.

This chapter contains an introduction to the basic elements of the MATLAB GUIs. It does not contain a complete description of components or GUI features, but it does provide us with the basics required to create functional GUIs for your programs.

2.3.   *How a graphical user interface works*

A graphical interface provides the user with a familiar environment in which to work. It contains pushbuttons, toggle buttons, lists, menus, text boxes, and so forth, all of which are already familiar to the user, so that he or she can concentrate on the purpose of the application instead of the mechanics involved in doing things. However, GUIs are harder for the programmer, because a GUI-based program must be prepared for mouse clicks (or possibly keyboard input) for any GUI element at any time. Such inputs are known "aw" events, and a program that responds to events is said to be event driven.

The three principal elements required to create a MATLAB Graphical User Interface are:

1. Components. Each item on a MATLABGUI (e.g., pushbuttons, labels, edit boxes) is a graphical component. The types of components include graphical controls (pushbuttons, toggle buttons, edit boxes, lists, sliders, etc) static elements (text boxes), menus, toolbars and axes. Graphical controls and text boxes are created by the function uicontrol, and menus are created by the functions uimenu and uicontextmenu. Toolbars are created by function uitoolbar. Axes, which are used to display graphical data, are created by the function axes.

2. Containers. The components of a GUI must be arranged within a container, which is a window on the computer screen. The most common container is a figure. A figure is a window on the computer screen that has a title bar along the top, and that can optionally have menus attached. In the past, figures have been created automatically whenever data was plotted. However, empty figures can be created with the function figure, and they can be used to hold any combination of components and other containers.

The other types of containers are panels

3. Callbacks. Finally, there must be some way to perform an action if a user clicks a mouse on a button or types information on any keyboard. A mouse click or a key press is an event, and the MATLAB program must respond to each event if the program is to perform its function. For example, if a user clicks on a button to be executed. The code executed implements the function of the button to be executed. The code executed in response to an event is known as a callback. There must be a callback to implement the function of each graphical component on the GUI.

As mentioned in advantage 6, the compiler can transform the program into an independent program installed into any computer. In order to do this, besides the

Appendices

compiler, another program with the extension .exe is necessary which will install into the computer/client all the necessary libraries.

For the needs of this research a graphical interface was developed in which the user can perform readings with the novel hardware developed, but also to perform calculations in the signals and to compare them with reference signals.

3. *Source code for the created MATLAB program*

```
function varargout = untitled(varargin)
% UNTITLED M-file for untitled.fig
%      UNTITLED, by itself, creates a new UNTITLED or raises the
existing
%      singleton*.
%
%      H = UNTITLED returns the handle to a new UNTITLED or the
handle to
%      the existing singleton*.
%
%      UNTITLED('CALLBACK',hObject,eventData,handles,...) calls the
local
%      function named CALLBACK in UNTITLED.M with the given input
arguments.
%
%      UNTITLED('Property','Value',...) creates a new UNTITLED or
raises the
%      existing singleton*.  Starting from the left, property value
pairs are
%      applied to the GUI before untitled_OpeningFunction gets
called.  An
%      unrecognized property name or invalid value makes property
application
%      stop.  All inputs are passed to untitled_OpeningFcn via
varargin.
%
%      *See GUI Options on GUIDE's Tools menu.  Choose "GUI allows
only one
%      instance to run (singleton)".
%
% See also: GUIDE, GUIDATA, GUIHANDLES
% Edit the above text to modify the response to help untitled
% Last Modified by GUIDE v2.5 28-Jan-2010 12:48:19
% Begin initialization code - DO NOT EDIT
gui_Singleton = 1;
gui_State = struct('gui_Name',       mfilename, ...
                   'gui_Singleton',  gui_Singleton, ...
                   'gui_OpeningFcn', @untitled_OpeningFcn, ...
                   'gui_OutputFcn',  @untitled_OutputFcn, ...
                   'gui_LayoutFcn',  [] , ...
                   'gui_Callback',   []);
if nargin && ischar(varargin{1})
    gui_State.gui_Callback = str2func(varargin{1});
end
if nargout
    [varargout{1:nargout}] = gui_mainfcn(gui_State, varargin{:});
else
```

```
    gui_mainfcn(gui_State, varargin{:});
end
% End initialization code - DO NOT EDIT


% --- Executes just before untitled is made visible.
function untitled_OpeningFcn(hObject, eventdata, handles, varargin)
% This function has no output args, see OutputFcn.
% hObject    handle to figure
% eventdata  reserved - to be defined in a future version of MATLAB
% handles    structure with handles and user data (see GUIDATA)
% varargin   command line arguments to untitled (see VARARGIN)

% Choose default command line output for untitled
handles.output = hObject;

% Update handles structure
guidata(hObject, handles);

% UIWAIT makes untitled wait for user response (see UIRESUME)
% uiwait(handles.figure1);


clc
global NSR
global VTfast
global VF
global VTslow
global VTpoly
global AFIB
global SVT
global ASYS
load('matlab_02.mat','NSR','VTfast','VF','VTslow','VTpoly','AFIB','SV
T','ASYS');
% --- Outputs from this function are returned to the command line.
function varargout = untitled_OutputFcn(hObject, eventdata, handles)
% varargout  cell array for returning output args (see VARARGOUT);
% hObject    handle to figure
% eventdata  reserved - to be defined in a future version of MATLAB
% handles    structure with handles and user data (see GUIDATA)
% Get default command line output from handles structure
varargout{1} = handles.output;
function edit1_Callback(hObject, eventdata, handles)
% hObject    handle to edit1 (see GCBO)
% eventdata  reserved - to be defined in a future version of MATLAB
% handles    structure with handles and user data (see GUIDATA)
% Hints: get(hObject,'String') returns contents of edit1 as text
%        str2double(get(hObject,'String')) returns contents of edit1
as a double

% --- Executes during object creation, after setting all properties.
function edit1_CreateFcn(hObject, eventdata, handles)
% hObject    handle to edit1 (see GCBO)
% eventdata  reserved - to be defined in a future version of MATLAB
% handles    empty - handles not created until after all CreateFcns
called
% Hint: edit controls usually have a white background on Windows.
%       See ISPC and COMPUTER.
if ispc && isequal(get(hObject,'BackgroundColor'),
get(0,'defaultUicontrolBackgroundColor'))
    set(hObject,'BackgroundColor','white');
end
```

> Here the variables are set. Matlab_02.mat that contains the reference values is loaded

Appendices

```matlab
% --- Executes on button press in pushbutton1.
function pushbutton1_Callback(hObject, eventdata, handles)
% hObject    handle to pushbutton1 (see GCBO)
% eventdata  reserved - to be defined in a future version of MATLAB
% handles    structure with handles and user data (see GUIDATA)
global VTfast
global NSR
global signal
global signalmikos
global time1
global xx
global nn
global x
axes(handles.axes1);
time1char=get(handles.edit1,'string');
time1=str2num(time1char);
%signal=wavrecord(time1*11025,11025);
signal=NSR;
signalmikos=[1:length(signal)]';
plot(signalmikos/11025,signal);
x=signal;
xx=x/max(x);
nn=signalmikos/11025;
function edit4_Callback(hObject, eventdata, handles)
% hObject    handle to edit4 (see GCBO)
% eventdata  reserved - to be defined in a future version of MATLAB
% handles    structure with handles and user data (see GUIDATA)
% Hints: get(hObject,'String') returns contents of edit4 as text
%        str2double(get(hObject,'String')) returns contents of edit4
as a double

% --- Executes during object creation, after setting all properties.
function edit4_CreateFcn(hObject, eventdata, handles)
% hObject    handle to edit4 (see GCBO)
% eventdata  reserved - to be defined in a future version of MATLAB
% handles    empty - handles not created until after all CreateFcns
called

% Hint: edit controls usually have a white background on Windows.
%       See ISPC and COMPUTER.
if ispc && isequal(get(hObject,'BackgroundColor'),
get(0,'defaultUicontrolBackgroundColor'))
    set(hObject,'BackgroundColor','white');
end

% --- Executes on button press in pushbutton2.
function pushbutton2_Callback(hObject, eventdata, handles)
% hObject    handle to pushbutton2 (see GCBO)
% eventdata  reserved - to be defined in a future version of MATLAB
% handles    structure with handles and user data (see GUIDATA)
global NSR
global signal
global signalmikos
global time1
global nn
global xx
clear a
clear b
clear n1
clear x1
```

Here the program reads the box named "edit 1" and reads the seconds it has to record. It waverecords and normalizes the recorded signal with command x/max(x) and transforms x into sec

Appendices

```
clear x
clear n
nikos=0;
x=signal;
xx=x/max(x);
nn=signalmikos/11025;
b=0;
a=imextendedmax(xx,0.9);
for i=2:length(a)-1
    if a(i)==1 & a(i-1)==0 & a(i+1)==1
        amin=(i);
    end
    if a(i)==1 & a(i-1)==1 & a(i+1)==0
            amax=(i);
            nikos(i)=max(xx(amin:amax))>0.85;
    end
end
n1=nn(a);
x1=xx(a);
plot(nn,xx,n1,x1,'r.')
b=sum(nikos~=0);
set(handles.edit4,'string',(b*60/time1));
function edit5_Callback(hObject, eventdata, handles)
% hObject    handle to edit5 (see GCBO)
% eventdata  reserved - to be defined in a future version of MATLAB
% handles    structure with handles and user data (see GUIDATA)
% Hints: get(hObject,'String') returns contents of edit5 as text
%        str2double(get(hObject,'String')) returns contents of edit5
as a double


% --- Executes during object creation, after setting all properties.
function edit5_CreateFcn(hObject, eventdata, handles)
% hObject    handle to edit5 (see GCBO)
% eventdata  reserved - to be defined in a future version of MATLAB
% handles    empty - handles not created until after all CreateFcns
called
% Hint: edit controls usually have a white background on Windows.
%       See ISPC and COMPUTER.
if ispc && isequal(get(hObject,'BackgroundColor'),
get(0,'defaultUicontrolBackgroundColor'))
    set(hObject,'BackgroundColor','white');
end


% --- Executes on button press in pushbutton3.
function pushbutton3_Callback(hObject, eventdata, handles)
% hObject    handle to pushbutton3 (see GCBO)
% eventdata  reserved - to be defined in a future version of MATLAB
% handles    structure with handles and user data (see GUIDATA)
global time1
noofpeaks=str2num(get(handles.edit5,'string'));
set(handles.edit7,'string',(noofpeaks*60)/time1)
function edit7_Callback(hObject, eventdata, handles)
% hObject    handle to edit7 (see GCBO)
% eventdata  reserved - to be defined in a future version of MATLAB
% handles    structure with handles and user data (see GUIDATA)
% Hints: get(hObject,'String') returns contents of edit7 as text
%        str2double(get(hObject,'String')) returns contents of edit7
as a double


% --- Executes during object creation, after setting all properties.
function edit7_CreateFcn(hObject, eventdata, handles)
```

Here the number of peak and eventually the heart rate is calculated
Calculation is simple and is based into how many times a rate higher than 0.85 is shown. All the signals are normalized, meaning that higher value in y axis is 1.

Appendices

```
% hObject    handle to edit7 (see GCBO)
% eventdata  reserved - to be defined in a future version of MATLAB
% handles    empty - handles not created until after all CreateFcns
called
% Hint: edit controls usually have a white background on Windows.
%        See ISPC and COMPUTER.
if ispc && isequal(get(hObject,'BackgroundColor'),
get(0,'defaultUicontrolBackgroundColor'))
    set(hObject,'BackgroundColor','white');
end


% --- Executes on button press in pushbutton5.
function pushbutton5_Callback(hObject, eventdata, handles)
% hObject    handle to pushbutton5 (see GCBO)
% eventdata  reserved - to be defined in a future version of MATLAB
% handles    structure with handles and user data (see GUIDATA)
global NSR
global signal
global signalmikos
global time1
global nn
global xx
pp=spline(nn,xx);
v=ppval(pp,nn);
plot(nn,xx,'b.',nn,v,'r')
pp1=mean(pp.coefs(100:end,1));
pp2=mean(pp.coefs(100:end,2));
pp3=mean(pp.coefs(100:end,3));
pp4=mean(pp.coefs(100:end,4));
ppcoefs=[pp1 pp2 pp3 pp4];
set(handles.edit9,'string',ppcoefs);
```

> Here the program performs spline fit in the normalized signal. With plot it prints with red over the normal that is blue. Meanwhile it prints in the box named "edit9" the variables it calculated

```
% --- Executes on button press in pushbutton6.
function pushbutton6_Callback(hObject, eventdata, handles)
% hObject    handle to pushbutton6 (see GCBO)
% eventdata  reserved - to be defined in a future version of MATLAB
% handles    structure with handles and user data (see GUIDATA)
zoom
function edit9_Callback(hObject, eventdata, handles)
% hObject    handle to edit9 (see GCBO)
% eventdata  reserved - to be defined in a future version of MATLAB
% handles    structure with handles and user data (see GUIDATA)

% Hints: get(hObject,'String') returns contents of edit9 as text
%        str2double(get(hObject,'String')) returns contents of edit9
as a double

% --- Executes during object creation, after setting all properties.
function edit9_CreateFcn(hObject, eventdata, handles)
% hObject    handle to edit9 (see GCBO)
% eventdata  reserved - to be defined in a future version of MATLAB
% handles    empty - handles not created until after all CreateFcns
called
% Hint: edit controls usually have a white background on Windows.
%        See ISPC and COMPUTER.
if ispc && isequal(get(hObject,'BackgroundColor'),
get(0,'defaultUicontrolBackgroundColor'))
    set(hObject,'BackgroundColor','white');
end


% --- Executes on selection change in listbox1.
```

```
function listbox1_Callback(hObject, eventdata, handles)
% hObject    handle to listbox1 (see GCBO)
% eventdata  reserved - to be defined in a future version of MATLAB
% handles    structure with handles and user data (see GUIDATA)
% Hints: contents = get(hObject,'String') returns listbox1 contents
as cell array
%        contents{get(hObject,'Value')} returns selected item from
listbox1


% --- Executes during object creation, after setting all properties.
function listbox1_CreateFcn(hObject, eventdata, handles)
% hObject    handle to listbox1 (see GCBO)
% eventdata  reserved - to be defined in a future version of MATLAB
% handles    empty - handles not created until after all CreateFcns
called
% Hint: listbox controls usually have a white background on Windows.
%        See ISPC and COMPUTER.
if ispc && isequal(get(hObject,'BackgroundColor'),
get(0,'defaultUicontrolBackgroundColor'))
    set(hObject,'BackgroundColor','white');
end
function edit10_Callback(hObject, eventdata, handles)
% hObject    handle to edit10 (see GCBO)
% eventdata  reserved - to be defined in a future version of MATLAB
% handles    structure with handles and user data (see GUIDATA)
% Hints: get(hObject,'String') returns contents of edit10 as text
%        str2double(get(hObject,'String')) returns contents of edit10
as a double


% --- Executes during object creation, after setting all properties.
function edit10_CreateFcn(hObject, eventdata, handles)
% hObject    handle to edit10 (see GCBO)
% eventdata  reserved - to be defined in a future version of MATLAB
% handles    empty - handles not created until after all CreateFcns
called
% Hint: edit controls usually have a white background on Windows.
%        See ISPC and COMPUTER.
if ispc && isequal(get(hObject,'BackgroundColor'),
get(0,'defaultUicontrolBackgroundColor'))
    set(hObject,'BackgroundColor','white');
end


% --- Executes on selection change in popupmenu1.
function popupmenu1_Callback(hObject, eventdata, handles)
% hObject    handle to popupmenu1 (see GCBO)
% eventdata  reserved - to be defined in a future version of MATLAB
% handles    structure with handles and user data (see GUIDATA)
% Hints: contents = get(hObject,'String') returns popupmenu1 contents
as cell array
%        contents{get(hObject,'Value')} returns selected item from
popupmenu1
global NSR
global VTfast
global VF
global VTslow
global VTpoly
global AFIB
global SVT
global ASYS
global a
element=get(handles.popupmenu1,'value');
```

```
if element==2
    xref=NSR;
end
if element==3
    xref=VTfast;
end
if element==4
    xref=VTslow;
end
if element==5
    xref=VTpoly;
end
if element==6
    xref=VF;
end
if element==7
    xref=AFIB;
end
if element==8
    xref=SVT;
end
if element==9
    xref=ASYS;
end
xxref=xref/max(xref);
nnref=[1:length(xxref)]'/11025;
ppref=spline(nnref,xxref);
ppref1=mean(ppref.coefs(:,1));
ppref2=mean(ppref.coefs(:,2));
ppref3=mean(ppref.coefs(:,3));
ppref4=mean(ppref.coefs(:,4));
pprefcoefs=[ppref1 ppref2 ppref3 ppref4];
set(handles.edit10,'string',pprefcoefs);

% --- Executes during object creation, after setting all properties.
function popupmenu1_CreateFcn(hObject, eventdata, handles)
% hObject    handle to popupmenu1 (see GCBO)
% eventdata  reserved - to be defined in a future version of MATLAB
% handles    empty - handles not created until after all CreateFcns
called
% Hint: popupmenu controls usually have a white background on
Windows.
%        See ISPC and COMPUTER.
if ispc && isequal(get(hObject,'BackgroundColor'),
get(0,'defaultUicontrolBackgroundColor'))
    set(hObject,'BackgroundColor','white');
end
function edit11_Callback(hObject, eventdata, handles)
% hObject    handle to edit11 (see GCBO)
% eventdata  reserved - to be defined in a future version of MATLAB
% handles    structure with handles and user data (see GUIDATA)

% Hints: get(hObject,'String') returns contents of edit11 as text
%        str2double(get(hObject,'String')) returns contents of edit11
as a double

% --- Executes during object creation, after setting all properties.
function edit11_CreateFcn(hObject, eventdata, handles)
% hObject    handle to edit11 (see GCBO)
% eventdata  reserved - to be defined in a future version of MATLAB
```

Here there is the popup menu that is installed in the program in order for the user to choose a particular signal and to see in the next box the reference numbers of spline fit for the specified signal.

Appendices

```
% handles    empty - handles not created until after all CreateFcns
called
% Hint: edit controls usually have a white background on Windows.
%       See ISPC and COMPUTER.
if ispc && isequal(get(hObject,'BackgroundColor'),
get(0,'defaultUicontrolBackgroundColor'))
    set(hObject,'BackgroundColor','white');
end
```